การนำส่งเรตินัลดีไฮด์ทางผิวหนังโดยใช้ไคโทซาน

นางสาวปิยะพรรณ ทรัพย์เมือง

วิทยานิพนธ์นี้ เป็นส่วนหนึ่งของการศึกษาตามหลักสูตรปริญญาวิทยาศาสตรมหาบัณฑิต
สาขาเทคโนโลยีชีวภาพ
คณะวิทยาศาสตร์ จุฬาลงกรณ์มหาวิทยาลัย
ปีการศึกษา 2554
ลิขสิทธิ์ของจุฬาลงกรณ์มหาวิทยาลัย

RETINALDEHYDE SKIN DELIVERY USING CHITOSAN

Miss Piyapan Supmuang

A Thesis Submitted in Partial Fulfillment of the Requirements
for the Degree of Master of Science Program in Biotechnology
Faculty of Science
Chulalongkorn University
Academic Year 2011

Thesis Title	RETINALDEHYDE SKIN DELIVERY USING CHITOSAN
By	Miss Piyapan Supmuang
Field of Study	Biotechnology
Thesis Advisor	Associate Professor Supason Wanichwecharungruang, Ph.D.

Accepted by the Faculty of Science, Chulalongkorn University in Partial Fulfillment of the Requirements for the Master's Degree

……..Dean of the Faculty of Science
(Professor Supot Hannongbua, Dr. rer. nat.)

THESIS COMMITTEE

.....Chairman
(Assistant Professor Warinthorn Chavasiri, Ph.D.)

.....Thesis Advisor
(Associate Professor Supason Wanichwecharungruang, Ph.D.)

……..Examiner
(Associate Professor Chanpen Chanchao, Ph.D.)

……..External Examiner
(Natthakitta Suwannateep, Ph.D.)

ปิยะพรรณ ทรัพย์เมือง : การนำส่งเรตินัลดีไฮด์ทางผิวหนังโดยใช้ไคโทซาน (RETINAL-DEHYDE SKIN DELIVERY USING CHITOSAN) อ. ที่ปรึกษาวิทยานิพนธ์หลัก: รศ.ดร. ศุภศร วนิชเวชารุ่งเรือง, 90 หน้า.

ในงานวิจัยนี้ประสบความสำเร็จในการเตรียมอนุภาคนาโนของเรตินิลิดีนซัคซินิลไคโทซาน เริ่มต้นจากทำการสังเคราะห์ซัคซินิลไคโทซานโดยอาศัยปฏิกิริยาของไคโทซานกับซัคซินิคแอนไฮไดรด์ พอลิเมอร์นี้สามารถเกิดการรวมตัวเป็นอนุภาคระดับนาโนในน้ำหมู่อะมิโนบนพื้นผิวของอนุภาคของซัคซินิลไคโทซานสามารถสร้างพันธะชิฟเบสกับเรตินัลดีไฮด์ ได้เรตินิลิดีนซัคซินิลไคโทซานที่มีขนาดอนุภาค 181 ± 8.71 นาโนเมตร ซึ่งสังเกตได้จากกล้องจุลทรรศน์อิเล็กตรอนแบบส่องกราด การศึกษาความเสถียรภายใต้การได้รับแสง ความร้อน (40 องศาเซลเซียส) และออกซิเจน พบว่าส่วนของเรตินิลิดีนที่ถูกกราฟท์อยู่ในอนุภาคนาโนซัคซินิลไคโทซานมีความเสถียรเพิ่มขึ้นอย่างเห็นได้ชัดเมื่อเปรียบเทียบกับเรตินัลดีไฮด์อิสระ ผลที่ได้แสดงให้เห็นว่าเรตินัลดีไฮด์อิสระสลายตัวที่เวลา 120 นาที ขณะที่เรตินิลิดีนซัคซินิลไคโทซานสลายตัวที่เวลา 180 นาที นอกจากนี้เมื่อทำการกักเก็บสารต้านอนุมูลอิสระไว้ในอนุภาคเรตินิลิดีนซัคซินิลไคโทซาน พบว่าความเสถียรของเรตินิดีนที่ถูกกราฟท์เพิ่มขึ้นเมื่อเปรียบเทียบกับอนุภาคเรตินิลิดีนซัคซินิลไคโทซาน อนุภาคนาโนเรตินิลิดีนซัคซินิลไคโทซานที่มีวิตามินอีบรรจุอยู่ภายในไม่สลายตัวที่เวลา 300 นาที การศึกษาการซึมผ่านผิวหนังของอนุภาคนาโนเรตินิลิดีนซัคซินิลไคโทซาน และอนุภาคนาโนเรตินิลิดีนซัคซินิลไคโทซานที่มีวิตามินอี พบว่ามีการสะสมอยู่ที่บริเวณรูขุมขน และสามารถซึมผ่านผิวหนังทางรูขุมขน ทั้งเรตินัลดีไฮด์ที่ถูกกราฟท์ และวิตามินอีที่ถูกกับเก็บสามารถถูกปลดปล่อยออกมาจากอนุภาคเข้าสู่เนื้อเยื่อผิวหนังบริเวณรอบๆ

สาขาวิชา.....เทคโนโลยีชีวภาพ.....ลายมือชื่อนิสิต.....

ปีการศึกษา.....2554.....ลายมือชื่อ อ.ที่ปรึกษาวิทยานิพนธ์หลัก.....

5272708123: MAJOR BIOTECHNOLOGY
KEYWORDS: RETINALDEHYDE/ CHITOSAN/ IMINE AND SKIN PENETRATION

PIYAPAN SUPMUANG: RETINALDEHYDE SKIN DELIVERY USING CHITOSAN. ADVISOR: ASSOC. PROF. SUPASON WANICHWECHARUNGRUANG, Ph.D., 90 pp.

In this research, nanoparticles of retinilidenesuccinylchitosan (R-NSC) were successfully prepared. *N*-succinylchitosan was synthesized based on reaction of chitosan with succinic anhydride. The obtained polymer could self-assemble into spherical nanoparticles in aqueous medium. The amino groups on the surface of the *N*-succinylchitosan particles could form Schiff base with retinaldehyde. The R-NSC nanoparticles gave the particle size of 181 ± 8.71 nm as observed by scanning electron microscope. The stability study under light, heat (40 °C) and oxygen exposure indicated that the retinilidene moieties in the N-SC nanoparticles was significantly more stable comparing to free retinaldehyde. The result showed at 120 min the free retinaldehyde was degraded while the R-NSC was degraded at 180 min. In addition, when antioxidant was loaded into the R-NSC particles, stability of retinilidene moieties was further improved comparing to R-NSC particles. The vitamin E loaded R-NSC particles was undegraded at 300 min. The penetration study of the R-NSC and vitamin E-loaded R-NSC particles indicated accumulation of the particles at the hair follicles, thus implying that the particles could penetrat into the skin *via* hair follicles. Both the grafted retinaldehyde and the loaded vitamin E could be released from the particles into the surrounding skin tissue.

Field of Study: ……Biotechnology…… Student's Signature……
Academic Year: ……2011…….. Advisor's Signature……

ACKNOWLEDGEMENTS

First of all, I would like to express my sincere appreciation to my thesis advisor, Associate Professor Dr. Supason Wanichwecharungruang for her helpful supervision, invaluable assistance and generous encouragement to fulfill my achievement.

I also sincerely thank Assistant Professor Dr. Warinthorn Chavasiri, Associate Professor Dr. Chanpen Chanchao and Dr. Natthakitta Suwannateep for their time and suggestions as the committee members. And I would like to thank the Graduate School, Chulalongkorn University for financial support.

Finally, I would like to specially thank my family and research group members for their advice and encouragement throughout my master study.

CONTENTS

Page

Page

Page

LIST OF TABLES

Table **Page**

LIST OF FIGURES

Figure **Page**

Figure **Page**

Figure **Page**

Figure **Page**

Figure **Page**

Figure **Page**

LIST OF SCHEMES

Scheme **Page**

LIST OF ABBREVIATIONS

λ	wavelength
%	percent
°C	degree Celsius
DG	degree of grafting
DS	degree of substitution
cm^2	square centimeter
h	hour
s	second
µg	microgram
µl	microliter
mg	milligram
ml	milliliter
mW	milliwatt
min	minute
MW	molecular weight
mm	millimeter
nm	nanometer
ppm	parts per million
cm^{-1}	per centimeter
SEM	Scanning electron microscope
TEM	Transmission electron microscope
DLS	dynamic light scattering
UV	ultraviolet
cm^{-1}	unit of wavenumber (IR)
DMSO	dimethyl sulfoxide
CLFM	confocal laser scanning fluorescent microscope
ATR-FTIR	attenuated total reflection-fourier transform infrared
NMR	nuclear magnetic resonance
N-SC	*N*-succinylchitosan

R-NSC	retinaldehyde grafted N-SC particles
Rho B	Lissamine rhodamine B sulfonyl chloride
BHT	butylated hydroxtoluene
Vit E	α-tocopherol
i.p.	in-plane
def.	deformation

CHAPTER I
INTRODUCTION

1.1 Vitamin A

Vitamin A, its derivatives and beta-carotene (pro vitamin A) have been popular additives in the pharmaceutical and cosmetics. Dietary sources of vitamin A include meat, liver, egg yolk and milk. Source of beta-carotene include carrots, tomatoes and other yellow vegetables [1]. Vitamin A is an essential compound for normal skin-cell proliferation and regulation [2]. The cosmetics benefit from vitamin A and its derivatives lie in their ability to regulate epithelial cell growth and differentiation, decrease of wrinkling and roughness, and lightening of lentigines and melasma [1, 3, 4]. Thus, the popular derivatives of vitamin A that are found in cosmetics include vitamin A alcohol (retinol), vitamin A esters (retinyl palmitate, retinyl acetate), vitamin A aldehyde (retinaldehyde), and tretinoin (retinoic acid) (Figure 1.1) [1]. Vitamin A in the form of retinol can be converted to retinaldehyde, which in turn is converted into the active form, retinoic acid, in the cells. In fact, retinaldehyde can be converted back to retinol again, but the active retinoic acid is a dead-end metabolite [5]. In the body, a small percentage of retinol is converted to its biologically active form, retinoic acid, through an intermediary, retinaldehyde. Most of retinol is converted to retinyl ester, its storage form [6]. It is the conversion of the other forms of vitamin A into retinoic acid that affords them any cosmetic benefits to the skin. Problems of vitamin A and their derivatives include skin irritation and instability exposure to light, heat and oxygen. UVB and UVA radiation usually reduce the vitamin A content in human epidermis [7, 8]. Degradation of vitamin A is accelerated by exposure to light, especially ultraviolet light at wavelengths below 415 nm [9]. Vitamin A is degraded faster under UVA light (320-400 nm) than under UVB light (280-320 nm) [10].

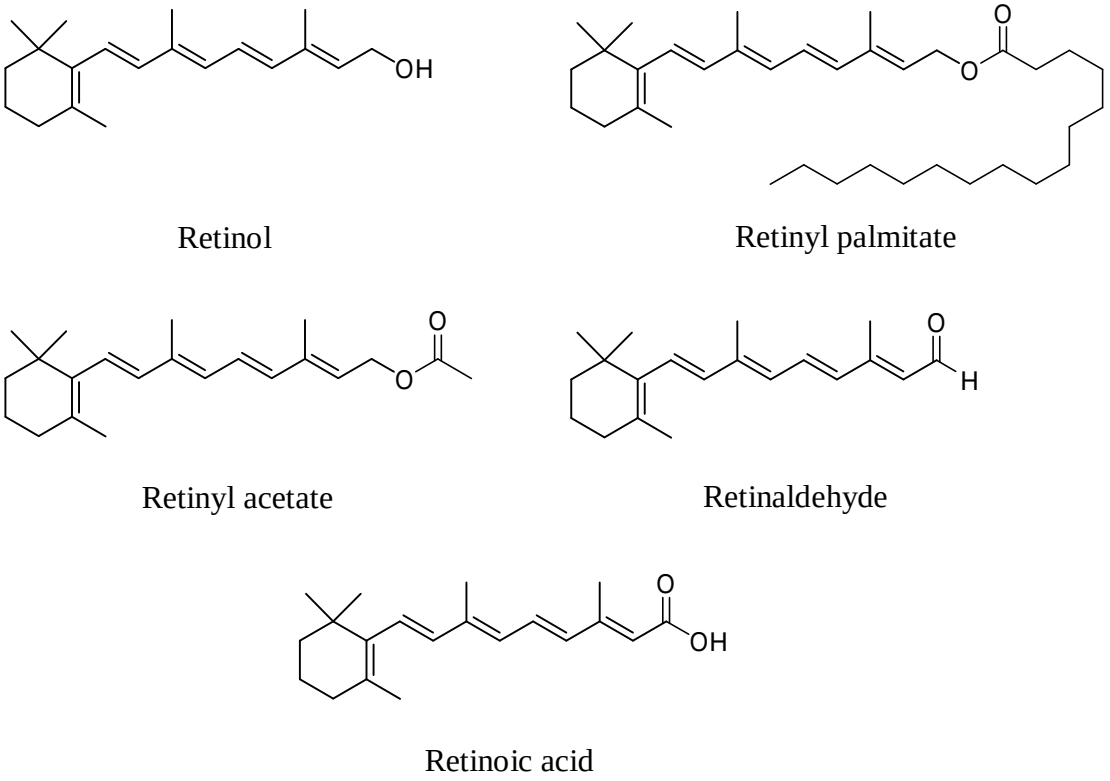

Figure 1.1 The derivatives of vitamin A are found in cosmetics

Retinaldehyde, vitamin A aldehyde is one of the popular vitamin A derivatives on the skin care product. It is the direct precursor to retinoic acid in the metabolic process. It is a much less irritant form of the vitamin A. Retinaldehyde is speculated to be 20-fold less effective than retinoic acid. Retinaldehyde is considered another vitamin A of limited efficacy. Studies have shown responses to increased epidermal thickness, enhance protein synthesis, increase production of collagen and repair skin of sun damage (such as wrinkles, pigmentation, rough and dry skin) [11, 12].

1.2 Mechanisms of vitamin A

Interaction of retinoic acid with nuclear receptor proteins leads to interaction with specific DNA sequences to affect transcription, resulting in either increased or decreased expression of specific proteins or enzymes [13]. The many gene expression changes induced by vitamin A, some specific ones that are likely essential to skin antiaging effects are those leading to thicker skin, which likely contributes to decrease

fine lines and wrinkle appearance; for example, increased epidermal proliferation and differentiation, increased production of epidermal ground substance (glycosamino-glycans, GAG) that bind water, thus increasing epidermal hydration and increased production of collagen [14]. The vitamin A is reported to reduce production of collagenase [15] and reduced skin wrinkling [16, 17]. Vitamin A also reduce expression of tyrosinase [18, 19], a key enzyme in the conversion of tyrosine to melanin.

1.3 Aging and photoaging

Aging is a natural, ineluctable, and complex process that reverses biological characteristics and leads to cellular death. On the other hand, the damage accumulation theory, which was introduced by Denham Harman, explains aging by the accumulation of alterations of the biomolecules that the organism cannot repair or eliminate completely [20, 21]. Skin aging begins with a redistribution of fat, decreased dermal elasticity [22] and continues with a progressive impairment of the regeneration of connective tissue components such as collagen and hyaluronate [23-25]. Besides natural aging, environmental conditions can accelerate aging. The environmental factor that accelerates skin aging is ultraviolet (UV) irradiation from the sun. This sun-induced skin aging, called photoaging that depends primarily on the degree of sun exposure (UV fraction of sunlight (280-400 nm), in particular UVB radiations (280–320 nm)). DNA photodamage and repair represent the predominant adverse effects of UVB on cells and tissues. The UVA (320-400 nm) represents about 96% of solar UV radiations are more involve the photo-sensitization of skin [26].

Use of vitamin A for antiaging

The first vitamin A used to treat skin aging was retinoic acid. The potential effects of retinoic acid on photodamaged skin were first observed by Kligman and co-worker in young women treated for tenacious acne [27]. Histologic findings of retinoic acid application to the skin include: (1) compaction of the stratum corneum, (2) dispersion of melanin granules, and (3) increased dermal collagen synthesis. These findings explain the smoother skin, healthy-looking glow, decreased pigmentation,

and decreased fine lines and wrinkles observed following a long-term topical treatment with retinoic acid. The limiting factor in vitamin A treatment is skin irritation characterized by erythema, burning, and dryness. Retinaldehyde, the precursor of retinoic acid, is much less of an irritant than retinoic acid. It was demonstrated to be well tolerated and effective in treating photodamage [8, 12].

1.4 Improvement stabilizing of vitamin A

The degradation of vitamin A in aqueous solution is rapid [28], the solubility of vitamin A in water is poor because of their low polarity. Dispersibility and stability can be improved by incorporating vitamin A into colloidal carrier particles. Carriers available at present include single and double emulsions [29-34], liposomes [35, 36], solid lipid nanoparticles [37-42] and polymeric micro- or nanoparticles [31, 43-45], complex with cyclodextrins [29, 47-49] and proteins [50, 51]. Many of these technologies have been developed for cosmetic or pharmaceutical applications.

1.5 Encapsulation of vitamin A applied to transdermal applications

The administration can be adapted to deliver vitamin A to skin. Encapsulation for skin deposition requires vitamins A protection against different stresses (light, heat and oxygen) and particles penetration through skin. The absorption can be divided in several steps: (1) drug deposition on skin, (2) drug diffusion through the stratum corneum to reach dermis or epidermis, and (3) molecule metabolization by dermal cell. However, vitamin A properties, particles cited afterwards have been mostly designed for local action. [52]

1.5.1 Lipid based carriers for vitamin A

The stratum corneum is composed by lipid bilayers, liposomes may pass through this barrier and could constitute a suitable drug carrier for dermal route. Liposomes surface charge might impact their drug deposition influence. This hypothesis has been tested with retinoic acid loaded particles [53, 54]. Surface charge of liposomes did not influence retinoic acid in vitro release. The membrane fluidity and permeability did not affect retinoic acid diffusion, and can also hypothesize that retinoic acid release and diffusion through stratum corneum. These preparations were

less efficient than retinoic acid ethanolic/water solution. It is generally accepted that ethanol might affect stratum corneum structure thus enhancing drug permeation. It can be hypothesized that oil and surfactant can interact physically with stratum corneum bilayers and diarrange this structured environment. Thus, surfactant characteristics have an impact on drug permeation. Retinoic acid protection against UV radiation by encapsulation has been studied with liposomes, niosomes [55], emulsion and lipid particles [38, 56]. Ourique et al. compared retinoic acid stability in nanocapsules and nanoemulsions [30]. Nanocapsules improved significantly retinoic acid photostability when compared to nanoemulsion formulated according to the same process without polymer. A reservoir form might maintain biological efficiencies while decreasing side effects. For example, retinoic acid topical administration often causes burning, erythema or peeling. Retinoic acid was found to be less irritating for the skin when deposited in SLNs gels than with commercial cream [38, 56]. SLNs could penetrate in stratum corneum which could explain the decrease of skin irritation.

1.5.2 Entrapment of vitamin A in molecular assemblies

The chitosan properties have been largely studied for nasal and oral administrations [57], studied previous results its charge might be of interest for dermal deposition [53]. For example, Retinol has been encapsulated in chitosan nanoparticles for cosmetic or pharmaceutical applications [43]. For further investigations concerning drug deposition are needed. Particles positive charge might be an advantage for retinol penetration.

1.6 Chitosan

Chitosan is a natural polymer derived from chitin by deacetylation (Figure 1.2). It consists unbranched chain of β-(1-4)-2-acetamido-2-acetamido-2-deoxy-β-d-glucose and β-(1-4)-2-amino-2-acetamido-2-deoxy-β-d-glucose as a repeating units [58]. It can be extracted from fungi, insect, lobster, shrimp and krill. This biopolymer and its derivatives have potential applications in the areas of biotechnology, biomedicine [59-62], agriculture, wastewater purification [63], environmental protection, food [64] and cosmetics [43]. Chitosan is non-toxic, biocompatible,

biodegradable and possesses anti-bacterial property [65-68]. Although chitosan should be useful for even more numerous applications, the compound suffers limitation on solubility, chitosan is soluble only in acid [69]. Thus various chemical modifications of chitosan structure have been reported for the improvement of its solubility [70]. One example among many is the preparation of chitosan Schiff bases by reacting chitosan with aldehydes and ketones [65, 71, 72, 108]

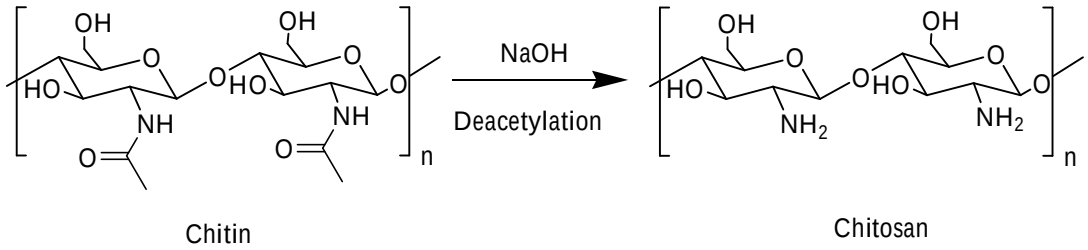

Figure 1.2 Deacetylation reaction of chitin

1.7 Skin

1.7.1 Skin structure

The structure of the skin can be included three main layers, the epidermis, dermis and fat layer (Figure 1.3). In addition to these structures, there are also several associated appendages: hair follicles, sweat glands, apocrine glands, and nails. The uppermost layer of the skin structure is the epidermis, has an approximately thickness 300 μm (Figure 1.4) [74]. The stratum corneum is the top layer of the epidermis, has an approximately thickness of 10 – 20 μm. It is the layer of the skin that we see from the outside. These cells are dead, contain a lot of keratin and are arranged in overlapping layers that impart a tough and waterproof character to the skin's surface (Figure 1.5) [76]. Dead skin cells are continually eliminate from the skin's surface. This is balanced by the dividing cells in the basal cell layer to produce a state of constant renewal. Also in the basal cell layer are cells called melanocytes that produce melanin. Melanin is a pigment that is absorbed into the dividing skin cells to help protect them against damage from sunlight (ultraviolet light). Melanin granules form a protective shield over the nuclei of the keratinocytes. The more melanin pigment present, the darker the color of your skin. The dermis contains a variable amount of

fat, and also collagen and elastin fibers which provide strength and flexibility to the skin. When the skin is exposed to sunlight, modified cholesterol in the dermis produces vitamin D. Nerves in the dermis detect heat, cold, pain, pressure and touch and relay this information to the brain. A sebaceous gland opens into each hair follicle and produces sebum, a lubricant for the hair and skin that helps repulse water, damaging chemicals and microorganisms. Sweat glands occur on all skin areas each person has more than 2 million. When the body needs to lose heat these glands produce sweat and moves to the skin's surface *via* the sweat duct. The innermost layer of the skin structure is the layer of subcutaneous fat. The fat stored in this layer represents an energy source for the body and helps to insulate the body against changes in the outside temperature. [77]

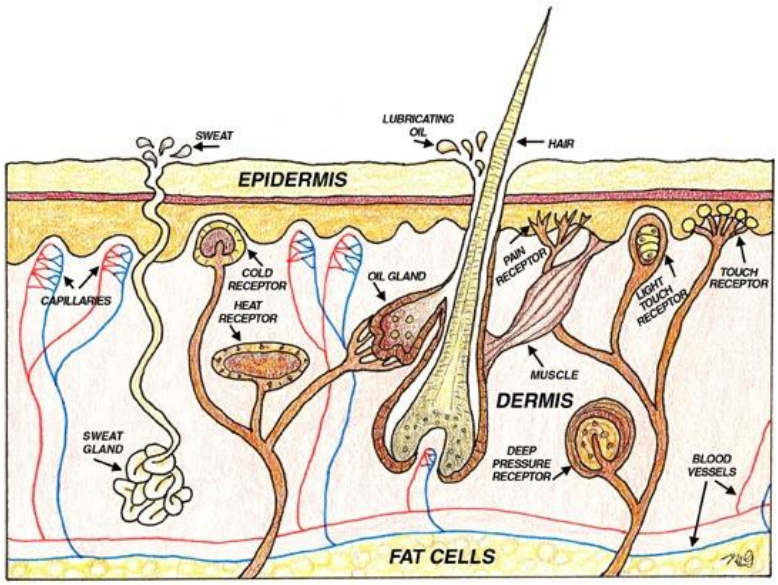

Figure 1.3 Simplified schematic cross-section of the human skin [http://www.swiss-creations.com/sc-14story.htm#The Human Skin]

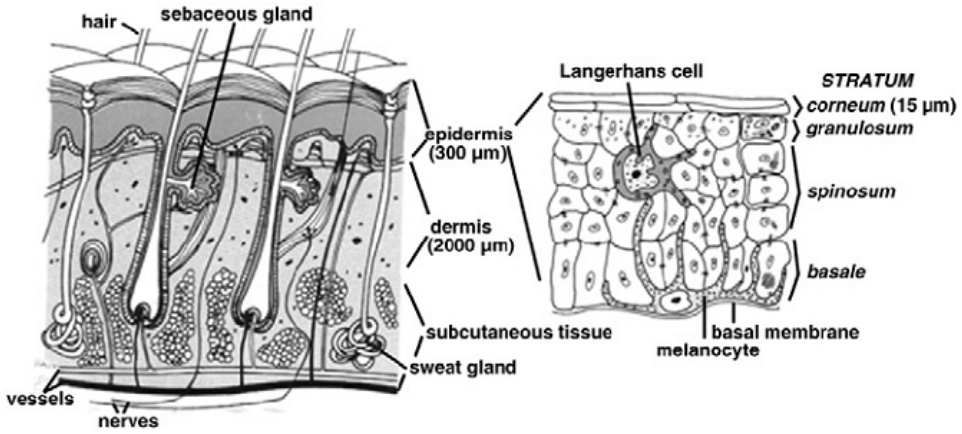

Figure 1.4 Structure of the skin. The skin consists of three main layers: epidermis, dermis, and subcutaneous fat tissue. The barrier function of the skin is located in the uppermost layer, the stratum corneum. [77]

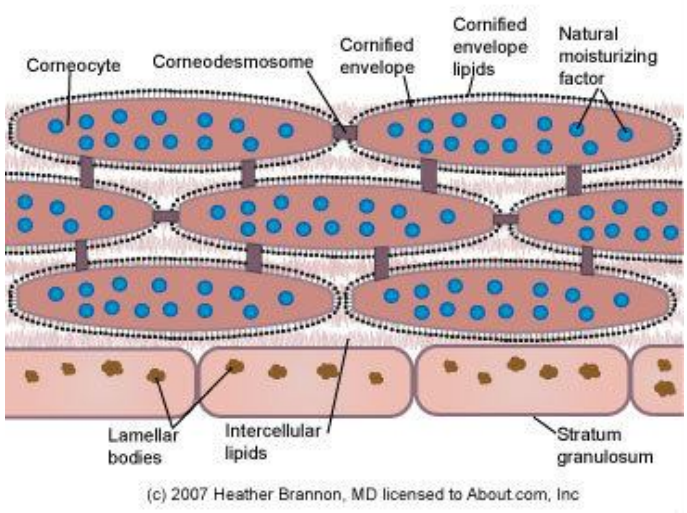

Figure 1.5 Structure of stratum corneum [http://www.zazana.com/babnee/id9571.aspx]

1.7.2 Skin functions

Skin functions include protection, heat regulation, immune response, biochemical synthesis and sensory detection. The epidermis, the most superficial layer and more specifically, the stratum corneum, plays the major role. With age, the skin's natural rejuvenation process slows drastically and the skin becomes thinner, drier, and less elastic. This aging process has intrinsic and extrinsic components. [78-80] Intrinsic aging comprises the genetically clinical, histological, and physiologic

changes that occur in the skin throughout the body with the passage of time. Extrinsic aging is a cumulative degenerative process induced by decades of exposure to harmful environmental conditions, mainly solar ultraviolet radiation. [78-81] Concurrent processes of intrinsic and extrinsic aging produce distinct skin changes, including development of fine and coarse wrinkles, leathery texture, mottled hyperpigmentation, and dryness. There is a marked loss of elasticity, and hyperkeratinization occurs, causing the corneocytes to adhere in excess, accounting for the thickening of the stratum corneum. In papillary dermis, photodamaged elastic fibers are short and fragmented, in contrast with the appearance of normal or nonphotodamaged elastic fibers, which are long, wavy, and nonfragmented. [78, 80, 81] The greater understanding of the skin structure and function has allowed the development of efficient care products with appreciable beneficial effects, [82] and both alpha-hydroxy acids and retinoids have a capacity of reducing cohesion between corneocytes and, consequently, decrease the width of the stratum corneum, especially in situations of hyperkeratosis. [83, 84]

1.7.3 Sites for particle delivery

Skin is a widely used route of delivery for drugs and is potentially a route for their delivery as nanoparticles. The nanoparticle drug delivery has been advertised as an enabling technology, its potential in treatment skin. The sites of skin for nanoparticles delivery include three major sites, the sweat gland, stratum corneum surface and hair follicle (Figure 1.6) [85]. The prospects of drug delivery using particles have results obtained in various studies demonstrate that the particles applied in cosmetic. Advantages of particulate carrier systems are the deep and preferred penetration into the hair follicle. In additions, the long storage time within the hair follicles [86]. Drug-loaded particles are only the transporter bringing the drug exactly to the specific target site within the hair follicles [87]. Then drug release from the nanoparticles into the target tissue. Nanostructures in drug delivery have been widely used in recent years because they can not only stimulate a sustained release but also protect labile drugs from degradation [88, 89].

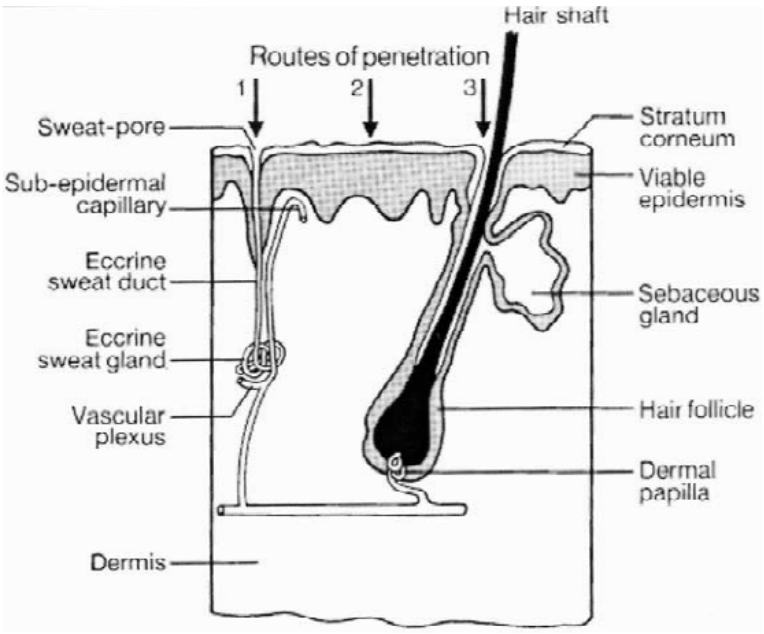

Figure 1.6 Sites in skin for nanoparticle delivery. Topical nanoparticle drug delivery takes place in three major sites: sweat gland (panel a), stratum corneum surface (panel b) and hair follicle (panel c). [85]

1.8 Antioxidant

Antioxidant is a molecule ability of inhibiting the oxidation of other molecules. Oxidation is a chemical reaction that transfers electrons or hydrogen from a substance to an oxidizing agent. Oxidation reactions can produce free radicals. In turn, these radicals can start chain reactions. When the chain reaction occurs in a cell, it can cause damage or death to the cell. Antioxidants terminate these chain reactions by removing free radical intermediates, and inhibit other oxidation reactions. They do this by being oxidized themselves, so antioxidants are often reducing agents such as substances in the vitamin: vitamin A, vitamin B, vitamin C, vitamin K and vitamin E and nonvitamin: coenzyme Q10, lipoic acid, butylated hydroxyanisole (BHA) and butylated hydroxyltoluene (BHT). In this research will be mentioned the vitamin E and BHT.

α-tocopherol (vitamin E)

α-tocopherol (vitamin E) is a lipid-soluble vitamin present in many food sources, especially soy, nuts, whole-wheat flour, and oils. The vitamin E is the most active and is important in protecting cellular membranes from lipid peroxidation by free radicals. Because of this ability to quench free radicals has been used to describe the actions of vitamin E and its derivatives. Several studies show their ability to reduce UV-radiation-induced erythema and edema, sunburn cell formation, and lipid peroxidation. [90-94] Clinical improvement skin aging has been documented with decrease in both skin wrinkling and skin tumor formation. [95-97] *In vitro* studies have showed the effects of α-tocopherol in reducing minimal erythema dose and the number of epidermal sunburn cells. Many studies have been performed on both tocopherol and tocopherol acetate. Tocopherol is the primary active form of vitamin E, the vitamin E esters have also been shown to penetrate the epidermis when applied topically [98]. The previous study found tocopherol sorbate, a less commonly used vitamin E derivative, to be photoprotective *via* its antioxidant actions as well. [95] All this data verifications the popularity of vitamin E and its derivatives as antioxidant, rejuvenating ingredients in cosmetics.

Although topical application of vitamin E demonstrates promising photoprotective effects, specifically when it is combined with other antioxidants, controlled studies in humans are needed before it can be recommended as an effective cosmeceutical agent for the treatment of both intrinsic and extrinsic aging. [6, 100]

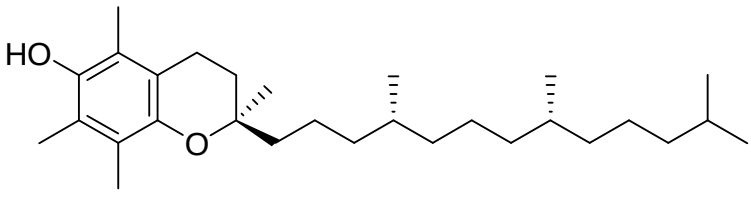

Figure 1.7 Structure of α-tocopherol

Butylated hydroxyltoluene (BHT)

Butylated hydroxyltoluene (BHT) has also been used as a food antioxidant to stabilize fats and oils, and to preserve the nutritional value of the diet of man and animals. BHT is an inhibitor of free radical-mediated processes agent. [100, 101] In some reviews on safety evaluation of hindered phenolic antioxidants, In monkeys, BHT induced fragmentation and the presence of large nuclear fibrils in hepatic nuclei [102, 103].

BHT has been found to have protective effects against UV-induced erythema on rabbit skin and to inhibit lipid peroxidation in mouse skin. [104, 105] That there have been so many studies on so many potential topical antioxidants certainly suggests even more potential product development in the future.[1]

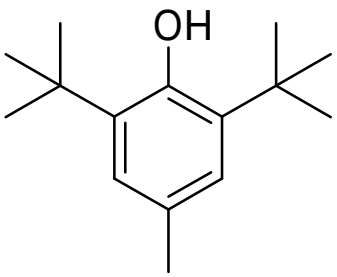

Figure 1.8 Structure of butylated hydroxyltoluene

1.9 Literature reviews of vitamin A improvement

Improvement of vitamin A by emulsion

In 2004, Hwang, S. R., *et al.* [29] encapsulated all-*trans* retinoic acid into phospholipid-based microemulsion. The process gave the encapsulation efficiency of higher than 99.9% and the ATRA loading of 32%. Microemulsion formulation of all-*trans* retinoic acid improved the solubility and chemical stability of all-*trans* retinoic acid compared with all-*trans* retinoic acid in 1% Tween 80 and methanol solution (Figure. 1.9) while maintained its pharmacokinetic profile and anti-cancer efficacy.

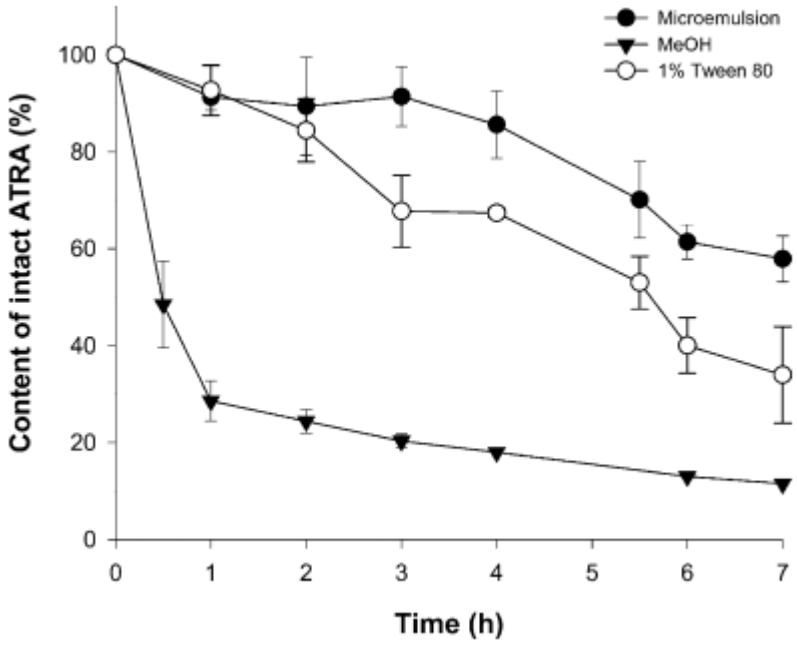

Figure 1.9 Comparison of stability of all-trans retinoic acid in various preparations during incubation at room temperature under light exposure. [29]

In 2009, Eskandar, N. G., *et al.* [33] prepared all-*trans*-retinol into nanoparticle-coated emulsions. The chemical stability was studied as a function of UVA+UVB irradiation, and storage temperature (4°C, ambient temperature, and 40°C) for emulsions stabilised with lecithin and oleylamine as the initial emulsifier with and without silica nanoparticle layers. A significant stability improvement (~2-fold increase in the half-life of the drug) was observed by nanoparticle incorporation into oleylamine-stabilised droplets (Figure 1.10). The nanoparticle layers can be used to enhance the chemical stability of active ingredients in emulsion carriers.

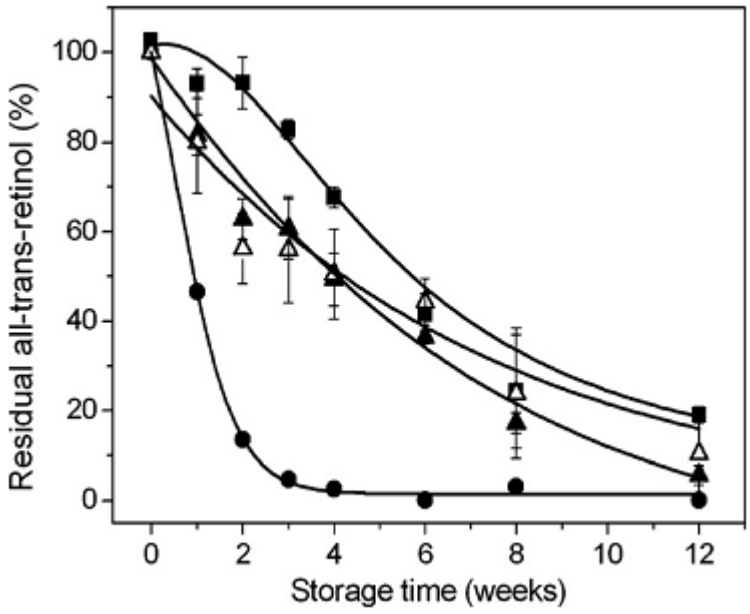

Figure 1.10 Long-term chemical stability at 4°C of all-trans-retinol incorporated into emulsions stabilised with no stabiliser (solid circles), only lecithin (solid squares), lecithin and silica nanoparticles in the oil phase (solid triangles), lecithin and silicananoparticles in the aqueous phase (open triangles). [33]

In 2012, Eskandar, N. G., *et al.* [34] prepared all-*trans*-retinol oil-in-water emulsions stabilised with conventional surfactants and silica nanoparticles. The stability was observed for silica-coated oleylamine emulsions at 4°C in their wet state. The result showed half-life of all-*trans*-retinol was 25.66 and 22.08 weeks for silica incorporation from the oil and water phases, respectively. This was ~4 times higher compared to the equivalent solid-state emulsions with drug half-life of 6.18 and 6.06 weeks at 4°C. Exceptionally, at a storage temperature of 40 ◦C, the chemical stability of the drug was 3 times higher in the solid-state freeze-drying compared to the wet emulsions. The dry particles confirmed that the promising to improve the chemical stability of water-labile compounds.

Improvement of vitamin A by lipid nanoparticles

In 2006, Jee, J. P., *et al.* [37] prepared all-*trans* retinol-loaded solid lipid nanoparticles (SLN) by hot melt homogenization method. The encapsulation efficiency was higher than 74% and drugs loading ranged from 2.17 to 2.94%. The

particles size of all-*trans* retinol-loaded SLN ranged from 90 to 240 nm and the zeta potentials ranged from -27 to -37 mV, suggesting acceptable electrostatic stability of all-*trans* retinol-loaded SLN. The photostability at 12 h of all-*trans* retinol in SLN was higher than free retinol in methanolic solution (Figure 1.11).

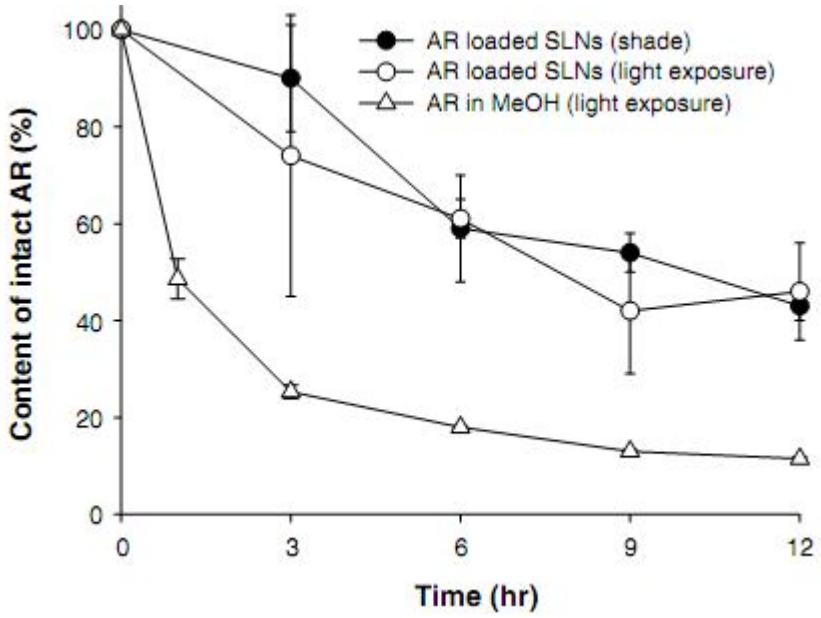

Figure 1.11 Effect of light on the chemical stability of AR in SLNs. And one group of samples was exposed to light and the other group was shaded from light. [37]

In 2007, Shah, K. A., *et al.* [38] encapsulated tretinoin (TRE) into solid lipid nanoparticles (SLN) by emulsification-solvent diffusion (ESD) technique. SLN of TRE has a particle sizes around 300-500 nm, the encapsulation efficiency of 35.5% to 48.9% and the ATRA loading of 3.55% to 4.89%. Encapsulation of TRE in SLN resulted in a significant improvement in its photostability in comparison to TRE in methanolic solution (Figure 1.12).

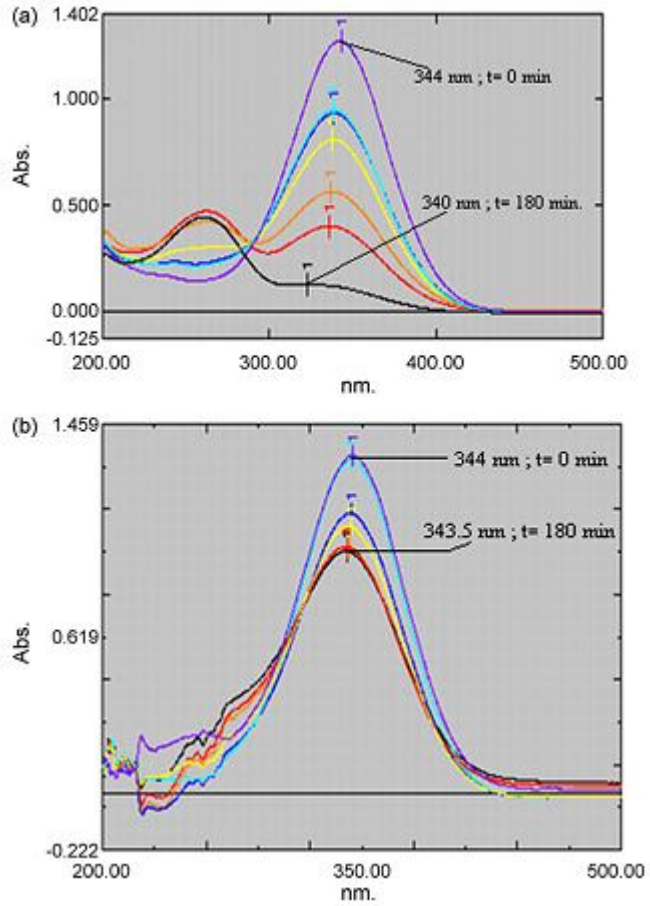

Figure 1.12 Photodegradation of TRE after exposure to sunlight for different durations (a) methanolic solution (b) SLN dispersion containing TRE. [38]

In 2007, Liu, J., *et al.* [40] prepared isotretinoin-loaded solid lipid nanoparticles. The isotretinoin-loaded SLN were formulated by hot homogenization method. The SLN formulations have high encapsulation efficiency ranging from 80% to 100% and drugs loading ranging from 19% to 24%. The isotretinoin-loaded SLN has low average size of 30-50 nm (Figure 1.13). These particles showed high accumulation of isotretinoin in skin and possened a significant skin targeting effect.

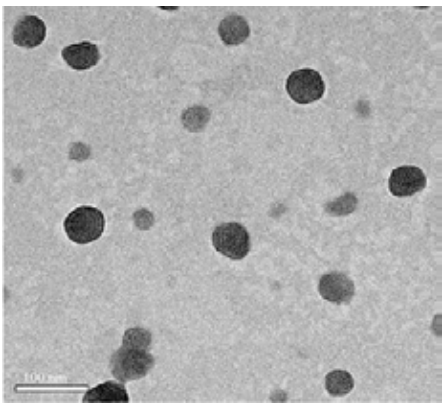

Figure 1.13 The TEM imaging of isotretinoin-loaded SLN. [40]

In 2009, Castro, G. A., *et al.* [41] investigated the influence of the formation of ion pairing between all-trans retinoic acid (RA) and a lipophilic amine (stearylamine; STE) on the drug encapsulation efficiency (EE) and stability of solid lipid nanoparticles (SLNs). The formulation without STE allowed only 13% of RA encapsulation, the EE for RA–STE-loaded SLNs was 94%. The stability studies showed a significant decrease in EE for the SLNs without STE, while, for SLNs loaded with RA and STE, the EE remained constant after 360 days. Skin irritation studies showed that the SLNs loaded with the ion pairing were significantly less irritating when compared to the marketed RA-cream. This novel SLN formulation represents a promising alternative for topical treatment of acne with RA.

In 2012, Ridolfi, D. M., *et al.* [42] prepared solid lipid nanoparticles containing tretinoin (SLN-TRE) and SLN-TRE containing chitosan (SLN-chitosan-TRE). The hydrodynamic mean diameter were 162.7 ± 1.4 and 284.8 ± 15.0 nm for SLN-TRE and SLN-chitosan-TRE, respectively. The SLN-chitosan-TRE exhibited high encapsulation efficiency, high physical stability in the tested period (one year) were not cytotoxic to keratinocytes and showed high antibacterial activity against *P. acnes* and *S. aureus.* Therefore chitosan-SLN can be good candidates to encapsulate TRE and to increase its therapeutic efficacy in the topical treatment of acne.

Improvement of vitamin A by polymeric nanoparticles

In 2006, Kim, D. G., *et al.* [43] prepared retinol-encapsulated chitosan nanoparticles by ultrasonication at an output power of 50W for 10 cycles of 2 s each on ice (Figure 1.14). Retinol-encasulated chitosan nanoparticles has a spherical shape and its particle size was around 50-200 nm. Particle size increased according to the increased drug content. The nanospheres gave the encapsulation efficiency higher than 60% with the highest retinol loading of 17.35%.

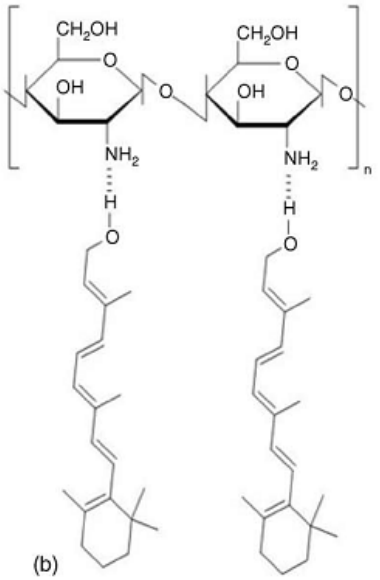

Figure 1.14 Structure of retinol-encapsulated nanoparticles. [43]

In 2007, Opanasopit, P., *et al.* [44] prepared amphiphilic grafted copolymer *N*-phthaloylchitosan-grafted poly(ethylene glycol) methyl ether (PLC-g-mPEG) using chitosan with four different degrees of deacetylation (DD) (80, 85, 90 and 95%). All-*trans* retinoic acid (ATRA) was incorporated into PLC-g-mPEG by dialysis method. The particle sizes of ATRA incorporated into micelles were about 80-160 nm depending on the initial drug-loaded and %DD of chitosan. It was found that %DD of chitosan, was a key factor in controlling the incorporation efficiency, stability of the drug-loaded micelles and drug release behavior. As the %DD increased, the incorporation efficiency and ATRA-loaded micelles stability increased.

In 2008, Ourique, A. F., *et al.* [30] prepared tretinoin-loaded nanocapsules by interfacial deposition of performed poly-ε-caprolactone. The TRE-encapsulated poly-ε-caprolactone nanoparticles presented encapsulation efficiency of >99.9% and drugs loading of 4.76%. These particles showed improved photostability of tretinoin over free tretinoin in a methanolic solution.

In 2009, Errico, C., *et al.* [45] encapsulated retinoic acid into poly (D, L-lactide-co-glycilide) (PLGA) and poly (3-hydroxybutylate) (PHB) nanoparticles using the dialysis method. The particles size of retinoic acid-loaded PLGA and PHB ranged from 107±39 to 549±170 nm and 50±20 to 53±17 nm, respectively. The size of PHB nanoparticles prepared techniques. The retinoic acid loading was 1.3% for retinoic acid-loaded PLGA and 1.04% for retinoic acid-loaded PHB.

Improvement of vitamin A by antioxidant

In 2002, Carlotti, M. E., *et al.* [31] tested photostability of vitamin A and vitamin A palmitate in different media. An O/W fluid emulsion with 0.5% w/w of retinyl palmitate, with and without butylated hydroxy toluene (BHT), was prepared. The fluid emulsion containing retinyl palmitate with and without BHT was stored at different temperatures and analysed every week for a month. BHT inhibited the photodegradation of both vitamins dissolved in octyl octanoate, suggesting that oxygen may be involved in their degradation. O/W emulsion promoted slightly the degradation of vitamin A ester. Butylated hydroxy toluene protected retinyl palmitate from degradation induced by light and heat.

1.10 Literature reviews of retinaldehyde

In 1998, Diridollou, S., *et al.* [46] has been used the moisturizing cream that containing 0.05% retinaldehyde for skin damage from sunlight comparing with general moisturizing cream. The result showed epidermal and dermal thickness, stiffness and elasticity of the skin was increased. Moreover, it also reduced the hardness of the skin comparing with general moisturizing cream.

In 1998, Creidi, P., *et al.* [8] treated skin damage from sunlight with the cream containing 0.05% retinaldehyde with 40 patients. And cream containing 0.05% retinoic acid with 40 patients. At week 18, a significant reduction of the wrinkle and roughness features was observed with both retinaldehyde and retinoic acid. But the retinoic acid caused more local irritation than retinaldehyde.

1.11 Literature reviews of chitosan

Chitosan derivatives

In 2002, Hu, Y., *et al.* [73] prepared chitosan-poly(acrylic acid) complex nanoparticles (CS-PAA nanoparticles) using template polymerization. The polymerization of acrylic acid in chitosan solution (CS as the template) was initiated by $K_2S_2O_8$. After successful polymerization, the solution changed from a clear solution to an emulsion. The inter- and intra- molecular complexation between negative charge from carboxyl groups (COO^-) of PAA and positive charge from amino groups (NH_3^+) of CS leading to the formation of nanoparticles. The obtained particles, at pH 4.5 in aqueous solution, showed well dispersion and good particle stability, and possesses positive charge and small size in the range of 200 - 300 nm (Figure 1.15).

Figure 1.15 TEM micrograph of CS-PAA nanoparticles at pH 4.5 [73]

In 2006, Aping, Z., *et al.* [70] synthesized *N*-succinyl-chitosan nanospheres (NSCS), succinyl was substituted at hydrogen atom of amino group in chitosan chains. In distilled water, NSCS easily dispersed into the stable and transparent dispersion. Examining of the dispersion indicated an assembling of polymer into

spherical particles. The self-assembly of the obtained nanospheres probably induce from the decrease in intermolecular H-bonding thus lower the crystallinity of the chitosan. The average size of the NSCS nanospheres was about 50–100 nm (Figure 1.16).

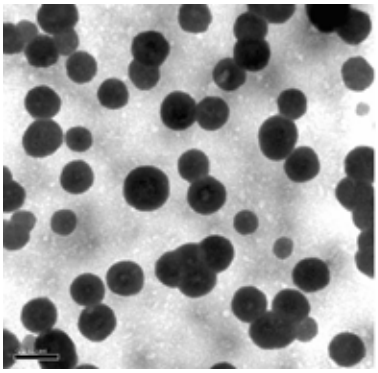

Figure 1.16 TEM micrographs of NSCS nanospheres [70]

In 2010, Luo, H., *et al.* [59] evaluted antitumor effects of N-succinyl-chitosan nanoparticles (NSCNP) in K562 cells. The results revealed NSCNP could inhibit the proliferation of K562 with an IC50 of 14.26 mg/ml (24 h), indicating that the antitumor effect of NSCNP achieved by necrosis and apoptosis induction in K562 cells.

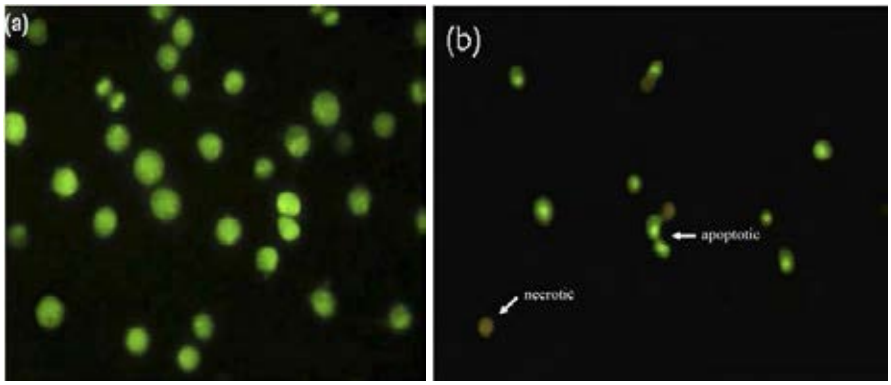

Figure 1.17 Fluorescent staining of nuclei in NSCNP-treated K562 cells by AO-EtBr. Cells with condensed and fragmented nuclei and cells necrotic were seen in the NSCNP (15 ug/ml, 24 h) treated cells (b), but not in the control cells (a) (Magnification 200×). [59]

Chitosan for drug delivery

In 2001, Janes, K. A., *et al.* [106] prepared chitosan nanoparticles by ionotropic gelation with sodium tripolyphosphate (TPP). The positive charge of DOX complexing with the polyanion, dextran sulfate and was loaded into nanoparticles. The effects of doxorubicin (DOX) encapsulation and/or release on cytotoxic activity relative to free DOX were studies. The evaluation of the activity of DOX-loaded nanoparticles in cell cultures indicated that those containing dextran sulfate were able to maintain cytostatic activity relative to free DOX, while DOX complexed to chitosan before nanoparticle formation showed slightly decreased activity. Additionally, confocal studies showed that DOX was not released in the cell culture medium but entered the cells while remaining associated to the nanoparticles.

In 2006, Opanasopit, P., *et al.* [44] prepared *N*-phthaloylchitosan-grafted poly(ethylene glycol) methyl ether (mPEG)(PLC-g-mPEG) and camptothecin (CPT) was loaded into micelles by dialysis method. The *in vitro* release bahaviors were studied in phosphate-buffered saline (PBS) at pH 7.4 for 96 hours by dialysis method. Release of CPT from the micelles was sustained. When compared to the unprotected CPT, CPT-loaded PLC-g-mPEG micelles were able to provent the hydrolysis of the lactone group of the drug.

In 2007, Xiangyang, X., *et al.* [62] prepared *N*-Succinyl-*N'*-octyl chitosan (SOC) by incorporated anticancer drug, doxorubicin (DOX), into polymeric micelles. The polymeric micelles containing doxorubicin in the core region exhibited a sustained release and more cytotoxic activity against HepG2, A549, BGC and K562 than doxorubicin alone, this can be attributed to an endocytosis mechanism rather than passive diffusion.

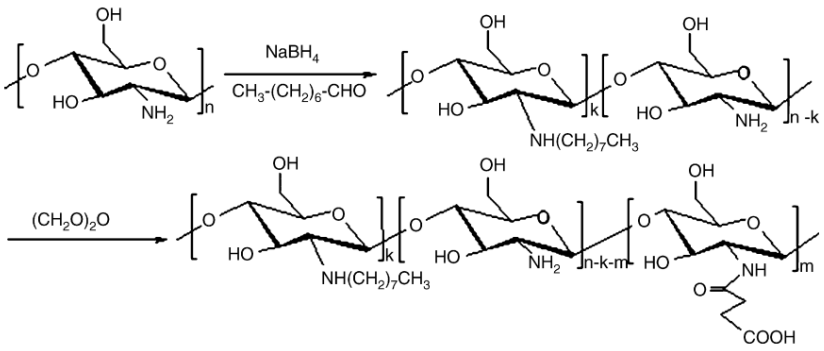

Figure 1.18 Synthesis of *N*-succinyl-*N*-octyl chitosan (SOC) [62]

In 2010, Hou, Z., *et al.* [60] entrapped hydroxycamptothecin (HCPT) into the NSC nanoparticles. The size of HCPT-loaded NSC (NSCH) nanoparticles were around 200 nm. The drug entrapment efficiency of NSCH reached up to 68.5% and the slower release of HCPT. *In vivo* studies, the NSCH nanoparticles showed tumor targeting and significant suppression of tumor growth after s.c. injection (close to the tumor) tomice bearing S180 sarcoma tumor. It indicated that NSCH had a lethal effect on the sarcoma cell. The results indicated that NSC nanoparticles had potential as a local sustained delivery system for hydrophobic antitumor drug.

In 2011, Mura, C., *et al.* [107] studied the *N*-succinyl chitosan matrices for selective colon delivery of 5-aminosalicylic acid. The drug was successfully loaded into the matrices reaching up to 95% entrapment efficiency. Swelling and drug release were studied at pH 1.2, 7.4, and in a pH gradient medium to simulate the gastro-intestinal transit. Main result of this study was a higher capability of *N*-succinyl chitosan to better control drug release in the simulated gastro-intestinal transit: *N*-succinyl chitosan gave the lowest release in acid medium (≅15%) and the highest in alkaline environment (≅92%).

Schiff base of chitosan

In 2009, Jin, X., *et al.* [65] synthesized the Schiff base of chitosan by the reaction of chitosan with citral working under high-intensity ultrasound. The maximum yield achieved was 86.4%. The results confirmed that amino groups on chitosan reacted with citral to form the Schiff base. The antimicrobial activities of

chitosan and Schiff base of chitosan were investigated against *Escherichia coil*, *Staphylococcus aureus* and *Aspergillus niger*. The results indicate that the antimicrobial activity of the Schiff base increases with an increase in the concentration. It was also found that the antimicrobial activity of the Schiff base was stronger than that of chitosan.

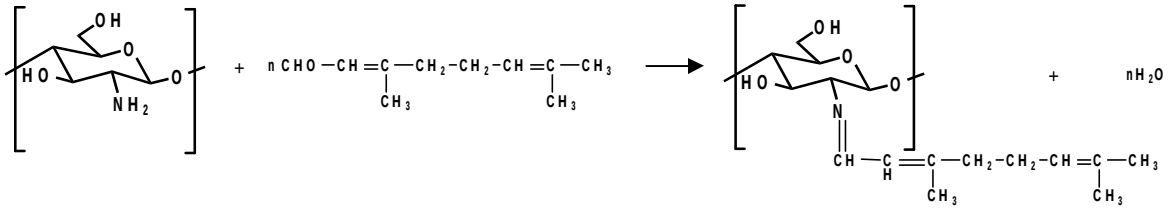

Figure 1.19 Synthesis Schiff base chitosan [65]

In 2010, Krishnapriya, K. R. and Kandaswamy, M. [63] synthesized a new chitosan biopolymer derivative (CTSL) by anchoring a new vanillin-based complexing agent or ligand, namely 4-hydroxy-3-methoxy-5-[(4-methylpiperazin-1-yl)methyl] benzaldehyde, (L) with chitosan (CTS) by means of condensation. The CTSL was employed to study the equilibrium adsorption of various metal ions, namely, Mn(II), Fe(II), Co(II), Cu(II), Ni(II), Cd(II), and Pb(II), as functions of pH of the solutions. The CTSL shows good adsorption pH ranges approximately of 6.5-7.0.

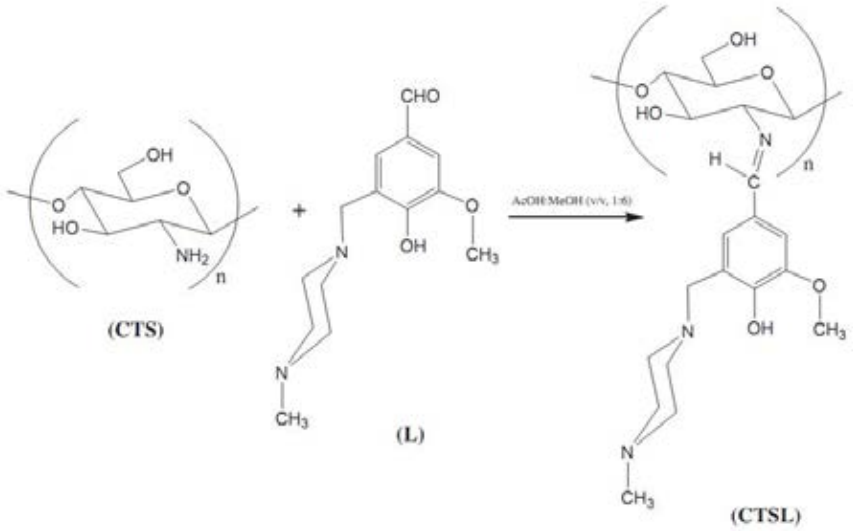

Figure 1.20 Synthesis of chitosan biopolymer derivative (CTSL) [63]

In 2011, Tree-udom, T., *et al.* [108] prepared the fragrant chitosan nanospheres using ultrasonication. The fabrication process involves a chemical reaction to covalently link the fragrant aldehydes with the amine functionalities of the *N*-succinylchitosan (NS-chitosan) carriers that simultaneously leads to an ultrasonic aided reorganization of the spheres in such a way that the grafted entities are at the particles' core. Localization of the grafted imine moieties at the core of the imine-NS-chitosan particles was confirmed. The obtained fragrant chitosan nanospheres not only showed up to 85-fold fragrance prolongation but also dispersed well in water.

1.12 Literature reviews of skin penetration

Penetration of particles

In 2003, Toll, R., *et al.* [109] investigated the penetration of fluorescence-labeled particles of different sizes between 750 and 6000 nm into the hair follicles by taking biopsies. It was found that the particles with the smaller diameter penetrated most excellently into the hair follicles. They demonstrated a selective penetration route of the microspheres into the HF. Optimal microsphere size proved to be approximately 1.5 μm, with a 55% rate of all HF, and with a maximum penetration depth of >2300 μm.

In 2007, Lademann, J., *et al.* [110] investigated the penetration and storage behavior of dye-containing nanoparticles (diameter 320 nm) into the hair follicles using porcine skin, which is a model for human tissue. It was found that the nanoparticles penetrate much deeper into the hair follicles than the dye in the non-particle form, if a massage had been applied (Figure 1.21). Without massage, similar results were obtained for both formulations (Figure 1.22). The result showed the nanoparticles were stored in the hair follicles up to 10 days, while the non-particle form could be detected only up to 4 days. Taking into consideration the surface structure of the hair follicles, it was assumed that the movement of the hairs may act as a pumping mechanism pushing the nanoparticles deep into the hair follicles.

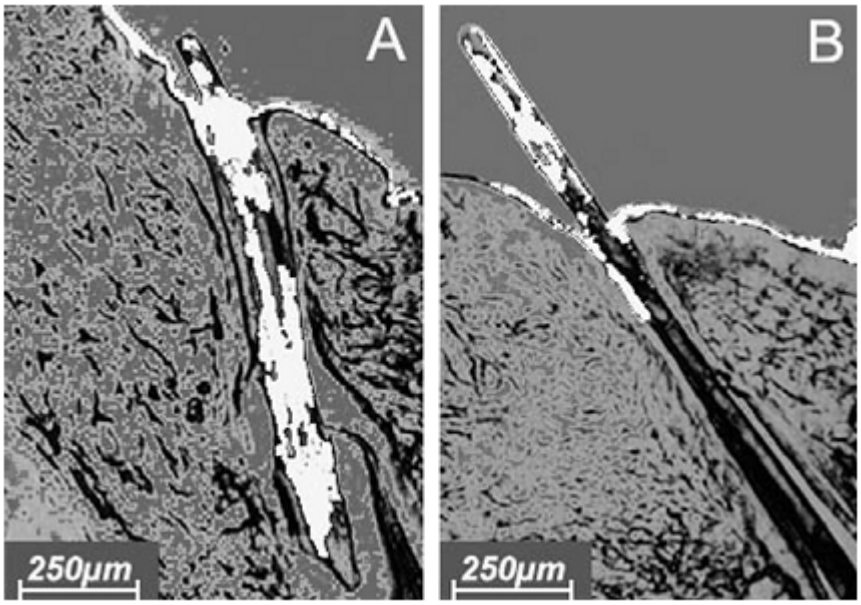

Figure 1.21 Superposition of a transmission and fluorescent image, demonstrating the in vitro penetration of the dye-containing formulation into the hair follicles of porcine skin after application of a massage. (A) Dye in particle form. (B) Dye in non-particle form. [110]

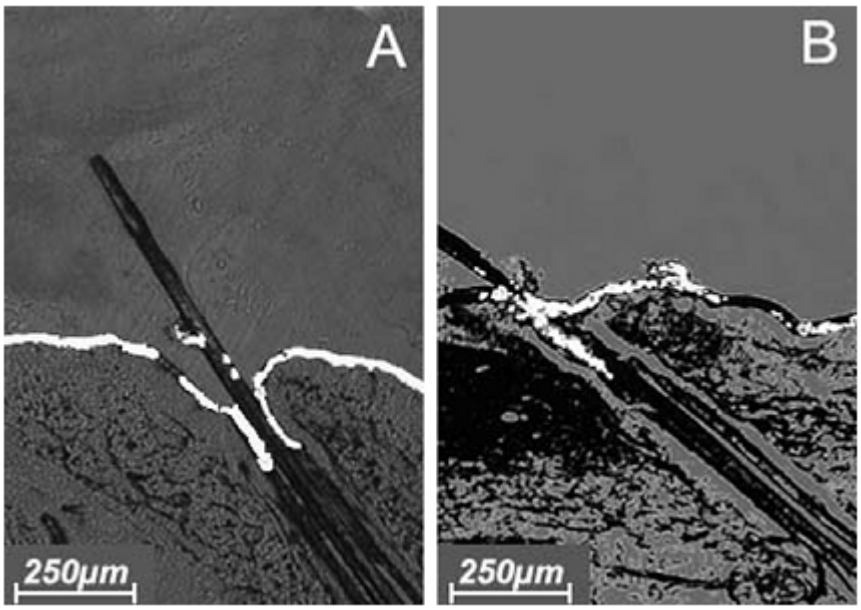

Figure 1.22 Superposition of a transmission and fluorescent image, demonstrating the in vitro penetration of the dye-containing formulation into the hair follicles of porcine skin without massage. (A) Dye in particle form. (B) Dye in non-particle form. [110]

In 2009, Kuchler, S., *et al*. [111] studied loading nile red to dendritic core-multishell (CMS) nanotransporters (20–30 nm) and solid lipid nanoparticles (SLNs, 150–170 nm). Pig skin penetration was studied *ex vivo* using a cream for reference. Interactions of SLNs and skin were followed by scanning electron microscopy, internalisation of the particles by viable keratinocytes by laser scanning microscopy. Incorporating nile red into a stable dendritic nanoparticle matrix, dye amounts increased 8-fold in the stratum corneum and 13-fold in the epidermis compared to the cream. The SLNs degradation at the stratum corneum surface, SLNs enhanced skin penetration less efficiently (3.8- and 6.3-fold).

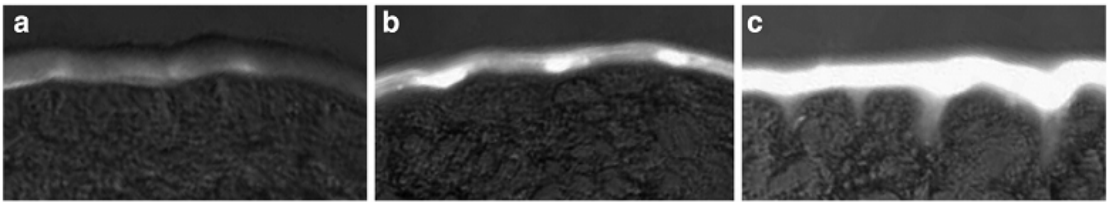

Figure 1.23 Penetration of nile red loaded cream (Panel a), SLN (Panel b), and dendrimer nanoparticles (Panel c) as seen by fluorescence microscopy. Comparisons between delivery vehicles are necessary to select the most appropriate delivery vehicle for a given drug. In this case the dendrimer nanoparticles enabled more nile red to penetrate deeper into porcine skin than the cream or the SLN. [111]

In 2010, Zhang, W., *et al*. [112] investigated the penetration and the distribution of poly(d,l-lactic-co-glycolic acid) (PLGA) nanoparticles in the human skin treated with microneedles. The distribution of nanoparticles, visualizing by confocal laser scanning microscopy (CLSM) showed that nanoparticles were delivered into the microconduits created by microneedles and permeated into the epidermis and the dermis. The result showed that (i) the permeation of nanoparticles into the skin was enhanced by microneedles, but no nanoparticle reached the receptor solution; (ii) much more nanoparticles deposited in the epidermis than those in the dermis; (iii) the permeation was in a particle size-dependent manner; and (iv) the permeation increased with the nanoparticle concentration increasing until a limit value was reached. The biodegradable nanoparticles would sustain drug release in the skin and supply the skin with drug over a prolonged period.

In 2011, Padois, K., *et al.* [113] prepared semi-synthetic triglycerides stabilized with a mixture of polysorbate and sorbitan oleate were loaded with 5% of minoxidil as carrier for skin drug delivery. *Ex vivo* skin penetration studies were performed using Franz-type glass diffusion cells and pig ear skin. *Ex vivo* skin corrosion studies were realized with a method derived from the Corrositex® test. Solid lipid nanoparticles suspensions were compared to commercial solutions in terms of skin penetration and skin corrosion. Solid lipid nanoparticles suspensions have been shown as efficient as commercial solutions for skin penetration and were non-corrosive while commercial solutions presented a corrosive potential.

Penetration of drug-loaded in particles

In 2007, Teichmann, A., *et al.* [114] studied the lipophilic dye curcumin incorporated in an oil-in-water microemulsion and in an amphiphilic cream was applied onto the skin of human volunteers. Using the method of tape stripping to remove the stratum corneum (SC), the depth profiles of the dye within the horny layer were compared. It was obvious that the microemulsion led to a penetration into the hair follicles, whereas, following application of the cream.

In 2011, Morgen, M., *et al.* [115] prepared amorphous drug/polymer nanoparticles from ethyl cellulose and UK-157,147 (systematic name (3S, 4R)-[6-(3-hydroxyphenyl)sulfonyl]-2,2,3-trimethyl-4-(2-methyl -3-oxo-2,3-dihydropyridazin-6-yloxy)-3-chromanol), a potassium channel opener, using sodium glycocholate (NaGC) as a surface stabilizer. *In vitro* testing with rabbit ear tissue, delivery of UK-157,147 to the follicles was demonstrated and distribution to the surrounding dermis (Figure 1.24). *In vivo* testing 100 nm nanoparticles with hamster ear model were well-tolerated, with no visible skin irritation. *In vivo* tests of smaller nanoparticles indicated targeted delivery to sebaceous glands. The nanoparticles released drug rapidly in *in vitro* nondip dissolution tests and were stable in suspension for 3 months. The results show selective drug delivery to the follicle by follicular transport of nanoparticles and rapid release of a poorly water-soluble drug.

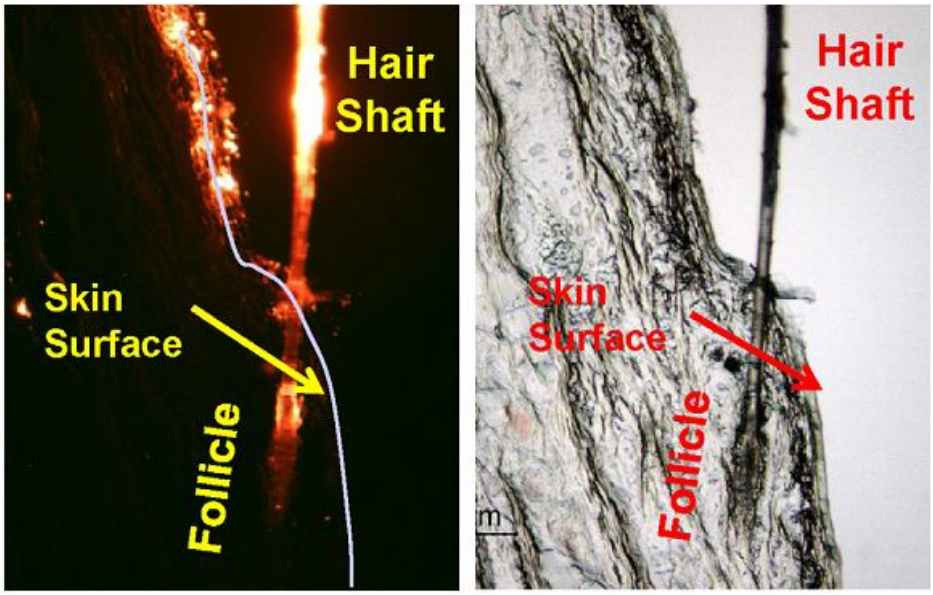

Figure 1.24 Fluorescent (left) and bright-field (right) microscopy images of rabbit ear tissue incubated for 2 h with 19:1:0.6 ethyl cellulose:MEH-PPV:NaGC fluorescent nanoparticles. [115]

In 2011, Kong, M., *et al.* [116] developed hyaluronic acid nanoemulsion to be applied as transdermal carrier for active lipophilic ingredient. *In vitro* skin penetration and histological examinations were carried out using α-tocopherol as model ingredient to assess skin permeability and bioavailability. The result showed nanoemuslion being able to penetrate across stratum corneum and diffuse deeper into dermis compared with the control group (ethanol solution) *via* follicular and intercellular pathway. No irritation has been found in dermis and skin surface indicated hyaluronic acid nanoemulsions could be successfully used as purcutaneous delivery carrier of active lipophilic ingredient and suitable for drug and cosmetic applications.

In 2012, Rancan, F., *et al.* [117] investigated the stability and release properties of biodegradable polylactic acid (PLA) particles upon topical application on human skin explants. PLA particles loaded with the hydrophilic fluorochrome 4-Di-2-Asp (DiAsp-PLA) were compared to PLA particles loaded with the lipophilic fluorochrome Bodipy 630/650 (BP-PLA). The result showed that BP-PLA particles released rapidly the loaded fluorochrome and lost the particulate morphology within a

few hours after application on skin surface. On the contrary, DiAsp-PLA particles maintained the particulate morphology, accumulated in hair follicles, and allowed a constant release of the incorporated fluorochrome for up to 16 h (Figure 1.25).

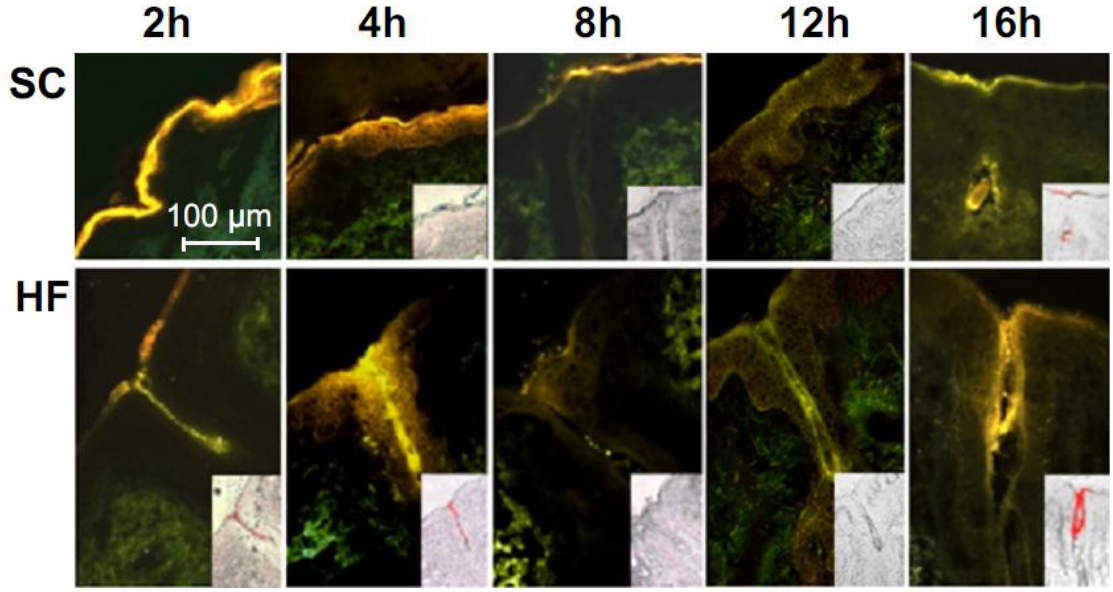

Figure 1.25 Semi-quantitative analysis of DiAsp-PLA particle accumulation in HFs. Representative fluorescence microscopy images of skin cryosections after topical treatment with DiAsp-PLA particles. The images show the time-dependent diffusion of DiAsp into stratum corneum (SC) and the accumulation of particles in hair follicles (HF). [117]

Penetration of vitamin A-loaded in particles

In 2006, Pople, P.V., *et al.* [118] investigated particulate carrier system such as solid lipid nanoparticles (SLN) for topical application of vitamin A palmitate and to study its beneficial effects on skin. The SLN dispersion was prepared using high-pressure homogenization technique and was incorporated into polymeric gels of Carbopol, Pemulen, Lutrol, and Xanthan gum for suitable application. The SLN dispersion showed mean particle size of 350 nm. *In vitro* release profile of vitamin A palmitate from nanoparticulate dispersion and its gel showed prolonged drug release up to 24 hours, which could be owing to embedment of drug in the solid lipid core. *In vitro* penetration studies showed almost 2 times higher drug concentration in the skin with lipid nanoparticle-enriched gel as compared with common gel, thus indicating

better localization of the drug in the skin (Figure 1.26). *In vivo* skin hydration studies in albino rats revealed increase in the thickness of the stratum corneum with improved skin hydration. The developed formulation was nonirritant to the skin. From the results indicated that SLN represents a promising particulate carrier having controlled drug release, improved skin hydration, and potential to localize the drug in the skin with no skin irritation.

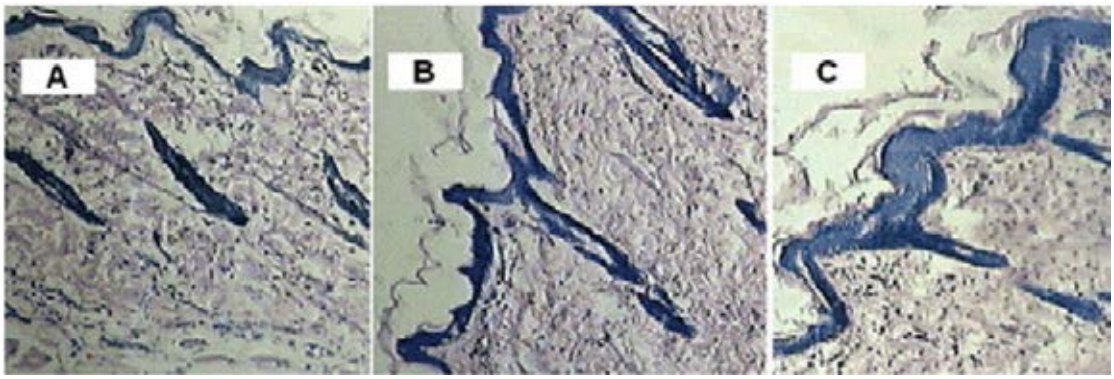

Figure 1.26 Photomicrographs of (A) untreated rat skin, (B) rat skin treated with conventional gel, and (C) rat skin treated with gel enriched with solid lipid nanoparticles. Magnification: 10×. [118]

In 2008, Mandawgade, S. D., *et al.* [157] investigated to develop solid lipid nanoparticles (SLNs) by using a simple microemulsion technique. Furthermore, the aim was to characterize these SLNs and evaluate its potential in the topical delivery of a lipophilic drug, tretinoin (TRN). TRN-loaded SLN-based topical gels were formulated and the gels were evaluated comparatively with the commercial product with respect to primary skin irritation, *in vitro* skin permeation. The results showed mean particle size <100 nm of the SLN dispersions with the novel lipids. Up to 46% of drug entrapment in the lipids was attained. Lesser skin irritancy, greater skin tolerance, and slow drug release was observed with the developed TRN-loaded SLN-based gels than the commercial product. The results of the characterization and evaluation established the safety for use, suitability and compatibility of lipids as a novel excipient.

In 2010, Teixeira, Z., *et al.* [119] prepared encapsulation of retinyl palmitate by poly(d,l-lactide) (PLA). Permeation studies were achieved using plastic surgery abdominal human skin by Franz diffusion cell. Retinyl palmitate permeates into deep skin layers. The confocal laser scanning microscopy (CLSM) showed that nanocapsules were distributed uniformly, suggesting that the permeation mechanism through skin is intercellular. The result showed the Nile blue-PLA nanocapsules and retinyl palmitate could be penetration up to 30 μm. Besides, it found that the most retinyl palmitate at the surface, while, the polymer penetrate deeper the retinyl palmitate (Figure 1.27).

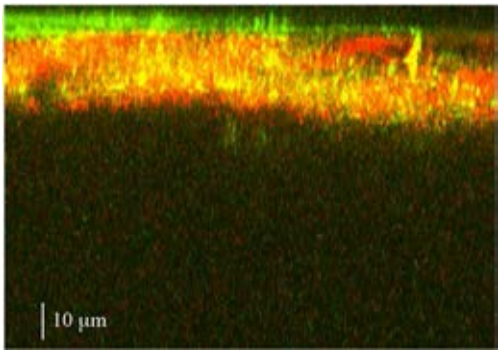

Figure 1.27 Confocal images of deeper layers into skin, cross-sectional image. Red fluorescence is polymeric shell (Nile blue-PLA nanocapsules); green fluorescence is retinyl palmitate. [119]

In 2011, Arayachukeat, S., *et al.* [120] prepared retinyl acetate (RA) loaded polymeric nanoparticle (NP) carriers using two different single polymers, ethyl cellulose (EC) and poly (ethylene glycol)-4-methoxycinnamoylphthaloylchitosan (PCPLC). The stability of RA to aqueous solution and UVA light was significantly improved when encapsulated with PCPLC, while EC encapsulation gave some improved stability in water but showed no improved photostability. *Ex vivo* application of the RA-loaded PCPLC NPs onto the surface of the freshly excised skin from a baby mouse indicated a significantly slower skin absorption rate for the encapsulated RA. However, 100% retention of the encapsulated RA in the skin tissue was observed after 24 h. Confocal fluorescent analysis of the skin pieces applied. The result indicated likely entry and accumulation of the PCPLC NPs and RA at the hair follicles.

Retinaldehyde was used in many cosmetic products for the treatment of dermatological diseases. Unfortunately, the retinaldehyde is insoluble in water and is easily damaged from light, heat and oxygen. Its structure contains aldehyde, which can easily react with amino group. Recently, Tree-udom and coworkers [108] reported a simple process for preparing water-soluble *N*-succinylchitosan, which could self-assembly in water to form nanospheres. Here we used the same reaction to obtain the *N*-succinylchitosan, and had retinaldehyde react with amino groups on this chitosan derivative, to prepare retinilidenesuccinylchitosan particles.

1.13 Research goals

1. Preparation of retinilidenesuccinylchitosan nanoparticles (R-NSC)
2. Encapsulation of the antioxidants into the R-NSC nanoparticles
3. Study the stability of the all prepared nanoparticles compared with free retinaldehyde
4. Study the skin penetration and release of the retinilidene moieties

CHAPTER II

EXPERIMENTAL

2.1 Materials and Chemicals

Chitosan powder with approximately 85% degree of deacetylation and 30,000 Da of viscosity-average molecular weight was purchased from Seafresh Chitosan (Lab) Co., Ltd (Bangkok, Thailand). Succinic anhydride (analytical grade) was purchased from Acros Organics (Geel, Belgium). Retinaldehyde and α-tocopherol (vitamin E) were purchased from Sigma Aldrich (Steinheim, Germany). BHT was purchased from Honghuat CO., LTD. Ethanol acetone and ethylacetate were purchased from ACI Labscan Limited (Bangkok, Thaiand). Acetic acid was purchased from Merck (Darmstadt, Germany). Lissamine rhodamine B sulfonyl chloride was purchased from Invitrogen (USA). Other reagents were analytical grade and were used without futher purification. Porcine ear skins were purchased from local slaughter house.

2.2 Preparation of *N*-succinylchitosan (N-SC)

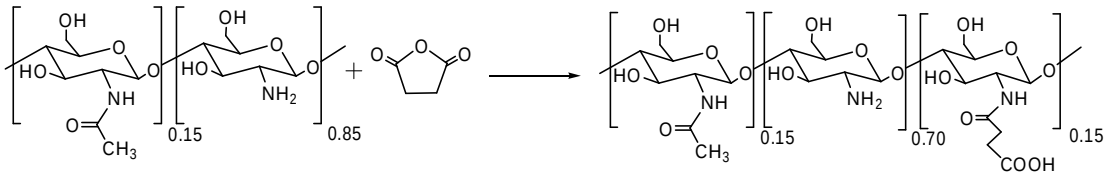

Scheme 2.1 Preparation of *N*-succinylchitosan [108]

The *N*-succinylchitosan (N-SC) was synthesized based on the method of Tree-udom (Scheme 2.1) [108]. Succinic anhydride was allowed to react with each glucosamine unit of chitosan at mole ratio of 1:5 (glucosamine unit:succinic anhydride). Chitosan 2.01 g (12.5 mmole) was dissolved in 70 mL of 2% (v/v) acetic acid. The succinic anhydride 0.25 g of (2.50 mmole) in 10 mL of acetone was slowly

dropped into the CS solution and the mixture was stirred at room temperature overnight. The precipitate was collected by filtration and repeatedly washed with excess acetone. The product was dried under vacuum for 24 h. Finally, a white powder was obtained. The product was characterized by Nuclear Magnetic Resonance (NMR) using a Varian mercury spectrometer (Variance Inc., Palo Alto, USA), operating at 400 MHz; Attenuated total reflectance-Fourier Transform Infrared (ATR-FTIR) using a Continuμm^{TM} infrared microscope equipped with a mercury-cadmium-telluride (MCT) detector, Nicolet 6700 FT-IR spectrometer (Thermo Electron Corporation, Madison, WI, USA) and a slide-on miniature germanium (Ge) internal reflection element, collecting at 64 scans in the mid-infrared region (4000–650 cm^{-1}); UV/Visible spectroscopy using a UV2500 spectrophotometer (Shimadzu Corporation, Kyoto, Japan), and a quartz cell of path length 1 cm, operating at 25 ^{0}C.

N-succinylchitosan (N-SC): 92% yields of white powder and 0.15 degree of succinyl grafting. ^{1}H NMR (D_2O, 400 MHz, δ, ppm): 1.88 (H of acetyl groups), 2.28-2.36 (methylene protons of the succinyl), 2.70 (H2 of glucosamine, GlcN), 3.48-3.75 (H2′ of *N*-acetylglucosamine, GlcNAc, H3, H4, H5 and H6 of GlcNAc and GlcN), 4.44 (H1 of GlcNAc and GlcN). ATR-FTIR (cm^{-1}): 3307 (N-H stretching and O-H stretching vibration), 2868 (C-H stretching vibration), 1638 (amide I (C=O stretching)), 1546 (amide II), 1379 (symmetric stretching vibration of COO^{-} and amide III), 1308 (amide III (C-N stretching)), 1150 (C-O-C stretching vibration), and 1026 (C-O stretching vibration). UV/Vis (deionized water, 25^{o}C) λ max: 250 nm.

2.3 Preparation of Retinilidenesuccinylchitosan nanoparticles (R-NSC)

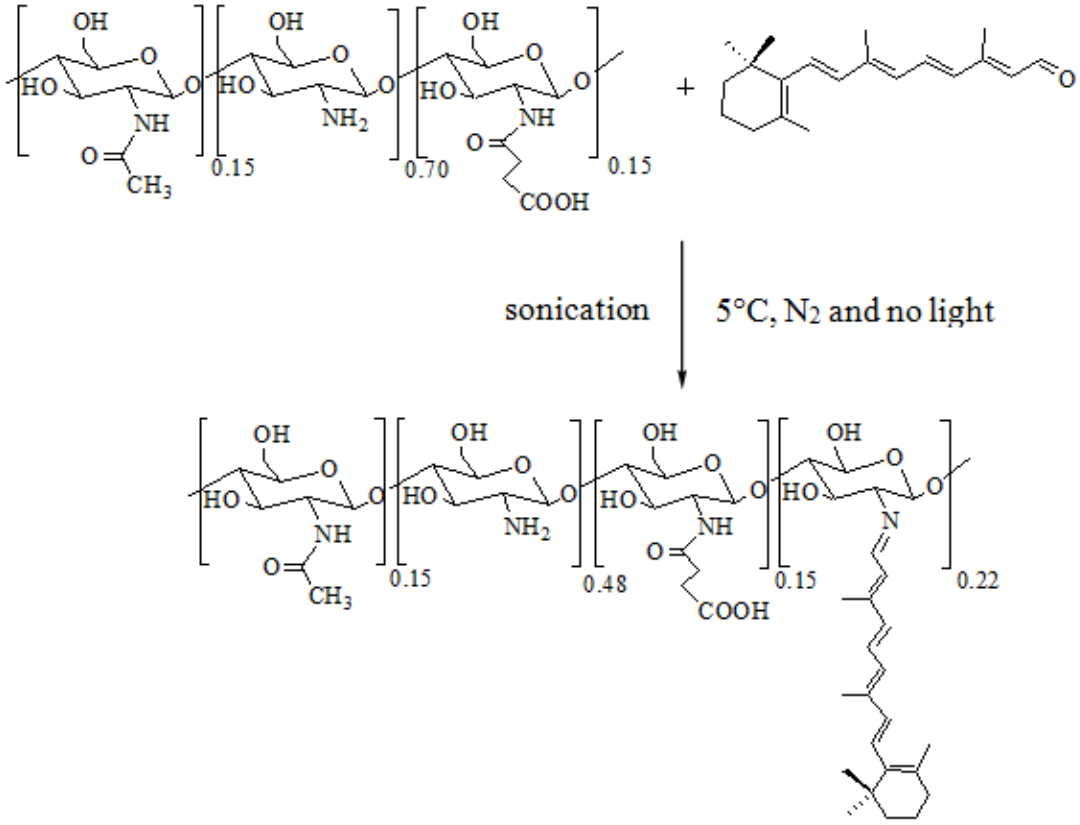

Scheme 2.2 Preparation of retinilidenesuccinylchitosan nanoparticles

Finding the optimum ratio between N-SC nanoparticles and retinaldehyde

Here the finding the optimum ratio between retinaldehyde and N-SC (no unreacted aldehyde left after the reaction but with maximum Schiff base formation) was carried out. The amine in N-SC nanoparticles was allowed to react with retinaldehyde at the moles ratio of N-SC to retinaldehyde of 1:1, 2:1 and 3:1. The mixtures were sonicated for 4 h under lightproof condition at 5°C in nitrogen atmosphere [108]. The imine bond formation was characterized through ATR-FTIR.

The best condition was then used to prepared retinilidenesuccinylchitosan for further study. The procedure involved adding retinaldehyde (15.86 mg in 1 ml of ethanol) drop-wise into aqueous N-SC particle suspension (46.28 mg in 19 ml of deionized water) under ultrasonic, no light, 5°C and nitrogen conditions. The mixture was continuously ultrasonicated (40 KHz) for 4 h. Dry particles were obtained by

freeze drying the aqueous suspension. The product was then characterized through ATR-FTIR.

Retinilidenesuccinylchitosan (R-NSC): Degree of retinaldehyde substitution: 0.22. ATR-FTIR (cm^{-1}): 3282 (N-H stretching and O-H stretching vibration), 2867 (C-H stretching vibration), 1620 (C=N stretching vibration), 1555 (amide II), 1150 (C-O-C stretching vibration), and 1023 (C-O stretching vibration).

2.4 Loading of α-tocopherol (vitamin E) and butylated hydroxytoluene (BHT) into R-NSC particles

Vitamin E-loaded R-NSC

The procedure was carried out at the weight ratio of α-tocopherol (vitamin E) and retinaldehyde of 1 to 3. The procedure involved adding retinaldehyde (15.86 mg) with α-tocopherol (10.57 mg) in 1.0 ml ethanol. Then slowly dropped the obtained mixture into aqueous N-SC particle suspension (46.28 mg, 19 ml water) under ultrasonic (40 KHz), light-proof, 5°C and N_2 atmospheric condition, and the mixture was continuously sonicated for another 4 h under such condition. The dry particles were obtained by freeze drying the aqueous suspension. The product was then subjected to ATR-FTIR, scanning electron microscope (SEM), transmission electron microscope (TEM), dynamic light scattering (DLS) and UV-Vis spectrophotometric analysis.

BHT-loaded R-NSC

The procedure was carried out at the weight ratio of butylated hydroxytoluene (BHT) and retinaldehyde of 1 to 3. The procedure involved adding retinaldehyde (15.86 mg) with α-tocopherol (10.57 mg) in 1.0 ml ethanol. Then the obtained mixture was slowly dropped into aqueous N-SC particle suspension (46.28 mg, 19 ml water) under ultrasonic (40 KHz), light-proof, 5°C and N_2 atmospheric condition, and the mixture was continuously sonicated for another 4 h under such condition. The dry particles were obtained by freeze drying the aqueous suspension. The product was

then subjected to ATR-FTIR, SEM, TEM, DLS and UV-Vis spectrophotometric analysis.

2.5 Morphology, Hydrodynamic diameter and Zeta potential of the nanoparticles

Nano-morphology of the products was observed using SEM and TEM. A drop of nanoparticles dispersion was placed on a glass slide and dried overnight. The sample was coated with a gold layer under vacuum at 15kV for 90s then mounted on a SEM stud for visualization at an accelerating voltage of 15kV. The TEM analysis on a JEM-2100 transmission electron microscope (JEOL, Tokyo, Japan) was used also used to acquire for morphology of the products. A drop of nanoparticle dispersion was placed onto carbon film coated on a copper grid and dried at room temperature. Observation was performed at 100-120 kV with 15 kV accelerating voltage.

The average hydrodynamic diameter, polydispersity index (PDI) and zeta potential values of samples were conducted by dynamic light scattering (DLS) technique using a Zetasizer nanoseries model S4700 (Malvern Instruments, Worcestershire, UK). Before measurement, the freshly prepared colloidal suspension was appropriately diluted and ultrasonicated for five minutes. All measurements were carried out in triplicate and mean values were reported.

2.6 Stability of retinilidene in the particles

Stability evaluation of the retinaldehyde in Schiff base nanoparticles: R-NSC, Vitamin E-loaded R-NSC and BHT-loaded R-NSC were carried out in comparison to the free retinaldehyde. The experiment was performed under a normal aqueous environment by monitoring the retinaldehyde concentration of the freshly prepared suspension (46.28 mg of N-SC which corresponded to 3 moles of retinilidene groups; 15.86 mg or 1 mole of retinal, in final volume of 50 ml) for five hours under light (UVA intensity of approximately 3-5 mW/cm^2, UVB intensity of approximately 0.1-0.12 mW/cm^2), heat (40°C) and oxygenated conditions. The suspension used in the experiment was prepared to give similar retinaldehyde final concentration of 20 ppm. Free retinaldehyde solutions of similar concentrations to those suspensions of

retinaldehyde in nanoparticles were freshly prepared in ethanol and the solutions were subjected to similar conditions. At each predetermined time, a 5 ml aliquot was withdrawn at 0, 30, 60, 120, 180, 240 and 300 min. The aliquots were subjected to retinaldehyde quantification by UV-visible absorption spectrophotometry. Degradation of retinal and retinilidene moiety in the R-NSC particles was quantitatively monitored through the decrease of absorbance at 375 and 352 nm, respectively. The experiments were carried out in triplicate.

2.7 Fluorescence labeled particles

To track the location of R-NSC particles in skin tissue, fluorophore Rhodamine B was covalently linked to the N-SC polymeric chains. The fluorophore Rhodmine B (Lissamine rhodamine B sulfonyl chloride) was first covalently linked to the SC by adding 0.01% of Rhodmine B into aqueous N-SC particle suspension under light-proof and N_2 atmosphere and the mixture was left overnight. The Rhodamine B-labeled N-SC polymer was then purified from free Rhodamine B by dialysis under light-proof condition. The Rho B-labeled N-SC was then grafted with retinaldehyde as previously described (Scheme 2.3). And the vitamin E was then encapsulated with Rho B-R-NSC at loading of approximately 7% (by weight) as previously described (Chapter II page 36). The obtained particles were subjected to confocal laser scanning fluorescent microscope (CLFM), SEM and DLS analysis.

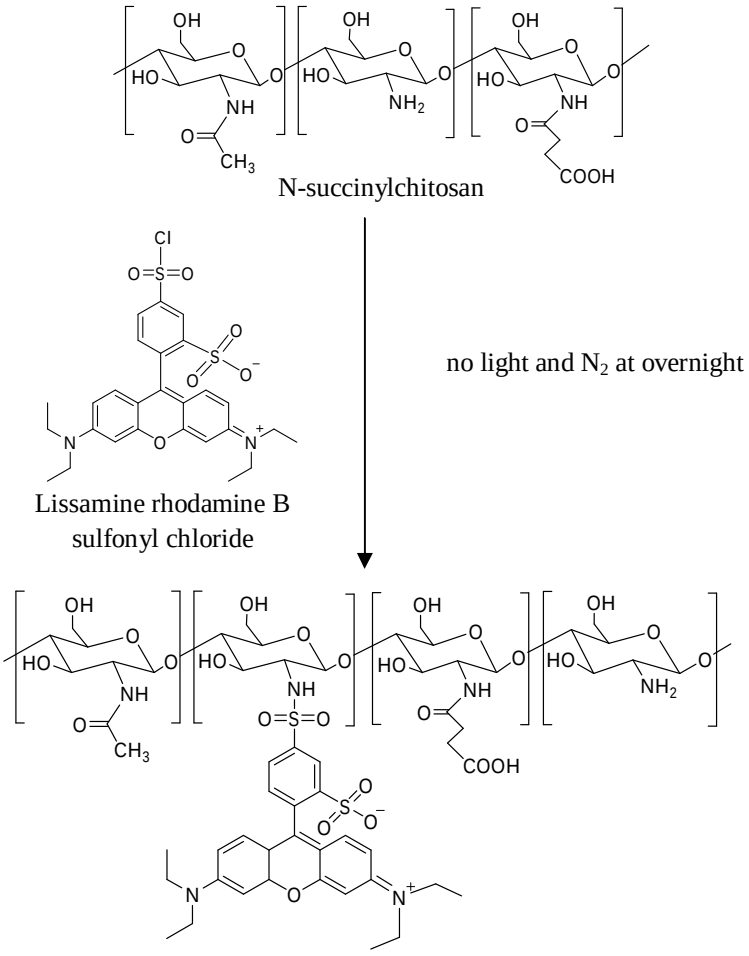

N-succinylchitosan grafted by Lissamine rhodamine B sulfonyl chloride (Rho B-labeled N-SC)

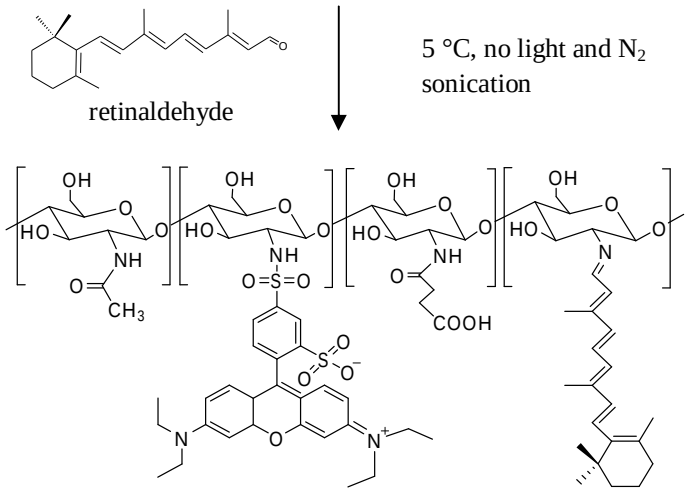

retinilidenesuccinylchitosan-Rho B (Rho B-R-NSC)

Scheme 2.3 Synthesis and structure of Rho B-labeled N-SC and Rho B-R-NSC.

2.8 Skin penetration

The fresh porcine ear skin of one month old White Large piglet was purchased from a local slaughter house and was used within 6 h. The freshly excised surgically skin piece possessed 2.43 ± 0.32 mm (mean ± SD) depth for the skin layers. It was cut into approximately 1.5 cm × 1.5 cm peices. The final coverage of Rho B-N-SC and retinal on the skin was ~20 and ~7 μg cm^{-2}, respectively. The Rho B-labeled R-NSC used in the experiment was prepared at the 0.01% (mol) of Rho-B to that of monomeric unit of the R-NSC. The CLFM system used was a Nikon Digital Eclipse C1-Si (Tokyo, Japan) equipped with Plan Apochromat VC 100×, Diode Laser and 85 YCA-series Laser (405 nm and 561 nm, respectively, Melles Griot, Carlsbad, CA, USA), a Nikon TE2000-U microscope, a 32-channel-PMT-spectral-detector and Nikon-EZ-C1 Gold Version 3.80 software. CLFM was used to capture the fluorescent signals of the Rhodamine B and the grafted retinilidene moieties together with the released retinal in the skin piece. Excitation was carried out at 405 and 561 nm while detection was done spectrally at 465-518, 537-587 and 587 nm for the porcine ear skin, retinaldehyde and Rhodamine B, respectively.

Penetration of the Rho B-R-NSC

The experiment was started by dropping 15 μl of the Rho B-R-NSC nanoparticles suspension (3085 ppm Rho B-labeled N-SC and 1057 ppm retinaldehyde) onto the porcine ear skin piece, massage for 2 min with roller (Figure 2.1) and left at 25 °C for 30 min. The piece was then analyzed by CLFM. Fluorescent spectral signals at 405-750 nm were collected from the sample piece, at various depths starting from ~20 μm (from the stratum corneum surface) down to ~200 μm depth. The obtained spectra of each pixel were then unmixed into retinaldehyde, Rho B-N-SC and porcine ear skin auto-fluorescent components using chemometric analysis (image algorithms) based on the spectral database constructed from fluorescent spectra of standard Rho B-N-SC, standard retinaldehyde and the porcine ear skin. Images indicating locations of retinaldehyde and Rho B-N-SC in the skin tissue were then constructed using the obtained resolved signals.

Figure 2.1 Image of roller.

Penetration of the vitamin E-loaded Rho B-R-NSC

The experiment was started by dropping 15 μl of the vitamin E-loaded Rho B-R-NSC nanoparticles suspension (3085 ppm Rho B-labeled N-SC, 1057 ppm retinaldehyde and 265 ppm vitamin E) onto the porcine ear skin piece using the same previously described procedure used for the unloaded particles. Fluorescent spectral signals at 405-750 nm were collected from the sample piece, at various depths starting from ~20 μm (from the stratum corneum surface) down to ~200 μm depth. The obtained spectra of each pixel were then unmixed into retinaldehyde, Rho B-N-SC, vitamin E and porcine ear skin auto-fluorescent components using chemometric analysis (image algorithms) based on the spectral database constructed from fluorescent spectra of standard Rho B-N-SC, standard retinaldehyde, vitamin E standard and the porcine ear skin. Images indicating locations of retinaldehyde, vitamin E and Rho B-NSC in the skin tissue were then constructed using the obtained resolved signals.

CHAPTER III

RESULTS AND DISCUSSION

3.1 Preparation and characterization of N-succinylchitosan (N-SC)

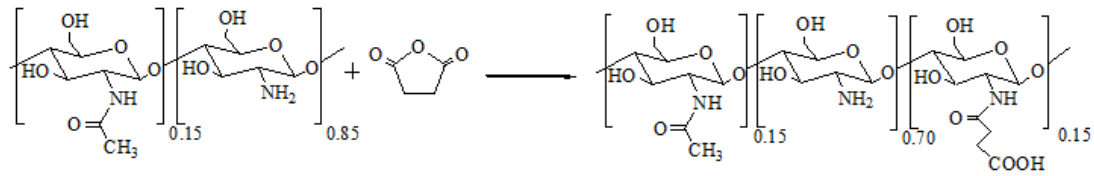

Scheme 3.1 Preparation of *N*-succinylchitosan.

The N-succinyl derivative of chitosan was prepared as shown in Scheme 3.1 *via* a succinylation reaction between amino group on chitosan chain and succinic anhydride to form *N*-succinylchitosan (N-SC) [108].

The physical appearance of the synthetic N-SC obtained from reactions conducted at mole ratios between the succinic anhydride: amino group of the chitosan of 1:5, were white powder (Figure 3.5a).

The successful succinyl moiety grafting was confirmed by NMR and ATR-FTIR. For ^{1}H NMR spectrum of N-SC in D_2O (Figure 3.1), signal appearing at 2.28-2.36 ppm assigned to dimethylene protons of grafted succinyl was observed. Using the integral ratio between 4H from ethyl group of succinyl and 1H from C2 of glucosamine unit (at 2.70 ppm) with 85% deacetylation degree, the degree of grafting or succinyl substitution was estimated from the ratio between the integrated area of the resonance peaks of the methylene protons of the grafted succinyl group, $I_{succinyl}$ (-C(O)CH_2CH_2C(O)-, 2.28-2.36 ppm) and that of the resonance peaks from hydrogen atoms in glucosamine units, I_{H2} (H2 of the Gln, 2.70 ppm), taking into account the degree of deacetylation of 0.85 for the starting chitosan, the degree of succinyl grafting was approximated to be 0.15. ATR-FTIR spectrum (Figure 3.2 and 3.3) showed new absorption band at 1635 cm^{-1} corresponding to COO^- stretching, 1548 cm^{-1} corresponding to N-H bending vibration of amide II and 1382 cm^{-1}

corresponding to C-N stretching vibration of amide III. The UV absorption spectrum of the N-SC showed λ_{max} at approximately 305 nm.

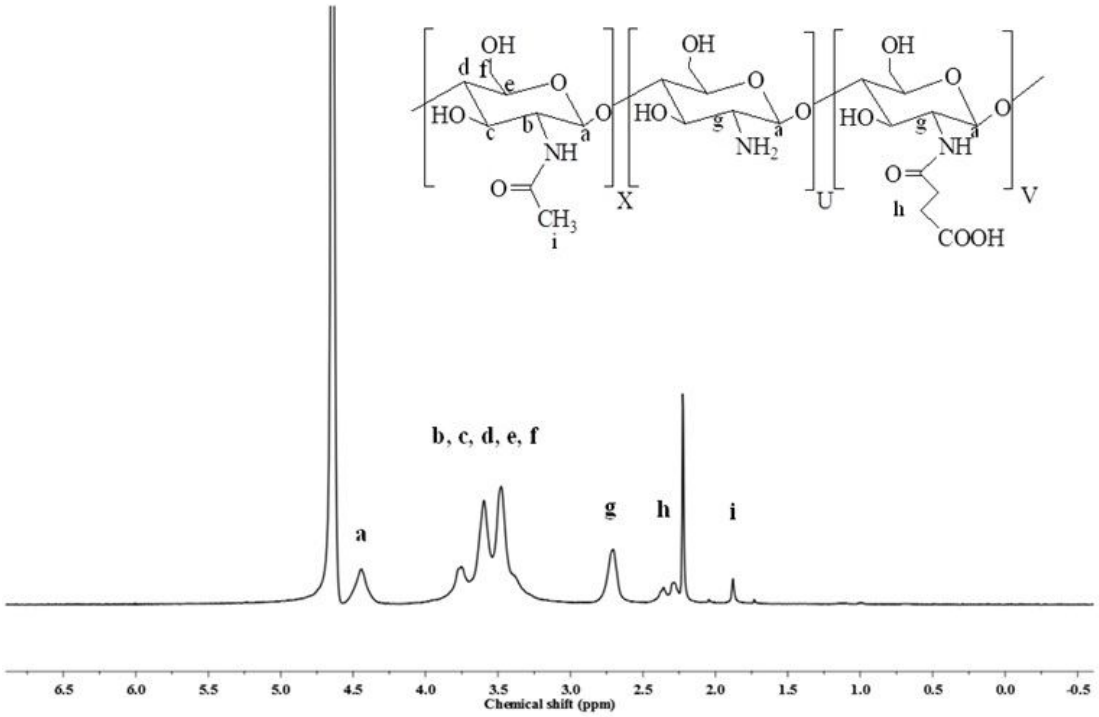

Figure 3.1 ^{1}H NMR spectrum of N-SC.

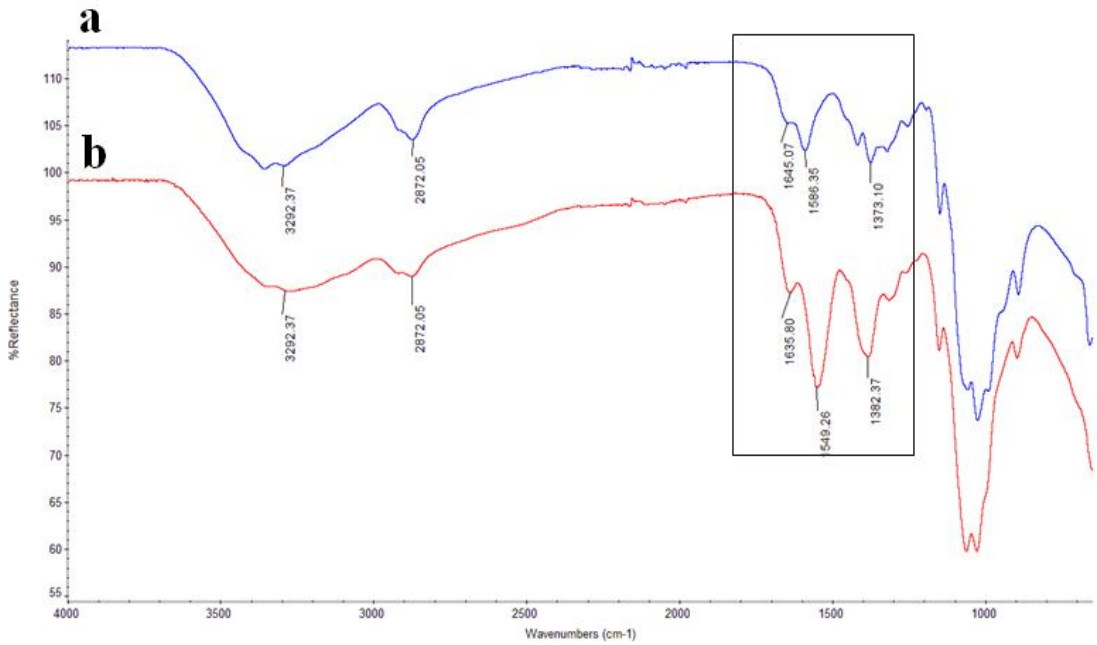

Figure 3.2 ATR-FTIR spectra of (a) chitosan and (b) N-SC.

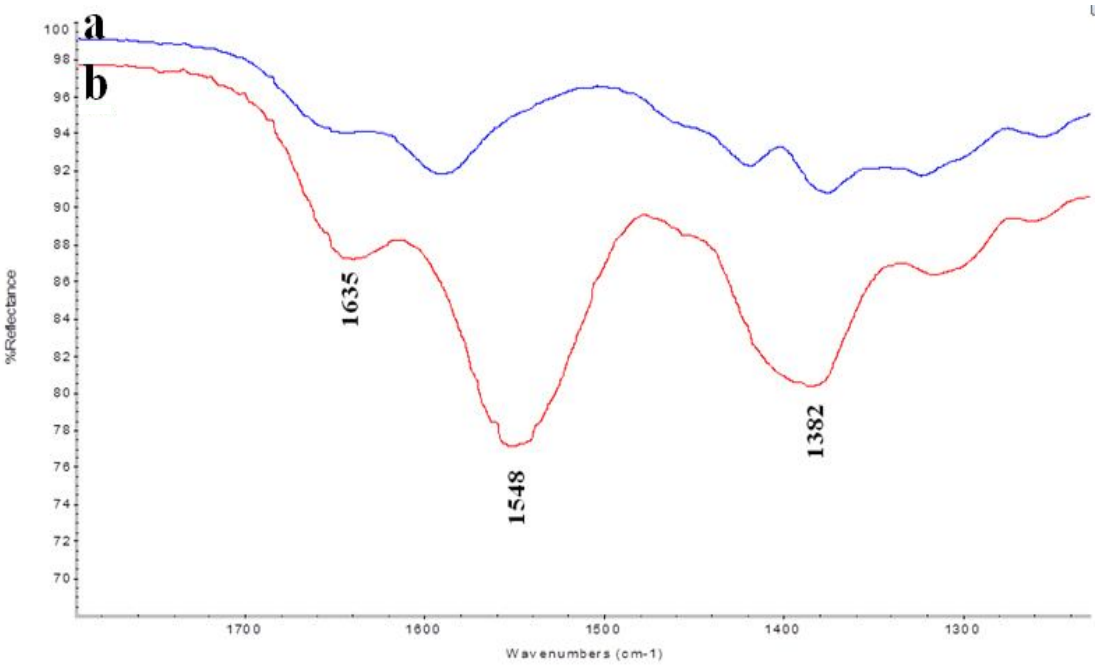

Figure 3.3 Expension of ATR-FTIR spectra of (a) chitosan and (b) N-SC.

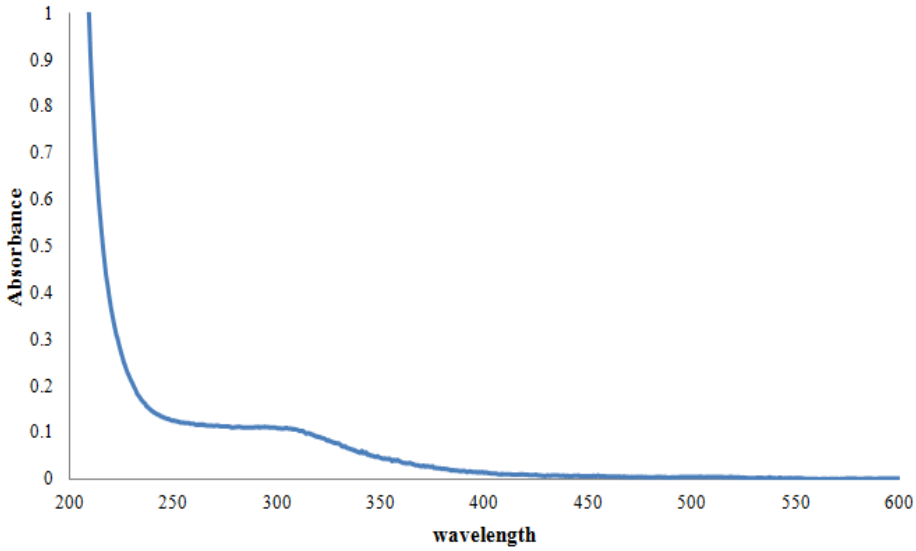

Figure 3.4 UV-visible absorption profiles of N-SC at concentration 500 ppm.

The main objective on preparing N-SC was to overcome the water insolubility of chitosan. As expected, it was found that the N-SC could easily disperse well in deionized water and self-assembly into the stable and transparent colloidal dispersion (Figure 3.5b).

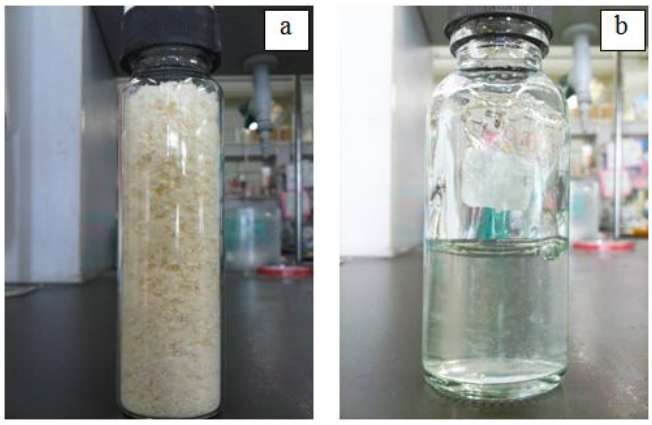

Figure 3.5 Image of N-SC powder (a) and N-SC suspension (b).

Morphology, Hydrodynamic diameter and Zeta potential of the nanoparticles

In water, N-SC could automatically self-assemble into water dispersible particulates. Morphology of particles was characterized with scanning electron microscope (SEM) and transmission electron microscope (TEM). The suspension of the sample was left to dry before being subjected to SEM and TEM analysis. SEM

and TEM images of the particles indicated a spherical morphology with the dry size of 181.59 ± 8.71 nm (Figure 3.6). In water, the hydrodynamic diameter of approximately 572 nm was obtained from the dynamic light scattering analysis with a narrow size distribution (PDI of 0.506) (Table 3.1 and 3.2). Figure 3.7 showed size distribution spectrum of N-SC measured by DLS. The size of the obtained particles was bigger than that observed by SEM and TEM. This indicated some swelling of the N-SC particles when suspended in water. The mean zeta potential of N-SC nanoparticles in water at pH 6.5 was 12.17 ± 1.75 mV. Amine groups in the polymer structure were speculated as the cause of the positive charge at the particle surface.

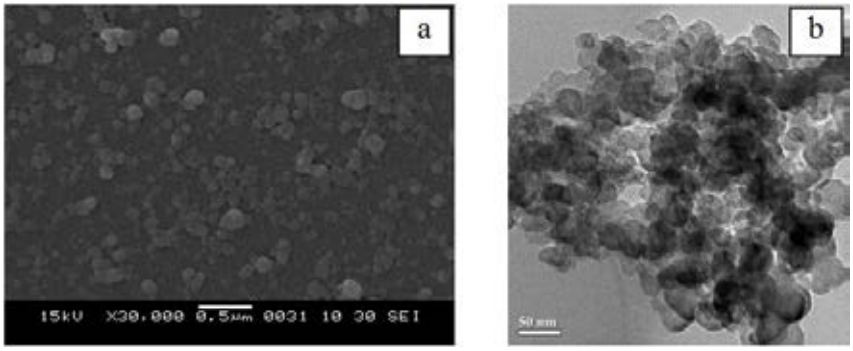

Figure 3.6 SEM image of N-SC nanoparticles at polymer concentration of 1000 ppm at 30,000xmagnification (a) and TEM image of N-SC nanoparticles at polymer concentration of 1000 ppm (b).

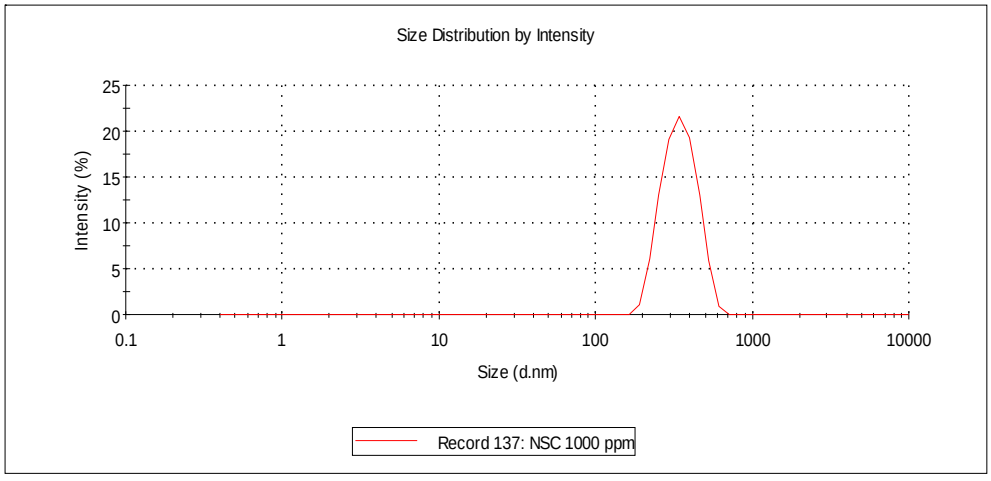

Figure 3.7 Size distribution of N-SC nanoparticles.

3.2 Preparation and characterization of retinilidenesuccinylchitosan (R-NSC)

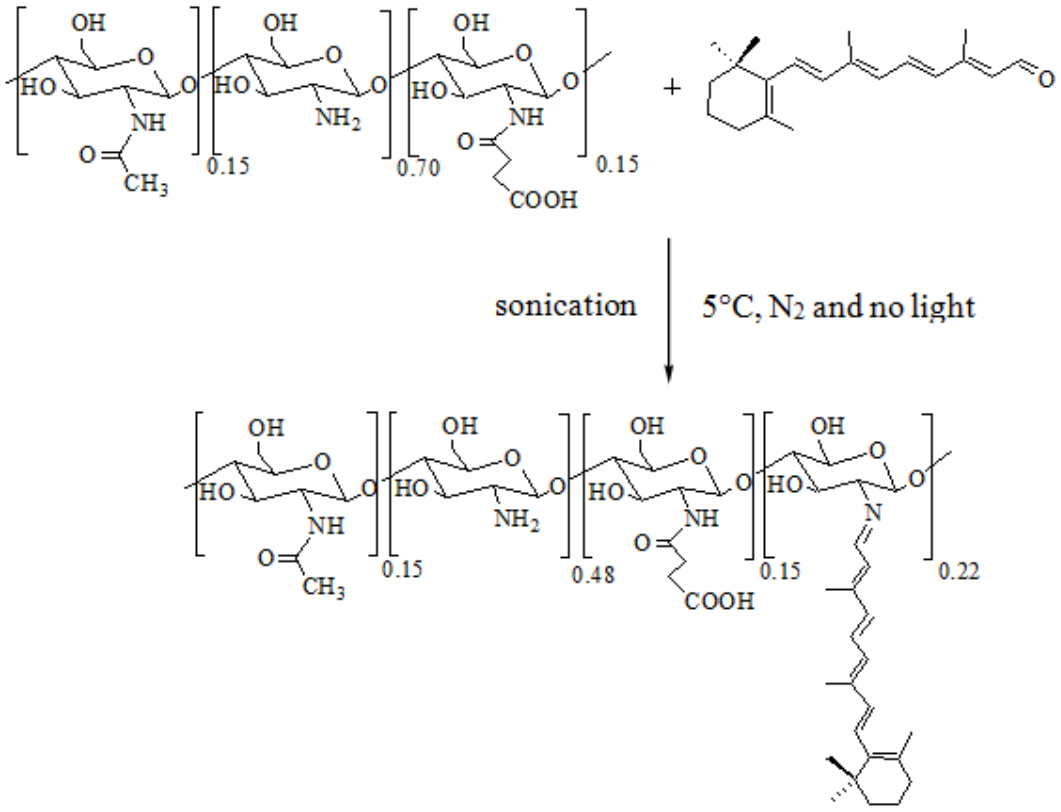

Scheme 3.2 Preparation of retinilidenesuccinylchitosan.

Finding the optimum ratio between N-SC nanoparticles and retinaldehyde

During the retinilidenesuccinylchitosan preparation (Scheme 3.2), N-SC reacted with retinaldehyde to produce Schiff base, retinilidenesuccinylchitosan (R-NSC). The imine bond formation was characterized through ATR-FTIR (1620 cm^{-1}, Figure 3.9, 3.10, 3.11 and 3.12 see full ATR-FTIR interpretation in Appendix B, Figure A6).

Three weight ratios of N-SC to retinaldehyde (1:1, 2:1 and 3:1) were experimented using 4 h sonication time [108], no light, 5°C and nitrogen conditions. The ATR-FTIR spectra of the products of the reaction conducted at N-SC: retinaldehyde mole ratio of 1:1 and 2:1 showed peaks at 1620 cm^{-1} from imine and 1713 cm^{-1} from aldehyde (Figure 3.9 and 3.10 (a) and (b)). On the other hand, IR spectra of products from reaction at 3:1 ratios showed no absorption peak at 1713 cm^{-1}, thus indicating no aldehyde functionality (Figure 3.9 and 3.10 (c)). This indicated

no left over aldehyde in the system. Therefore the N-SC: retinaldehyde at the mole ratio of 3:1 (weight ratio of 46.28:15.86 mg) was used to prepare R-NSC for further study. The physical appearance of the R-NSC obtained was yellow solution. (Figure 3.8)

Figure 3.8 Image of retinilidenesuccinylchitosan suspension.

It was estimated that R-NSC product possessed a degree of imine substitution of approximately 0.22 (Scheme 3.2). A degree of retinaldehyde substitution (DS) or retinilidene moieties was quantitatively estimated by hydrolyzing the material with 0.1 M HCl, followed with partitioning with ethylacetate and quantifying the released retinaldehyde in the ethylacetate layer using UV-visible spectroscopic analysis with the aid of calibration curve (see appendix C for full details of DS determination procedure).

UV-visible absorption spectrum of retinaldehyde showed maximum absorption at 375 nm while that of R-NSC showed maximum absorption at 352 nm (Figure 3.13). The blue shift of absorption indicated the change from retinaldehyde to retinilidene moieties.

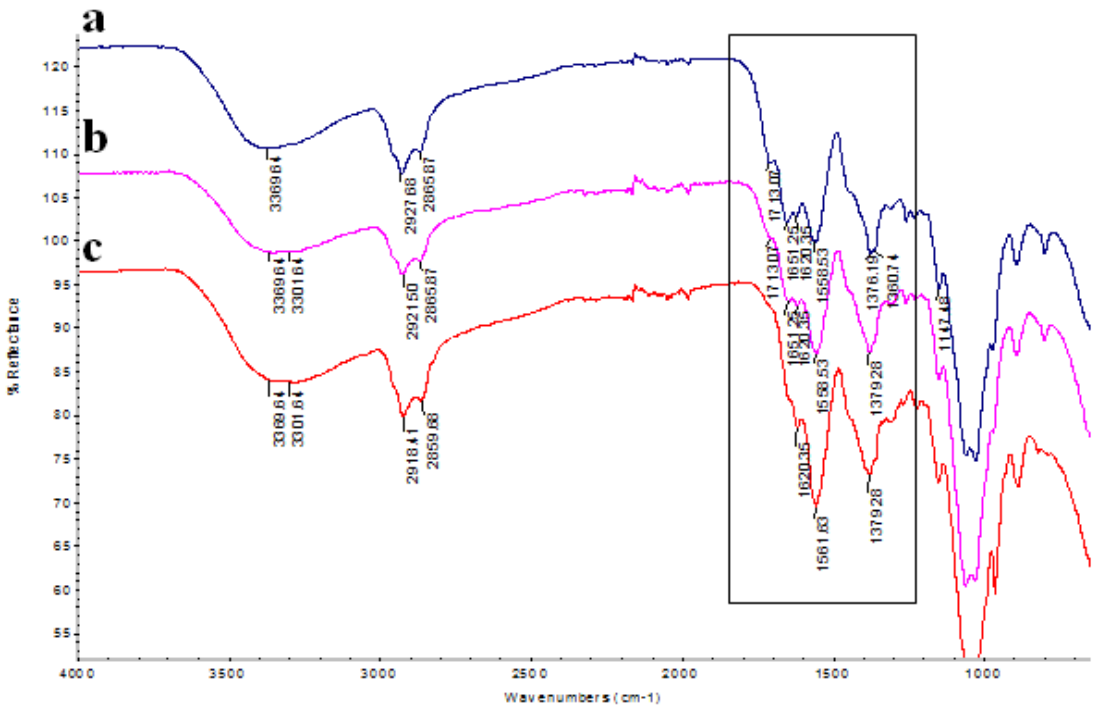

Figure 3.9 ATR-FTIR spectra of retinilidenesuccinylchitosan studies on imine formation at N-SC: retinaldehyde mole ratio of (a) 1:1, (b) 2:1 and (c) 3:1.

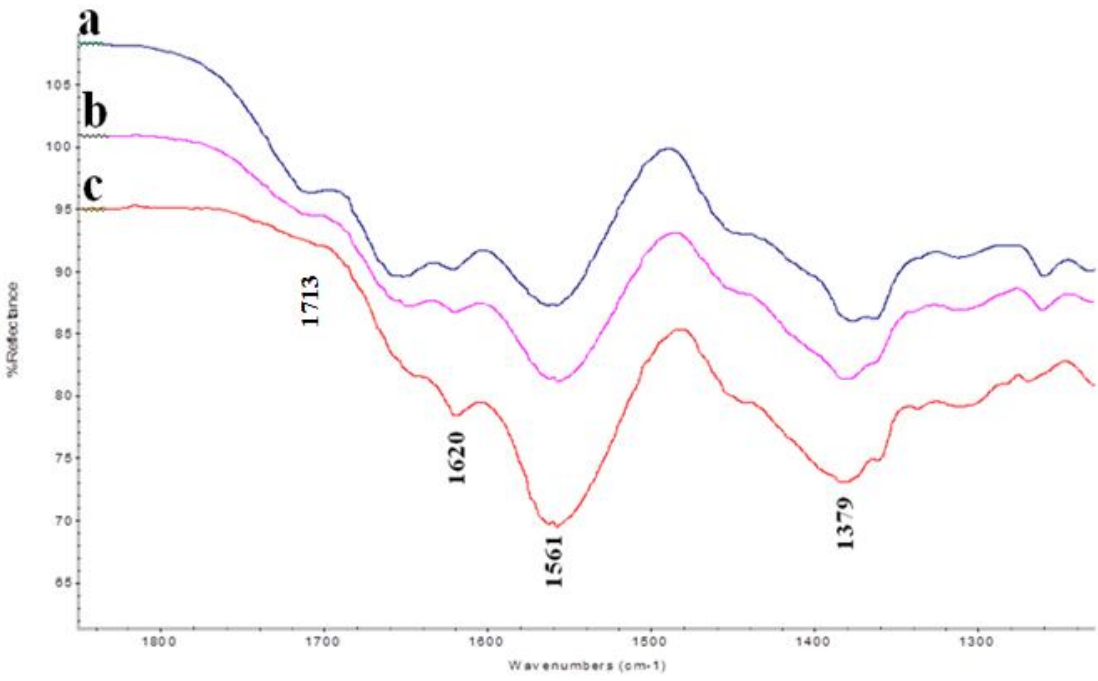

Figure 3.10 Expansion of ATR-FTIR spectra of retinilidenesuccinylchitosan obtained at N-SC: retinaldehyde mole ratio of (a) 1:1, (b) 2:1 and (c) 3:1.

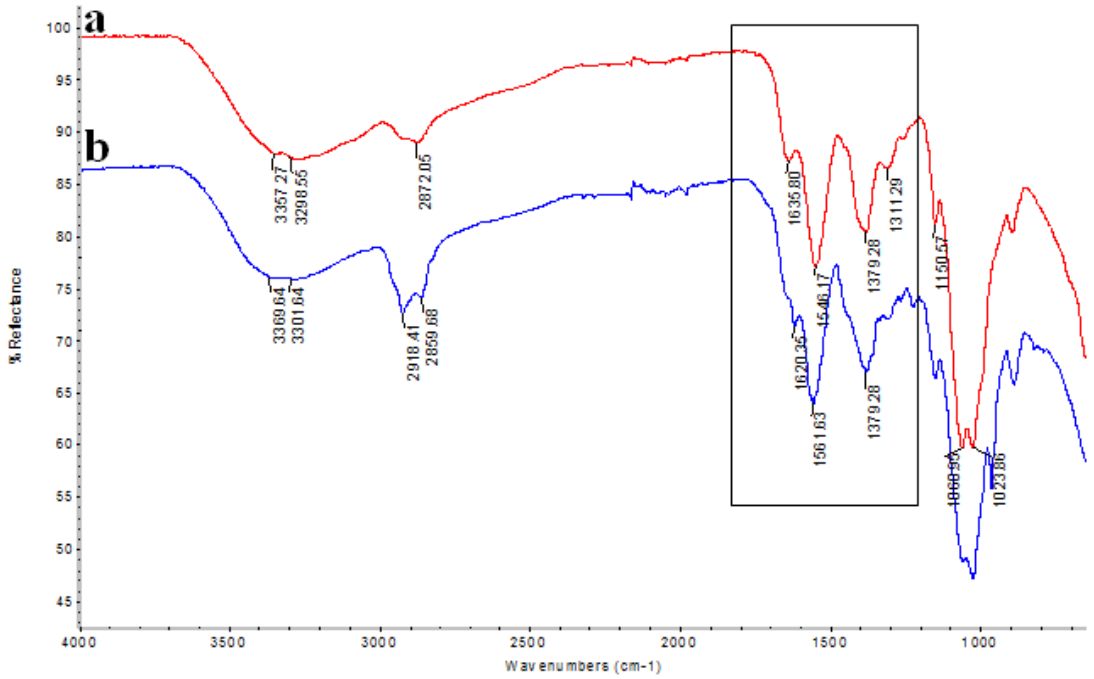

Figure 3.11 ATR-FTIR spectra of (a) N-SC and (b) retinilidenesuccinylchitosan prepared at N-SC: retinaldehyde mole ratio of 3:1, 4 h reaction time.

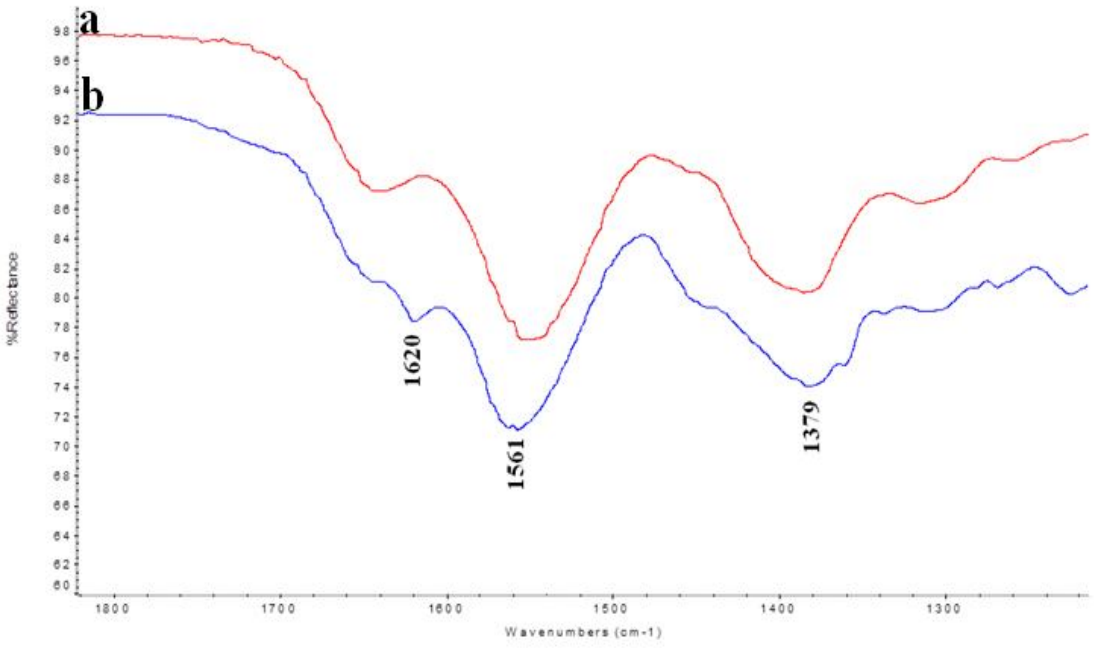

Figure 3.12 Expansion of ATR-FTIR spectra of (a) N-SC and (b) retinilidenesuccinylchitosan obtained at N-SC: retinaldehyde mole ratio of 3:1, 4 h reaction time.

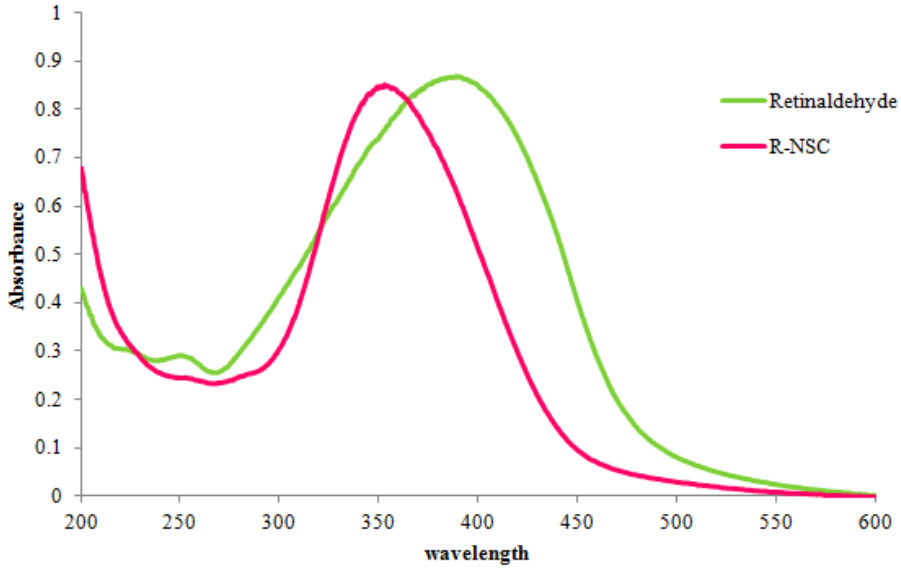

Figure 3.13 UV-visible absorption profiles of free retinaldehyde at concentration of 20 ppm (—) and N-SC at concentration of 925 ppm with retinaldehyde at concentration of 20 ppm (—).

Morphology, Hydrodynamic diameter and Zeta potential of the R-NSC nanoparticles

The R-NSC particles can be dispersed in water. SEM and TEM image of R-NSC particles indicated spherical morphology with the dry size of 240.10 ± 28.81 nm (Figure 3.14). Comparing to the dry size of N-SC (181 ± 8.71 nm), aldehyde grafted N-SC particles were bigger in size. In water, the hydrodynamic diameter of approximately 943 nm (PDI of 0.244) (obtained from the dynamic light scattering analysis) (Table 3.1 and 3.2) was observed. The difference between the dry size (240 nm) and hydrated size (943 nm) implied severse swelling of the particles in water. Figure 3.15 showed size distribution spectrum of R-NSC measured by DLS. The mean zeta potential of R-NSC particles in water of pH 6.5 was 29.73 ± 0.23 mV, indicating unagglomorated nature of the particles.

It was expected that the hydrophobicity of retinilidene moieties would be at the core of the nanospheres, while carboxyl group of the succinic anhydride and the hydroxyl group of the glucosamine rings would be at the surface of the nanospheres during the self-assembling process.

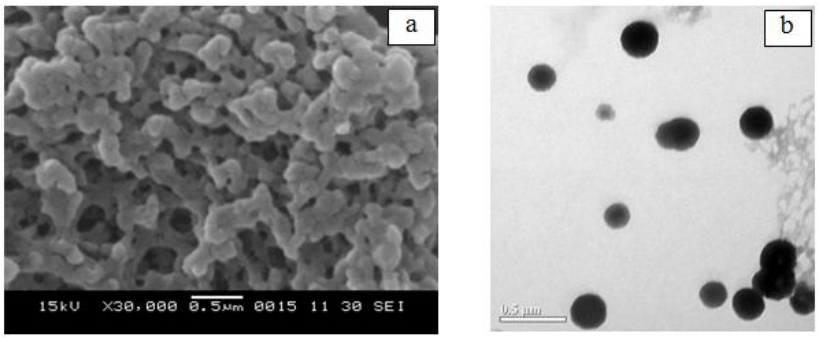

Figure 3.14 SEM image of R-NSC nanoparticles at polymer concentration of 1000 ppm at 30,000xmagnification (a) and TEM image of R-NSC nanoparticles at polymer concentration of 1000 ppm (b).

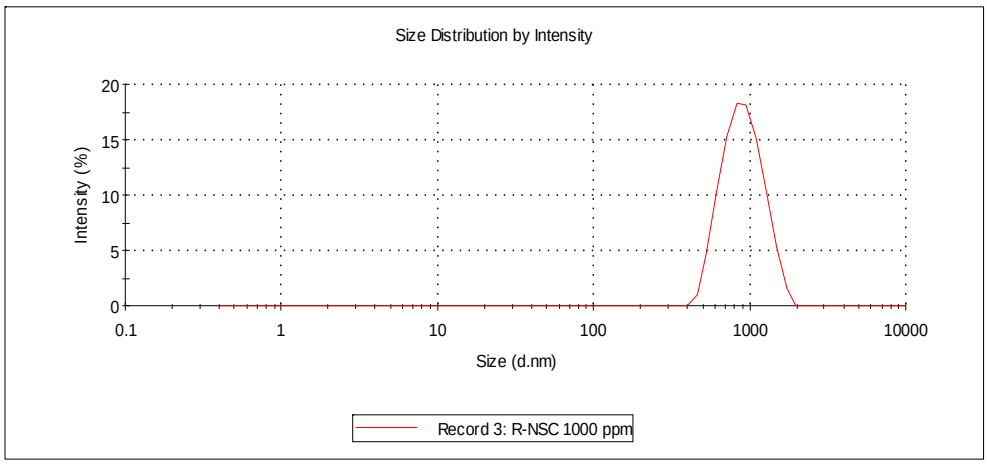

Figure 3.15 Size distribution of R-NSC nanoparticles.

3.3 Loading of α-tocopherol (vitamin E) and butylated hydroxytoluene (BHT) into R-NSC particles

Vitamin E-loaded R-NSC and BHT-loaded R-NSC

Here we wanted to further improve the retinilidene stability by surrounding them with antioxidants. Two hydrophobic antioxidants, vitamin E and butylated hydroxyltoluene were therefore, encapsulated into the R-NSC particles, with the intention that these antioxidants would protect the retinilidene from being easily oxidized. The loading of approximately 7% (by weight) was obtained for the BHT-loaded R-NSC and the vitamin E-loaded R-NSC particles. This was inferred

from the fact that there was no free vitamin E or BHT left in the system when 5.29 mg of the antioxidant was sonicated with 62.14 mg of R-NSC in the aqueous environment. The ATR-FTIR spectra of the products showed showed peaks at 1620 cm^{-1} from imine. The result showed vitamin E and BHT were not reacted with chitosan (Figure 3.16 and 3.17).

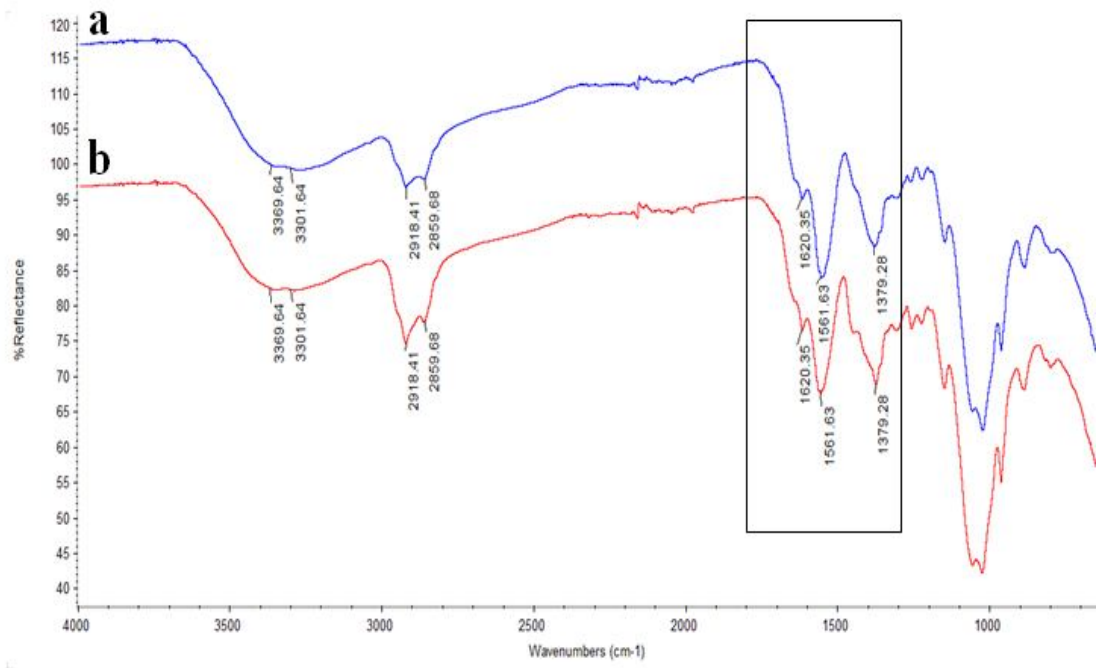

Figure 3.16 ATR-FTIR spectra of (a) BHT-loaded R-NSC and (b) vitamin E-loaded R-NSC prepared at N-SC: retinaldehyde mole ratio of 3:1 and 7.42% antioxidants (BHT and vitamin E), reaction time for 4 h.

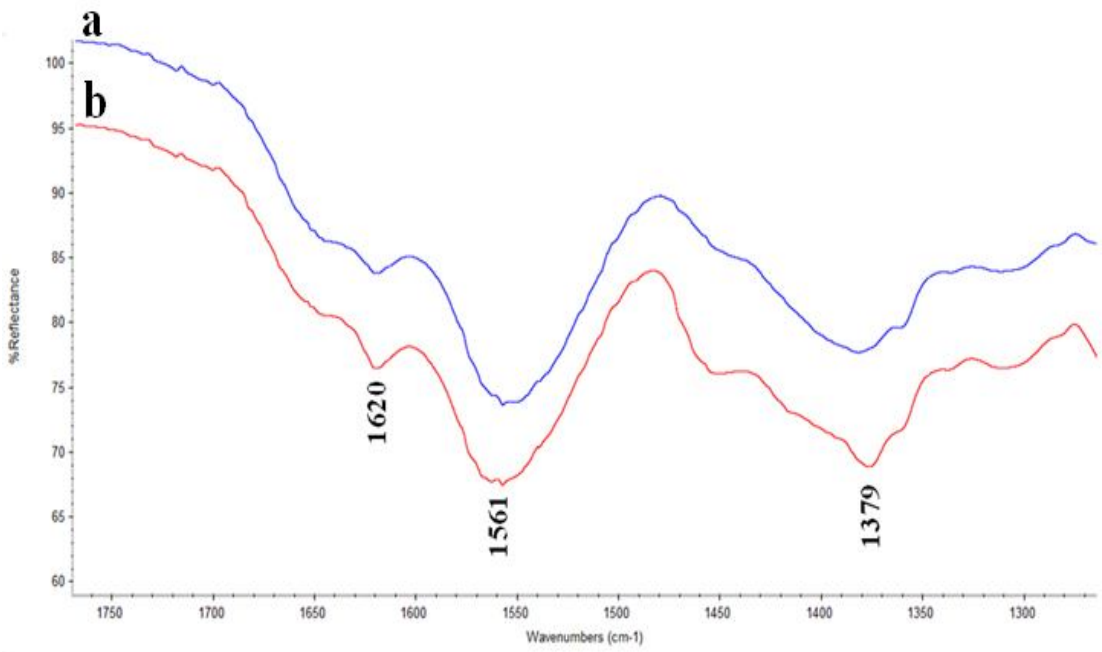

Figure 3.17 Expansion of ATR-FTIR spectra of (a) BHT-loaded R-NSC and (b) vitamin E-loaded R-NSC prepared at N-SC: retinaldehyde mole ratio of 3:1 and 7.42% antioxidants (BHT and vitamin E), reaction time for 4 h.

Morphology, Hydrodynamic diameter and Zeta potential of the antioxidant loaded nanoparticles

The BHT-loaded R-NSC and vitamin E-loaded R-NSC particles could be dispersed in water. SEM and TEM image of BHT-loaded R-NSC particles indicated the particles with the dry size of 180.44 ± 9.33 nm (Figure 3.18a and b). However, inhomogeniety of the particle's core was also observed, implying phase separation between BHT and the R-NSC matrix. SEM and TEM image of vitamin E-loaded R-NSC particles indicated spherical morphology with the dry size of 162.44 ± 20.79 nm (Figure 3.18c and d) with homogeneous spherical core. This implied no phase separation between vitamin E and R-NSC matrix. In water, the hydrodynamic diameter of approximately 888 and 791 nm (PDI of 0.529 and 0.551) of BHT-loaded R-NSC and vitamin E-loaded R-NSC, respectively, were obtained (Table 3.1 and 3.2). The hydrated size was bigger than the dry size (SEM and TEM), indicating same swelling of the two particles when being suspended in water. The mean zeta potential

of BHT-loaded R-NSC and vitamin E-loaded R-NSC particles in water of pH 6.5 were 28.77 ± 0.85 and 25.47 ± 0.76 mV, respectively, implying acceptablev stability of the two particles suspension in water.

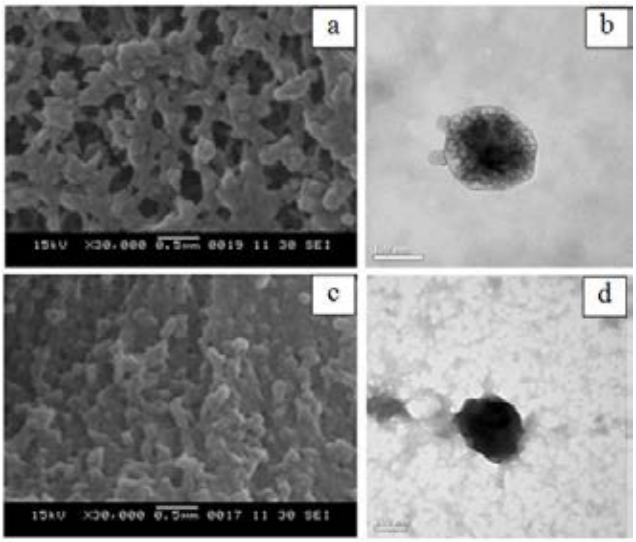

Figure 3.18 SEM and TEM image of BHT-loaded R-NSC particles (a, b) and Vitamin E-loaded R-NSC particles (c, d).

3.4 Stability of retinilidene in the particles

The stability of retinilidene moieties in the R-NSC, vitamin E-loaded R-NSC and BHT-loaded R-NSC particles were evaluated in water under light (UVA 3-5 mW/cm^2 and UVB of 0.1-0.12 mW/cm^2), heat (40°C) and oxygen (stirring at 300 rpm) exposures. The amount of retinilidene was quantified through the UV absorption at 352 nm (λ_{max} of retinilidene moieties). The results indicated that the retinilidene in the R-NSC was significantly more stable than the free retinaldehyde (Figure 3.19a and b). At 60 min, 88% of free retinaldehyde were degraded, however, only 66% of retinilidene in the R-NSC particles were degraded (Figure 3.20). This indicated improved stability the vitamin A derivative in the R-NSC form over the free retinaldehyde form. Upon encapsulation with BHT and vitamin E, the retinilidene stability was further improved. At 120 min, 72% of retinilidene in the BHT-loaded R-NSC were degraded, while, only 39% of retinilidene in the vitamin E-loaded R-NSC particles were degraded (Figure 3.19c and d). Therefore, the retinilidene in the vitamin E-loaded R-NSC particles was more stable than those retinilidene in the free retinaldehyde, R-NSC and BHT-loaded R-NSC particles (Figure 3.20).

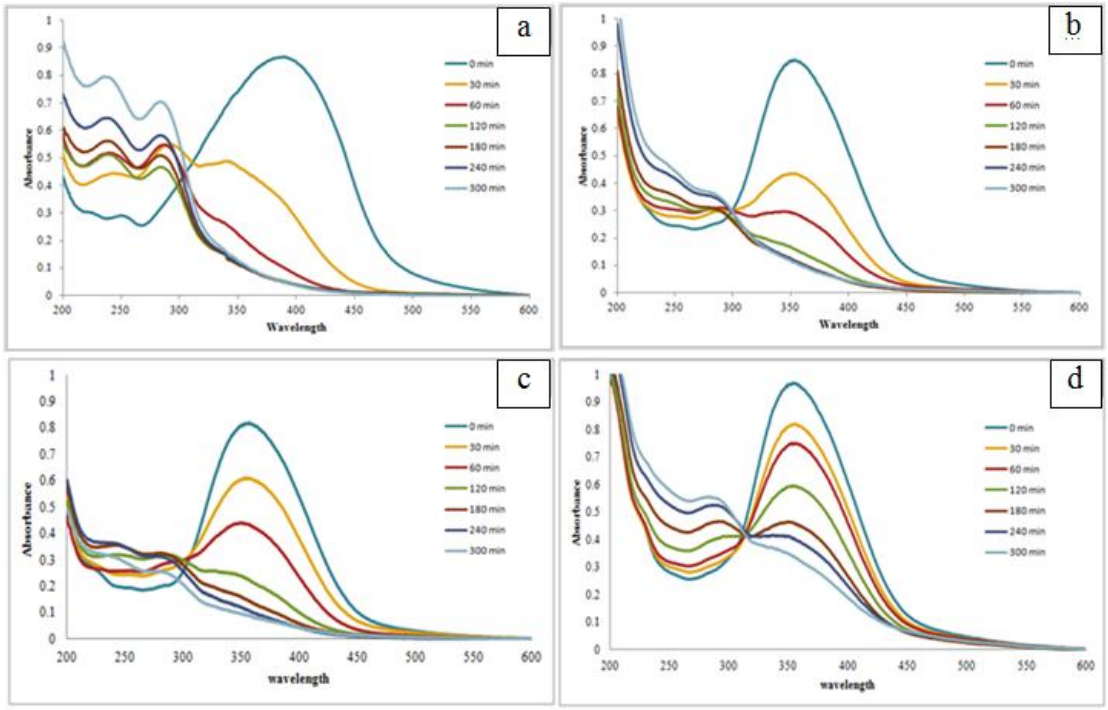

Figure 3.19 Stability (depicted as absorption at 352 nm) of free retinaldehyde (a), R-NSC particles (b), BHT-loaded R-NSC particles (c) and vitamin E-loaded R-NSC particles (d) in an aqueous environment when kept at 40°C with light and air exposures, for various times.

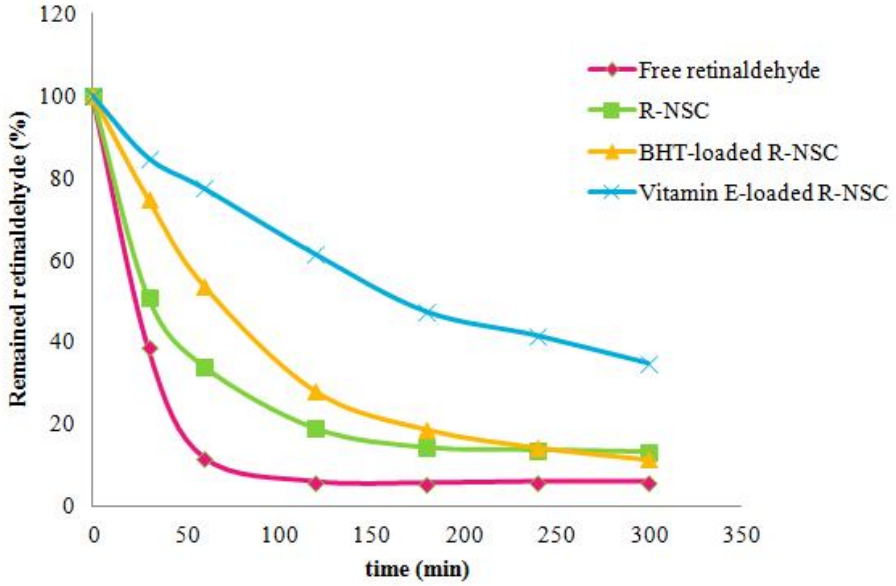

Figure 3.20 Retinaldehyde/retinilidene stability profiles of R-NSC particles, BHT-loaded R-NSC particles, vitamin E-loaded R-NSC particles and free retinaldehyde.

From above experiments, the stable vitamin A derivative in the form of nanoparticle could be fabricated. In the next section, ability of the new vitamin A particles to release the retinaldehyde was demonstrated in conjunction with their ability to penetrate skin tissue.

3.5 Fluorescence labeled particles

The N-SC particles were not fluorescent, therefore, to track the location of particles in skin tissue, fluorophore Rhodamine B was covalently linked to the N-SC polymeric chains. Rhodmine B (Lissamine rhodamine B sulfonyl chloride) was first covalently linked to the N-SC particles by adding 0.01% of Rhodamine B into aqueous N-SC particles suspension to obtained Rho B-labeled N-SC. Figure 3.21 shows that the Rho B-labeled N-SC particles give fluorescent emission at 587 nm. Then the RhoB-labeled N-SC was grafted with retinaldehyde (Chapter II page 36) to obtained Rho B-R-NSC particles. Since fluorescent signals from retinaldehyde and Rho B-N-SC did come from the same location (Figure 3.22). The CLSM image of the Rho B-R-NSC particles is shown in Figure 3.22a. The CLSM image was resolved into retinilidene/retinaldehyde and Rho B components using fluorescent spectrum of retinaldehyde and Rhodamine B as reference (Figure 3.22b and c).

Vitamin E was encapsulated with Rho B-R-NSC particle at the vitamin E loading of approximately 7% (by weight). Since fluorescent signals from retinaldehyde, Rho B-N-SC and vitamin E did come from the same location (Figure 3.23). The CLSM image of vitamin E-loaded Rho B R-NSC particles is shown in Figure 3.23a. Here the fluorescence from vitamin E component could be resolved, thus the particles showed three fluorescent components, retinaldehyde, Rho B and vitamin E (Figure 3.23b, c and d).

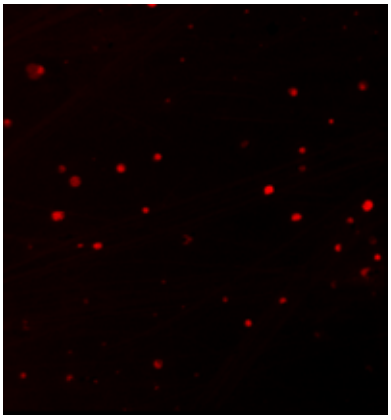

Figure 3.21 Confocal laser scanning fluorescence microscopy images showing Rho B-N-SC particles.

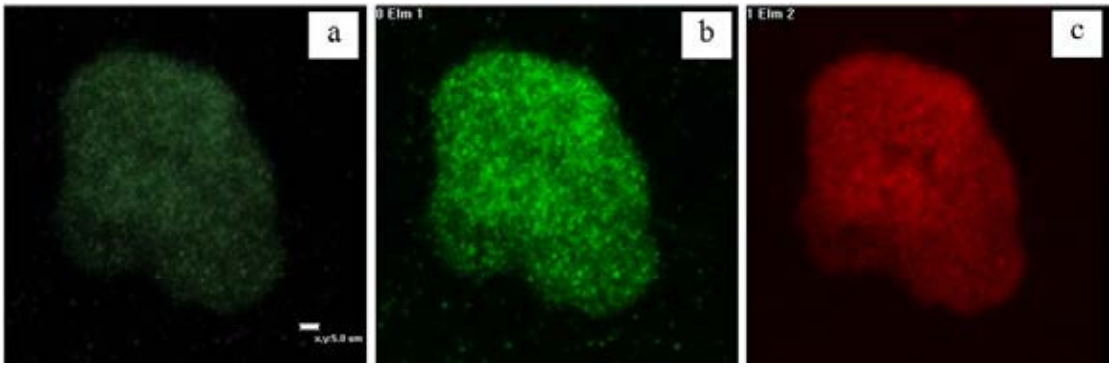

Figure 3.22 Confocal laser scanning fluorescence microscopic images showing Rho B-R-NSC particles (a) resolved fluorescent image of the retinaldehyde (b) and Rho B-SC (c).

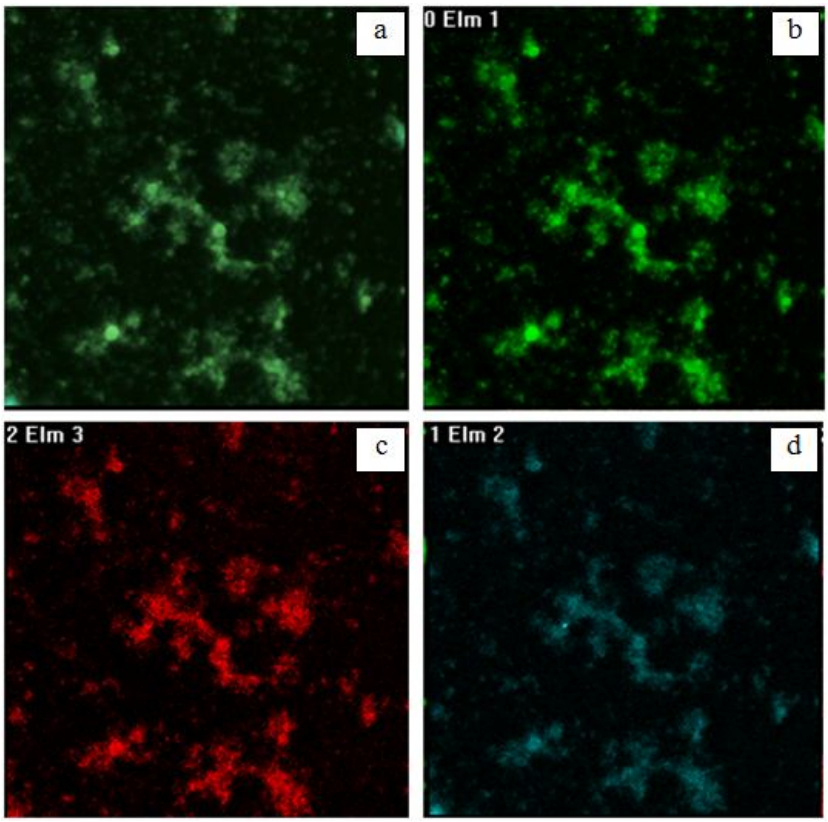

Figure 3.23 Confocal laser scanning fluorescence microscopy images showing Rho B-R-NSC particles (a), and resolved fluorescent image of the retinaldehyde (b), Rho B-SC (c) and vitamin E (d).

Morphology, Hydrodynamic diameter and Zeta potential of the nanoparticles

The Rho B-R-NSC and vitamin E-loaded Rho B R-NSC could be dispersed in water. SEM image of Rho B-R-NSC and vitamin E-loaded Rho B- R-NSC particles indicated spherical morphology of the particles with the dry size of 1348.00 ± 168.68 and 684.72 ± 200.76 nm, respectively (Figure 3.24). In water, the hydrodynamic diameter of approximately 1587 and 883 nm (PDI of 0.995 and 0.605) of Rho B-R-NSC and vitamin E-loaded Rho B R-NSC, respectively, were obtained from the dynamic light scattering analysis (Table 3.1 and 3.2). The bigger size of the hydrated particles comparing to the dry particles, indicated swelling of the R-NSC particles when suspended in water. The mean zeta potential of Rho B-R-NSC and vitamin E-

loaded Rho B R-NSC particles in water of pH 6.5 were 19.80 ± 0.20 and 18.87 ± 0.45 mV, respectively, indicating modurate stability of these particles in water.

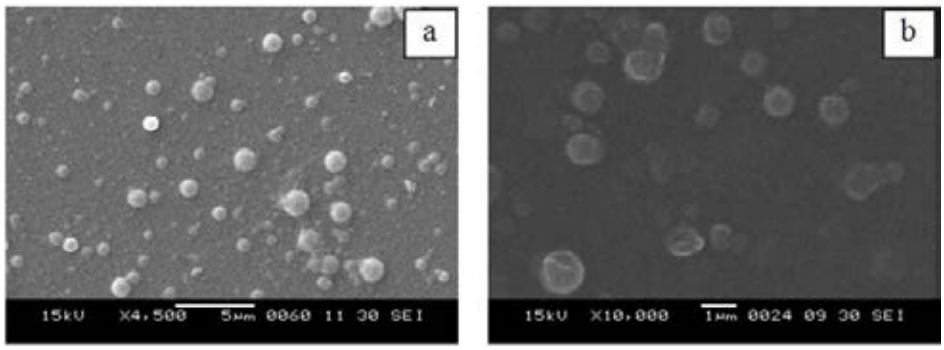

Figure 3.24 SEM images of Rho B-R-NSC (a) and vitamin E-loaded Rho B- R-NSC (b) particles.

Table 3.1 The size of particles.

Particles	Particles size from SEM, TEM (nm)	Hydrodynamic diameter from DLS (nm)
N-SC	181.59 ± 8.71	572.33 ± 8.35
R-NSC	240.10 ± 28.81	943.33 ± 5.60
BHT-loaded R-NSC	180.44 ± 9.33	888.00 ± 1.57
Vitamin E-loaded R-NSC	162.44 ± 20.79	791.00 ± 10.32
RhoB-R-NSC	1348.00 ± 168.68	1587.66 ± 57.33
Vitamin E-loaded RhoB-R-NSC	684.72 ± 200.76	883.00 ± 12.83

Table 3.2 The polydispersity index and zeta potential of particles.

Particles	PDI	Zeta potential (mV)
N-SC	0.506	12.17 ± 1.75
R-NSC	0.244	29.73 ± 0.23
BHT-loaded R-NSC	0.529	28.77 ± 0.85
Vitamin E-loaded R-NSC	0.551	25.47 ± 0.76
RhoB-R-NSC	0.995	19.80 ± 0.20
Vitamin E-loaded RhoB-R-NSC	0.605	18.87 ± 0.45

3.6 Skin penetration

Penetration of the Rho B-R-NSC

Ex-vivo skin penetration of the Rho B-R-NSC particles was carried out and the retinaldehyde release from the penetrated particles into the skin tissue was evaluated on the fresh porcine ear skin using CLFM. The experiment was started by dropping 15 µl of the Rho B-R-NSC nanoparticles suspension (3085 ppm Rho B-labeled N-SC and 1057 ppm retinaldehyde) onto the porcine ear skin piece, massaging for 2 min and leaving at 25°C for 30 min. The final coverage of Rho B-N-SC and retinal on the skin was ~20 and ~7 µg cm^{-2}, respectively. The obtained spectra of each pixel were then unmixed into retinaldehyde, Rho B-N-SC and porcine ear skin auto-fluorescent components using chemometric analysis (image algorithms) based on the spectral database constructed from fluorescent spectra of standard retinaldehyde, Rho B-N-SC and the porcine ear skin. The resolved CLSM pictures indicated fluorescence signals of retinaldehyde and Rho B-N-SC at various areas in the porcine ear skin. The result indicated that the Rho B-R-NSC could penetrated into the skin tissue *via* hair follicles. Their accumulation at the hair follicles was obvious. This indicated that the hair follicles was the major route of the Rho B-R-NSC particles skin penetration (Figure 3.25). Since fluorescent signals from retinaldehyde and Rho B-N-SC did not always come from the same location (Figure 3.26), it was concluded that the retinaldehyde

was released from the RhoB-N-SC particles and could diffuse into the surrounding tissue. In facts, by measuring the ratio of fluorescent intensity of retinaldehyde to that of RhoB-N-SC along the depth of the skin, it was observed that the ratios increased with the depth of the skin (Table 3.3). It indicated the dissociation of retinaldehyde from the RhoB-N-SC particles. The hydrophobic of retinaldehyde molecules appear to moved faster into the deeper skin layer comparing to the RhoB-N-SC.

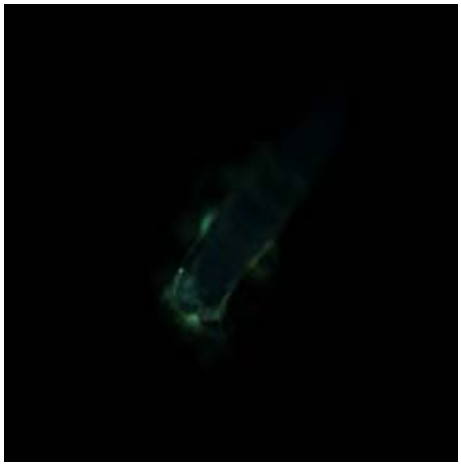

Figure 3.25 Confocal laser scanning fluorescence microscopy image showing accumulation of Rho B-R-NSC particles in hair follicle.

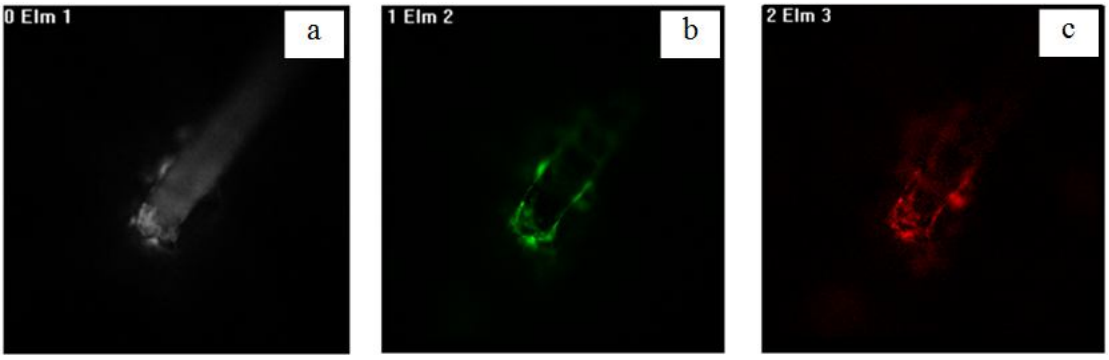

Figure 3.26 Confocal laser scanning fluorescence microscopy image showing unresolved fluorescent image of the porcine ear skin at ~10 μm depth from the stratum corneum surface, 30 mins after the Rho B-R-NSC nanoparticles suspension was supplied; (a) superimposed image of the fluorescent spectrum of porcine ear skin (gray), (b) retinaldehyde (green) and (c) Rho B-N-SC (red).

Table 3.3 The fluorescent intensity of retinaldehyde ($I_{Retinaldehyde}$) and Rho B-N-SC ($I_{RhoB\text{-}N\text{-}SC}$) around of the hair follicle, at various depths from stratum corneum area.

Depth (μm)	**Fluorescent intensity (I)**		$\mathbf{I_{Retinaldehyde}/I_{RhoB\text{-}N\text{-}SC}}$
	$\mathbf{I_{Retinaldehyde}}$	$\mathbf{I_{RhoB\text{-}N\text{-}SC}}$	
10	61.70	16.43	3.76
20	61.41	16.15	3.80
30	60.09	14.70	4.09
40	57.52	12.98	4.43
50	53.85	11.31	4.76
60	49.30	9.614	5.13
70	43.56	7.991	5.45
80	37.93	6.586	5.76
90	32.59	5.320	6.13
100	28.49	4.452	6.40
110	25.17	3.809	6.61
120	22.59	3.149	7.17
130	20.40	2.809	7.26
140	18.82	2.499	7.53
150	17.56	2.161	8.13
160	16.42	1.912	8.59
170	15.55	1.734	8.97
180	14.67	1.548	9.48
190	13.99	1.382	10.12
200	12.71	1.275	10.71

Penetration of the vitamin E-loaded Rho B-R-NSC

Ex-vivo skin penetration of the vitamin E-loaded Rho B R-NSC particles was carried out and the retinaldehyde and vitamin E release from the penetrated particles into the skin tissue was evaluated using the same procedure used for Rho B-R-NSC except that the additional fluorescent component of vitamin E was deduced from the output fluorescent signals, in addition to those of Rho B and retinaldehyde. The resolved CLSM pictures indicated fluorescence signals of retinaldehyde, vitamin E and Rho B-N-SC at various areas in the porcine ear skin. The result indicated that the vitamin E-loaded Rho B-R-NSC could penetrated into the skin tissue *via* hair follicles. This indicated that the hair follicles was the major route during the skin penetration of the vitamin E-loaded Rho B-R-NSC particles (Figure 3.27). Since fluorescent signals from retinaldehyde, vitamin E and Rho B-N-SC did not always come from the same location (Figure 3.28), it was concluded that the retinaldehyde and vitamin E were released from the Rho B-N-SC particles and could diffuse into the surrounding tissue. In facts, by measuring the ratio of fluorescent intensity of retinaldehyde and vitamin E to that of Rho B-N-SC along the depth of the skin, it was clear that the ratios slightly increased with the depth of the skin, it was concluded that the retinaldehyde and Rho B-N-SC could penetrate into the skin simultaneously. The retinaldehyde was released from the particles more slowly than the release of vitamin E (Table 3.4). This indicated the dissociation of retinaldehyde and vitamin E from the RhoB-N-SC particles. The hydrophobic of retinaldehyde and vitamin E molecules appear to moved faster into the deeper skin layer comparing to the RhoB-N-SC.

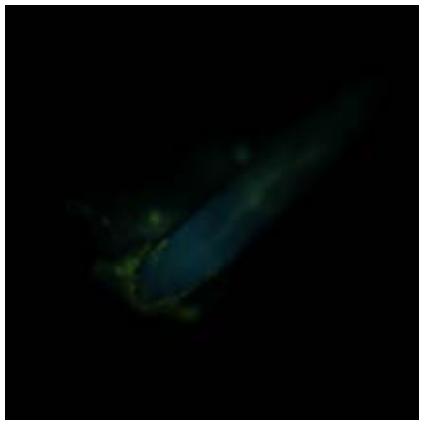

Figure 3.27 Confocal laser scanning fluorescence microscopy image showing accumulation of vitamin E-loaded Rho B-R-NSC particles in hair follicle.

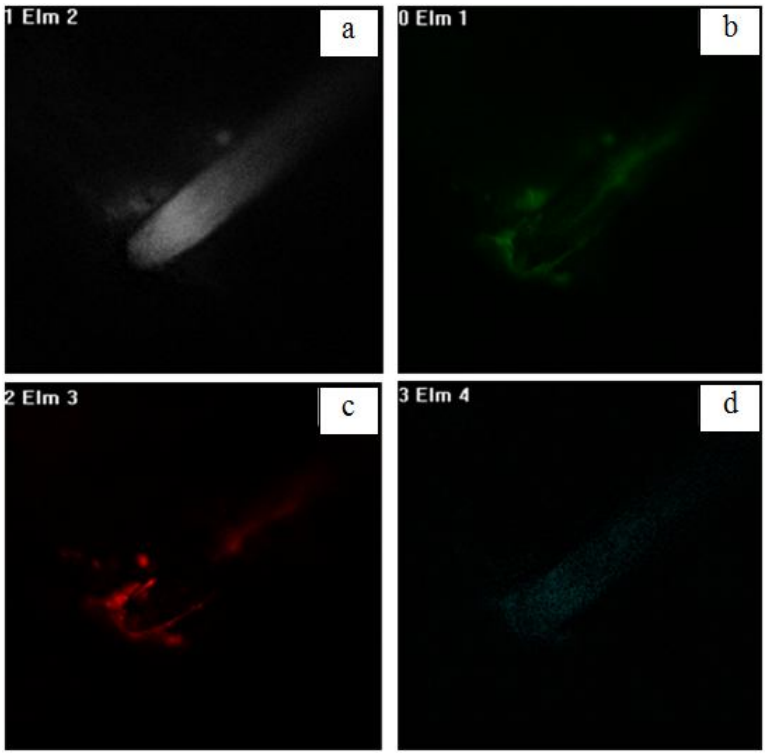

Figure 3.28 Confocal laser scanning fluorescence microscopy image showing unresolved fluorescent image of the porcine ear skin at ~10 μm depth from the stratum corneum surface, 30 mins after the vitamin E-loaded Rho B R-NSC nanoparticles suspension was applied; (a) superimposed image of the fluorescent spectrum of porcine hair (gray), (b) retinaldehyde fluorescent component (green), (c) Rho B-N-SC fluorescent component (red) and (d) vitamin E fluorescent component (light blue).

Table 3.4 The fluorescent intensity of retinaldehyde ($I_{Retinaldehyde}$), vitamin E ($I_{Vitamin\ E}$) and Rho B-N-SC ($I_{RhoB\text{-}N\text{-}SC}$) around of the hair follicles, at various depths from stratum corneum area.

Depth (μm)	**Fluorescent intensity (I)**			**$I_{Retinaldehyde}$/ $I_{RhoB\text{-}N\text{-}SC}$**	**$I_{Vitamin\ E}$/ $I_{RhoB\text{-}N\text{-}SC}$**
	$I_{Retinaldehyde}$	**$I_{Vitamin\ E}$**	**$I_{RhoB\text{-}N\text{-}SC}$**		
10	66.36	12.26	67.31	0.99	0.18
20	60.15	11.65	59.89	1.00	0.19
30	54.00	10.44	51.76	1.04	0.20
40	47.88	9.456	44.36	1.07	0.21
50	42.34	8.623	38.01	1.11	0.22
60	37.68	7.843	33.18	1.14	0.23
70	33.87	7.459	29.49	1.15	0.25
80	30.68	6.773	26.08	1.18	0.26
90	27.41	6.544	23.50	1.17	0.28
100	25.09	6.046	21.20	1.18	0.29
110	22.80	5.786	19.12	1.19	0.30
120	21.04	5.749	17.45	1.21	0.33
130	19.34	5.386	15.84	1.22	0.34
140	17.92	5.328	14.42	1.24	0.37
150	16.62	5.327	13.30	1.25	0.40
160	15.50	5.124	12.49	1.27	0.41
170	14.42	4.898	11.53	1.29	0.42
180	13.72	4.818	10.62	1.31	0.45
190	13.00	4.790	10.05	1.33	0.48
200	12.55	4.768	9.483	1.34	0.50

CHAPTER IV

CONCLUSION

In this research, nanoparticles of retinilidenesuccinylchitosan (R-NSC) were successfully prepared. Chitosan was first reacted with succinic anhydride to obtain *N*-succinylchitosan (N-SC) with degree succinyl substitution of 0.15 to obtain transparent colloidal suspension. The imine formation of R-NSC derived from the grafting reaction of aldehyde group of retinaldehyde onto amino group of N-SC chains. The obtained Schiff base product, had a degree of imine substitution of 0.20 and the dry particles were spherical with the diameter of 181 ± 8.71 nm. The stability of retinilidene moieties in the N-SC nanoparticles was significantly improved comparing to free retinaldehyde. In addition, when antioxidant was loaded into the R-NSC particles, stability of retinidene moieties could be improved. The vitamin E and BHT-loaded R-NSC particles showed great stability comparing to R-NSC particles.

The N-SC particles were not fluorescent. Therefore, Rhodamine B was covalent linked to amino group of the N-SC polymeric chains to obtain Rho B-N-SC. The Rho B-N-SC particles gave fluorescent emission at 587 nm. The *ex-vivo* skin permeation of the R-NSC and vitamin E-loaded R-NSC particles suspension was investigated on porcine ear skin using confocal laser scanning fluorescent microscope (CLSM). Fluorescent images of the porcine ear skin applied with R-NSC and vitamin E-loaded R-NSC particles suspension showed that the particles accumulated at the hair follicles. This indicated that the R-NSC particles could be permeated into the skin tissue *via* hair follicles. Both the grafted retinaldehyde and loaded vitamin E could be released from the particles because their fluorescent signal could be detected away from the fluorescent labeled N-SC particles. Hence, the grafted retinaldehyde improved the stability and solubility properties of retinaldehyde and enhances skin permeation. Thus, applications of these stable vitamin A derivative particles in cosmetics and dermatology are hopeful for treatment skin diseases.

REFERENCES

[1] Mary P, L. Antioxidants and vitamins in cosmetics. *Clinics in Dermatology* 19, 4(2001), 467-473.

[2] Michele, V. Overview. *Journal of the American Academy of Dermatology* 36, 6(1997): S91.

[3] Rafal, E. S., et al. Topical Tretinoin (Retinoic Acid) Treatment for Liver Spots Associated with Photodamage. *New England Journal of Medicine* 326, 6(1992): 368-374.

[4] Weiss, J. S., et al. Topical Tretinoin Improves Photoaged Skin. *JAMA: The Journal of the American Medical Association* 259, 4(1988): 527-532.

[5] Pugliese, P. T. The skin's antioxidant systems. *Dermatology Nursing* 10, 6(1998): 401–416.

[6] Manela-Azulay, M. and Bagatin, E. Cosmeceuticals vitamins. *Clinics in Dermatology* 27, 5(2009): 469-474.

[7] Griffiths, C. E. M., et al. Topical tretinoin (retinoic acid) improves melasma. A vehicle-controlled, clinical trial. *British Journal of Dermatology* 129, 4(1993): 415-421.

[8] Creidi, P., et al. Profilometric evaluation of photodamage after topical retinaldehyde and retinoic acid treatment. *Journal of the American Academy of Dermatology* 39, (1998): 960-965.

[9] Garcia-Fuentes, M. Torres, D. and Alonso, M. J. Design of lipid nanoparticles for the oral delivery of hydrophilic macromolecules. *Colloids and Surfaces B: Biointerfaces* 27, 2-3(2003): 159-168.

[10] Failloux, N., Bonnet, I., Perrier, E. and Baron, M.-H. Effects of light, oxygen and concentration on vitamin A1. *Journal of Raman Spectroscopy* 35, 2(2004): 140-147.

[11] Duell, E. A., Kang, S. and Voorhees J. J. Unoccluded retinol penetrates human skin in vivo more effectively than unoccluded retinyl palmitate or retinoic acid. *Journal Investigative Dermatology* 109, (1997): 301-309.

[12] Saurat, J. H., et al. Topical Retinaldehyde on Human Skin: Biologic Effects and Tolerance. *Journal Investigative Dermatology* 103, 6(1994): 770-774.

[13] Bissett, D. L. Common cosmeceuticals. *Clinics in Dermatology 27, 5(2009):* 435-445.

[14] Varani, J., Fisher, G. J., Kang, S. and Voorhees, J.J. Molecular mechanisms of intrinsic skin aging and retinoid-induced repair and reversal. *Journal Investigative Dermatology Symposium Proceedings* 3, 1(1998): 57-60.

[15] Kang, S., et al. Application of Retinol to Human Skin In Vivo Induces Epidermal Hyperplasia and Cellular Retinoid Binding Proteins Characteristic of Retinoic Acid but Without Measurable Retinoic Acid Levels or Irritation. *Journal Investigative Dermatology* 105, 4(1995): 549-556.

[16] Gonzalez, S., Moran, M. and Kochevar, I. E. Chronic Photodamage in Skin of Mast Cell-deficient Mice. *Photochemistry and Photobiology* 70, 2(1999): 248-253.

[17] Kligman, A. M., Baker, T. J. and Gordon, H.L. Long-term histologic follow-up of phenol face peels. *Plastic Reconstructive Surgery* 75, 5(1985): 652-659.

[18] Reynolds, N. J., et al. Retinoic acid metabolites exhibit biological activity in human keratinocytes, mouse melanoma cells and hairless mouse skin in vivo. *Journal of Pharmacology and Experimental Therapeutics* 266, 3(1993):1636-1642.

[19] Gendimenico, G. J. and Mezick, J. A. Pharmacological Effects of Retinoids on Skin Cells. *Skin Pharmacology and Physiology* 6, 1(1993): 24-34.

[20] Harman, D., Aging: a theory based on free radical and radiation chemistry. *Journal of Gerontology* 2, (1957): 298-300.

[21] Harman, D. Aging: Overview. *Annals of the New York Academy of Sciences* 928, 1(2001): 1-21.

[22] Stern, R. S. Treatment of Photoaging. *New England Journal of Medicine* 350, 15(2004): 1526-1534.

[23] Ghersetich, I., Lotti, T., Campanile, G., Grappone, C. and Dini, G. Hyaluronic acid in cutaneous intrinsic aging. *International Journal of Dermatology* 33, 2(1994): 119-122.

[24] Meyer, L. J. and Stern, R. Age-dependent changes of hyaluronan in human skin. *Journal Investigative Dermatology* 102, 3(1994): 385–389.

[25] Fligiel, S. E. G., et al. Collagen Degradation in Aged/Photodamaged Skin In Vivo and After Exposure to Matrix Metalloproteinase-1 In Vitro. *Journal Investigative Dermatology 120*, 5(2003): 842-848.

[26] Trautinger, F. Mechanisms of photodamage of the skin and its functional consequences for skin ageing. *Clinical and Experimental Dermatology* 26, 7(2001): 573-577.

[27] Kligman, A. M., Grove, G. L., Hirose, R. and Leyden, J. J. Topical tretinoin for photoaged skin. *Journal of the American Academy of Dermatology* 15, 4(1986): 836-859.

[28] Semenova, E. M., Cooper, A., Wilson, C. G. and Converse, C. A. Stabilization of All-*trans*-retinol by Cyclodextrins: A Comparative Study Using HPLC and Fluorescence Spectroscopy. *Journal of Inclusion Phenomena and Macrocyclic Chemistry* 44, 1(2002): 155-158.

[29] Hwang, S. R., Lim, S.-J., Park, J.-S. and Kim, C.-K. Phospholipid-based microemulsion formulation of all-trans-retinoic acid for parenteral administration. *International Journal of Pharmaceutics* 276, 1-2(2004): 175-183.

[30] Ourique, A. F., Pohlmann, A. R., Guterres, S. S. and Beck, R. C. R. Tretinoin-loaded nanocapsules: Preparation, physicochemical characterization, and photostability study. *International Journal of Pharmaceutics* 352, 1-2(2008): 1-4.

[31] Carlotti, M. E., Rossatto, V. and Gallarate, M. Vitamin A and vitamin A palmitate stability over time and under UVA and UVB radiation. *International Journal of Pharmaceutics* 240, 1-2(2002): 85-94.

[32] Yoshida, K., Sekine, T., Matsuzaki, F., Yanaki, T. and Yamaguchi, M. Stability of vitamin A in oil-in-water-in-oil-type multiple emulsions. *Journal of the American Oil Chemists' Society* 76, 2(1999): 1-6.

[33] Eskandar, N. G., Simovic, S. and Prestidge, C. A. Chemical stability and phase distribution of all-trans-retinol in nanoparticle-coated emulsions. *International Journal of Pharmaceutics* 376, 1-2(2009): 186-194.

[34] Eskandar, N. G., Simovic, S. and Prestidge, C. A. Solid-state nanoparticle coated emulsions for encapsulation and improving the chemical stability of all-trans-retinol. *International Journal of Pharmaceutics* 423, 2(2012): 384-391.

[35] Diaz, C., Vargas, E. and Gatjens-Boniche, O. Cytotoxic effect induced by retinoic acid loaded into galactosyl-sphingosine containing liposomes on human hepatoma cell lines. *International Journal of Pharmaceutics* 325, 1-2(2006): 108-115.

[36] Sinico, C., et al. Liposomes as carriers for dermal delivery of tretinoin: in vitro evaluation of drug permeation and vesicle-skin interaction. *Journal of Controlled Release* 103, 1(2005): 123-136.

[37] Jee, J.-P., Lim, S.-J., Park, J.-S. and Kim, C.-K. Stabilization of all-trans retinol by loading lipophilic antioxidants in solid lipid nanoparticles. *European Journal of Pharmaceutics and Biopharmaceutics* 63, 29(2006): 134-139.

[38] Shah, K. A., Date, A. A., Joshi, M. D. and Patravale, V. B. Solid lipid nanoparticles (SLN) of tretinoin: Potential in topical delivery. *International Journal of Pharmaceutics* 345, 1-2(2007): 163-171.

[39] Lim, S.-J. and Kim, C.-K. Formulation parameters determining the physicochemical characteristics of solid lipid nanoparticles loaded with all-trans retinoic acid. *International Journal of Pharmaceutics* 243, 1-2(2002): 135-146.

[40] Liu, J., et al. Isotretinoin-loaded solid lipid nanoparticles with skin targeting for topical delivery. *International Journal of Pharmaceutics* 328, 2(2007): 191-195.

[41] Castro, G. A., et al. Formation of ion pairing as an alternative to improve encapsulation and stability and to reduce skin irritation of retinoic acid loaded in solid lipid nanoparticles. *International Journal of Pharmaceutics* 381, 1(2009): 77-83.

[42] Ridolfi, D. M., et al. Chitosan-solid lipid nanoparticles as carriers for topical delivery of tretinoin. *Colloids and Surfaces B: Biointerfaces* 93, 0(2012): 36-40.

[43] Kim, D.-G., et al. Retinol-encapsulated low molecular water-soluble chitosan nanoparticles. *International Journal of Pharmaceutics* 319, 1-2(2006): 130-138.

[44] Opanasopit, P., Ngawhirunpat, T., Rojanarata, T., Choochottiros, C. and Chirachanchai, S. Camptothecin-incorporating N-phthaloylchitosan-g-mPEG self-assembly micellar system: Effect of degree of deacetylation. *Colloids and Surfaces B: Biointerfaces* 60, 1(2007): 117-124.

[45] Errico, C., Gazzarri, M. and Chiellini, F. A novel method for the preparation of retinoic acid-loaded nanoparticles. *International Journal of Molecular Sciences* 10, 5(2009): 2336-47.

[46] Diridollou, S., et al. Study of the effects of retinaldehyde on the skin using ultrasound and rheological techniques. *Journal of Dermatological Science* 16, 1(1998): S214.

[47] Qi, Z. H. and Shieh, W. J. Aqueous Media for Effective Delivery of Tretinoin. *Journal of Inclusion Phenomena and Macrocyclic Chemistry* 44, 1(2002): 133-136.

[48] Lin, H. S., Chean, C. S., Ng, Y. Y., Chan, S. Y. and Ho, P. C. 2-Hydroxypropyl-β-cyclodextrin increases aqueous solubility and photostability of all-trans-retinoic acid. *Journal of Clinical Pharmacy and Therapeutics* 25, 4(2000): 265-269.

[49] Yap, K. L., Liu, X., Thenmozhiyal, J. C. and Ho, P. C. Characterization of the 13-cis-retinoic acid/cyclodextrin inclusion complexes by phase solubility, photostability, physicochemical and computational analysis. *European Journal of Pharmaceutical Sciences* 25, 1(2005): 49-56.

[50] Zsila, F., Bikadi, Z. and Simonyi, M. Retinoic acid binding properties of the lipocalin member β-lactoglobulin studied by circular dichroism, electronic absorption spectroscopy and molecular modeling methods. *Biochemical Pharmacology* 64, 11(2002): 1651-1660.

[51] Dufour, E. and Haertle, T. Binding of retinoids and β-carotene to β-lactoglobulin. Influence of protein modifications. *Biochimica et Biophysica Acta (BBA) - Protein Structure and Molecular Enzymology* 1079, 3(1991): 316-320.

[52] Gonnet, M., Lethuaut, L. and Boury, F. New trends in encapsulation of liposoluble vitamins. *Journal of Controlled Release* 146, 3(2010): 276-290.

[53] Montenegro, L., Panico, A. M., Ventimiglia, A. and Bonina, F. P. In vitro retinoic acid release and skin permeation from different liposome formulations. *International Journal of Pharmaceutics* 133, 1(1996): 89-96.

[54] Manconi, M., Sinico, C., Valenti, D., Lai, F. and Fadda, A. M. Niosomes as carriers for tretinoin: III. A study into the in vitro cutaneous delivery of vesicle-incorporated tretinoin. *International Journal of Pharmaceutics* 311, 1-2(2006): 11-19.

[55] Manconi, M., et al. Niosomes as carriers for tretinoin: II. Influence of vesicular incorporation on tretinoin photostability. *International Journal of Pharmaceutics* 260, 2(2003): 261-272.

[56] Mandawgade, S. D. and Patravale, V. B. Development of SLNs from natural lipids: Application to topical delivery of tretinoin. *International Journal of Pharmaceutics* 363, 1-2(2008): 132-138.

[57] Hejazi, R. and Amiji, M. Chitosan-based gastrointestinal delivery systems. *Journal of Controlled Release* 89, 2(2003): 151-165.

[58] Kurita, K. Chitin and Chitosan: Functional Biopolymers from Marine Crustaceans. *Marine Biotechnology* 8, 3(2006): 203-226.

[69] Luo, H., Li, J. and Chen, X. Antitumor effect of N-succinyl-chitosan nanoparticles on K562 cells. *Biomedicine & Pharmacotherapy* 64, 8(2010): 521-526.

[60] Hou, Z., et al. Synthesis and evaluation of N-succinyl-chitosan nanoparticles toward local hydroxycamptothecin delivery. *Carbohydrate Polymers* 81, 4(2010): 765-768.

[61] Ubaidulla, U., Khar, R. K., Ahmad, F. J., Sultana, Y. and Panda, A. K. Development and characterization of chitosan succinate microspheres for the improved oral bioavailability of insulin. *Journal of Pharmaceutical Sciences* 96, 11(2007): 3010-3023.

[62] Xiangyang, X., et al. Preparation and characterization of N-succinyl-N′-octyl chitosan micelles as doxorubicin carriers for effective anti-tumor activity. *Colloids and Surfaces B: Biointerfaces* 55, 2(2007): 222-228.

[63] Krishnapriya, K. R. and Kandaswamy, M. A new chitosan biopolymer derivative as metal-complexing agent: synthesis, characterization, and metal (II) ion adsorption studies. *Carbohydrate Research* 345, 14(2010): 2013-2022.

[64] Mohammed, A. Chitosan application for active bio-based films production and potential in the food industry: Review. *LWT - Food Science and Technology* 43, 6(2010): 837-842.

[65] Jin, X., Wang, J. and Bai, J. Synthesis and antimicrobial activity of the Schiff base from chitosan and citral. *Carbohydrate Research* 344, 6(2009): 825-829.

[66] Muzzarelli, R. and Muzzarelli, C. Chitosan Chemistry: Relevance to the biomedical sciences. *Advances in Polymer Science* 186, (2005): 151-209.

[67] Harish Prashanth, K. V. and Tharanathan, R. N. Chitin/chitosan: modifications and their unlimited application potential-an overview. *Trends in Food Science & Technology* 18, 3(2007): 117-131.

[68] Pillai, C. K. S., Paul, W. and Sharma, C. P. Chitin and chitosan polymers: Chemistry, solubility and fiber formation. *Progress in Polymer Science* 34, 7(2009): 641-678.

[69] Cravotto, G., Tagliapietra, S., Robaldo, B. and Trotta, M. Chemical modification of chitosan under high-intensity ultrasound. *Ultrasonics Sonochemistry* 12, 1-2(2005): 95-98.

[70] Aiping, Z., Tian, C., Lanhua, Y., Hao, W. and Ping, L. Synthesis and characterization of N-succinyl-chitosan and its self-assembly of nanospheres. *Carbohydrate Polymers* 66, 2(2006): 274-279.

[71] Guo, Z., et al. Antifungal properties of Schiff bases of chitosan, N-substituted chitosan and quaternized chitosan. *Carbohydrate Research* 342, 10(2007): 1329-1332.

[72] Sun, T., Xu, P., Liu, Q., Xue, J. and Xie, W. Graft copolymerization of methacrylic acid onto carboxymethyl chitosan. *European Polymer Journal* 39, 1(2003): 189-192.

[73] Hu, Y., et al. Synthesis and characterization of chitosan–poly(acrylic acid) nanoparticles. *Biomaterials* 23, 15(2002): 3193-3201.

[74] Bal, S. M., Ding, Z., van Riet, E., Jiskoot, W. and Bouwstra, J. A. Advances in transcutaneous vaccine delivery: Do all ways lead to Rome? *Journal of Controlled Release* 148, 3(2010): 266-282.

[75] Watt F.M. Terminal differentiation of epidermal keratinocytes, *Current. Opinion Cell Biology* 1, (1989): 1107–1115.

[76] Michaels, A. S., Chandrasekaran, S. K. and Shaw, J. E. Drug permeation through human skin: Theory and *in vitro* experimental measurement. *AIChE Journal* 21, 5(1975): 985-996.

[77] Bouwstra, J. A. and Honeywell-Nguyen, P. L. Skin structure and mode of action of vesicles. *Advanced Drug Delivery Reviews* 54, (2002): S41-S55.

[78] Kneedler, J. A., Sky, S. S. and Sexton, L. R. Understanding alpha-hydroxy acids. *Dermatology Nursing* 10, 4(1998): 265–266.

[79] Kempers, S., Katz, H. I., Wildnauer, R. and Green, B. An evaluation of the effect an alpha hydroxy acid-blend skin cream in the cosmetic improvement of symptoms of moderate to severe xerosis, epidermolytic hyperkeratosis, and ichthyosis. *Cutaneous Medicine for the Practitioner* 61, 6(1998): 347–350.

[80] Kligman, A. M. Guidelines for the use of topical tretinoin (Retin-A) for photoaged skin. *Journal of the American Academy of Dermatology* 21, 3(1989): 650-654.

[81] Atwater, E. General dermatology: updates on alpha hydroxy acid product benefits. *Dermatology Nursing* 7, (1995): 139–40.

[82] Haug, R. H. Alpha hydroxy acids in skin care: Clark CP. Clin Plast Surg 23:49, 1996. *Journal of Oral and Maxillofacial Surgery* 54, 8(1996): 1039.

[83] Silverman, A. K., Ellis, C. N. and Voorhees, J. J. Hypervitaminosis A syndrome: A paradigm of retinoid side effects. *Journal of the American Academy of Dermatology* 16, 5(1987): 1027-1039.

[84] Haug, R. H. Considerations in alpha hydroxy acid peels: Slavin JW. Clin Plast Surg 25:45, 1998. *Journal of Oral and Maxillofacial Surgery* 56, 10(1998): 1220.

[85] Barry, B. W. Drug delivery routes in skin: a novel approach. *Advanced Drug Delivery Reviews* 54, (2002): S31-S40.

[86] Lademann, J., et al. Hair Follicles - An Efficient Storage and Penetration Pathway for Topically Applied Substances. *Skin Pharmacology and Physiology* 21, 3(2008): 150-155.

[87] Lademann, J., et al. Penetration and storage of particles in human skin: Perspectives and safety aspects. *European Journal of Pharmaceutics and Biopharmaceutics* 77, 3(2011): 465-468.

[88] Panyam, J. and Labhasetwar, V. Biodegradable nanoparticles for drug and gene delivery to cells and tissue. *Advanced Drug Delivery Reviews* 55, 3(2003): 329-347.

[89] Soppimath, K. S., Aminabhavi, T. M., Kulkarni, A. R. and Rudzinski, W. E. Biodegradable polymeric nanoparticles as drug delivery devices. *Journal of Controlled Release* 70, 1-2(2001): 1-20.

[90] Roshchupkin, D. I., Pistsov, M. Y. and Potapenko, A. Y. Inhibition of ultraviolet light-induced erythema by antioxidants. *Archives of Dermatological Research* 266, 1(1979): 91-94.

[91] Darr, D., Dunston, S., Faust, H. and Pinnell, S. Effectiveness of antioxidants (vitamin C and E) with and without sunscreen as topical photoprotectants. *Acta Dermatology Venereologica* 76, 4(1996): 264–268.

[92] Ritter, E. F., et al. Modulations of ultraviolet light-induced epidermal damage: Beneficial effects of tocopherol. *Plastic Reconstructive Surgery* 100, 4(1997): 973-980.

[93] Lopez, T., Thiele, Shindo, H. and Packer. Topical application of α-tocopherol modulates the antioxidant network and diminishes ultraviolet-induced

oxidative damage in murine skin. *British Journal of Dermatology* 138, 2(1998): 207-215.

[94] Yuen, K. S. and Halliday, G. M. α-Tocopherol, an Inhibitor of Epidermal Lipid Peroxidation, Prevents Ultraviolet Radiation from Suppressing the Skin Immune System. *Photochemistry and Photobiology* 65, 3(1997): 587-592.

[95] Jurkiewicz, B. A., Bissett, D. L. and Buettner, G. R. Effect of Topically Applied Tocopherol on Ultraviolet Radiation-Mediated Free Radical Damage in Skin. *Journal Investigative Dermatology 104*, 4(1995): 484-488.

[96] Bissett, D. L., Hillebrand, G. G. and Harnon, D. P. The hairless mouse as a model of skin photoaging: Its use to evaluate photoprotective materials. *Photo-dermatology* 6, 5(1989): 228–233.

[97] Gensler, H. L. and Magdaleno, M. Topical vitamin e inhibition of immunosuppression and tumorigenesis induced by ultraviolet irradiation. *Nutrition and Cancer* 15, 2(1991): 97-106.

[98] Beijersbergen van Henegouwen, G. M. J., Junginger, H. E. and de Vries, H. Hydrolysis of RRR-α-tocopheryl acetate (vitamin E acetate) in the skin and its UV protecting activity (an in vivo study with the rat). *Journal of Photochemistry and Photobiology B: Biology* 29, 1(1995): 45-51.

[99] Darvin, M., Zastrow, L., Sterry, W. and Lademann, J. Effect of Supplemented and Topically Applied Antioxidant Substances on Human Tissue. *Skin Pharmacology and Physiology* 19, 5(2006): 238-247.

[100] Alekperov, U. K. and Shcherbakov, V. K. An incomplete metaphase block and other effects accompanying the action of ionol on mitosis. *Tsitologia* 9, (1967): 606-609.

[101] Askerov, I. T., Abutalybov, M. G. and Alekperov, U. K. A comparative study of polyploidizing effects of colchiein and ionol. *Tsitologia* 15, (1973): 341-843.

[102] Hathway, D. E. Metabolic fats in animals of hindered phenolic antioxidants in relation to their safety evaluation and antioxidant function. *Advanced Food Research* 15, (1966): 1-56.

[103] Branen, A. L. Toxicology and biochemistry of butylated hydroxyyanisole and butylated hydroxytoluene. *Journal American Oil Chemists' Society* 52, (1975): 59-63.

[104] Khettab, N., et al. Photoprotective effect of vitamins A and E on polyamine and oxygenated free radical metabolism in hairless mouse epidermis. *Biochimie* 70, 12(1988): 1709-1713.

[105] Roshchupkin, D. I., Pistsov, M. Y. and Potapenko, A. Y. Inhibition of ultraviolet light-induced erythema by antioxidants. *Archives of Dermatological Research* 266, 1(1979): 91-94.

[106] Janes, K. A., Fresneau, M. P., Marazuela, A., Fabra, A. and Alonso, M. a. J. Chitosan nanoparticles as delivery systems for doxorubicin. *Journal of Controlled Release* 73, 2-3(2001): 255-267.

[107] Mura, C., et al. In vitro study of N-succinyl chitosan for targeted delivery of 5-aminosalicylic acid to colon. *Carbohydrate Polymers* 85, 3(2011): 578-583.

[108] Tree-udom, T., Wanichwecharungruang, S. P., Seemork, J. and Arayachukeat, S. Fragrant chitosan nanospheres: Controlled release systems with physical and chemical barriers. *Carbohydrate Polymers* 86, 4(2011): 1602-1609.

[109] Toll, R., et al. Penetration Profile of Microspheres in Follicular Targeting of Terminal Hair Follicles. *Journal Investigative Dermatology* 123, 1(2003): 168-176.

[110] Lademann, J., et al. Nanoparticles-An efficient carrier for drug delivery into the hair follicles. *European Journal of Pharmaceutics and Biopharmaceutics* 66, 2(2007): 159-164.

[111] Kuchler, S., et al. Nanoparticles for skin penetration enhancement - A comparison of a dendritic core-multishell-nanotransporter and solid lipid nanoparticles. *European Journal of Pharmaceutics and Biopharmaceutics* 71, 2(2009): 243-250.

[112] Zhang, W., et al. Penetration and distribution of PLGA nanoparticles in the human skin treated with microneedles. *International Journal of Pharmaceutics* 402, 1-2(2010): 205-212.

[113] Padois, K., et al. Solid lipid nanoparticles suspension versus commercial solutions for dermal delivery of minoxidil. *International Journal of Pharmaceutics* 416, 1(2011): 300-304.

[114] Teichmann, A., et al. Comparison of stratum corneum penetration and localization of a lipophilic model drug applied in an o/w microemulsion and an amphiphilic cream. *European Journal of Pharmaceutics and Biopharmaceutics* 67, 3(2007): 699-706.

[115] Morgen, M., et al. Targeted delivery of a poorly water-soluble compound to hair follicles using polymeric nanoparticle suspensions. *International Journal of Pharmaceutics* 416, 1(2011): 314-322.

[116] Kong, M., Chen, X. G., Kweon, D. K. and Park, H. J. Investigations on skin permeation of hyaluronic acid based nanoemulsion as transdermal carrier. *Carbohydrate Polymers* 86, 2(2011): 837-843.

[117] Rancan, F., et al. Stability of polylactic acid particles and release of fluorochromes upon topical application on human skin explants. *European Journal of Pharmaceutics and Biopharmaceutics* 80, 1(2012): 76-84.

[118] Pople, P. V. and Singh, K. K. Development and evaluation of topical formulation containing solid lipid nanoparticles of vitamin A. *AAPS PharmSciTech* 7, 4(2006): E1-E7.

[119] Teixeira, Z., et al. Retinyl palmitate flexible polymeric nanocapsules: Characterization and permeation studies. *Colloids and Surfaces B: Biointerfaces* 81, 1(2010): 374-380.

[120] Arayachukeat, S., Wanichwecharungruang, S. P. and Tree-Udom, T. Retinyl acetate-loaded nanoparticles: Dermal penetration and release of the retinyl acetate. *International Journal of Pharmaceutics* 404, 1-2(2011): 281-288.

APPENDICES

APPENDIX A

1. Determination of degree of succinyl substitution

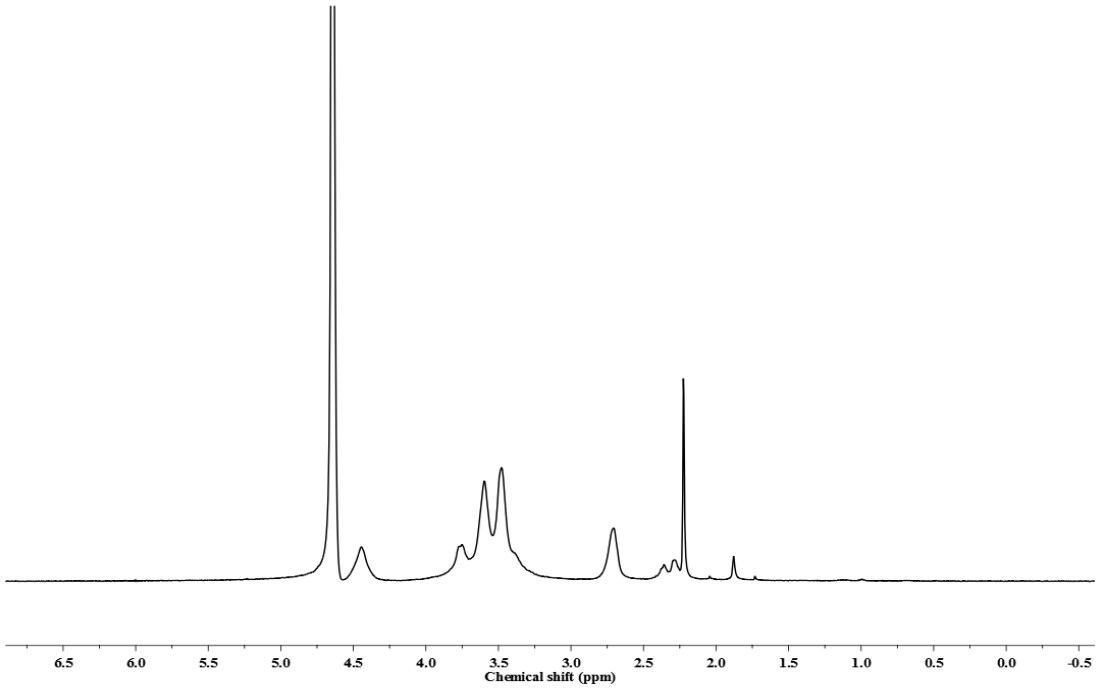

Figure A1. ^{1}H NMR spectrum of *N*-succinylchitosan (N-SC)

The degree of grafting could be determined using equation (1):

$$DG = \frac{I_{graft} \text{ x } DD}{n \text{ x } I_{cs}} \quad (1)$$

I_{graft} = the intensity of grafted moiety
DD = the amount of deacetylation degree
n = number of protons of grafted moiety
I_{cs} = the intensity of hydrogen atom of chitosan's glucosamine unit

From the ^{1}H NMR spectrum (Figure A1), using the integral ratio between 4H from ethyl group of succinyl (2.28-2.36 ppm) and 1H from C2 of glucosamine unit (at 2.7 ppm) with 85% deacetylation degree:

$$DG = \frac{0.70 \text{ x } 0.85}{4 \text{ x } 1}$$

$$DG = 0.15$$

The degree of succinyl substitution could be estimated as 0.15.

APPENDIX B

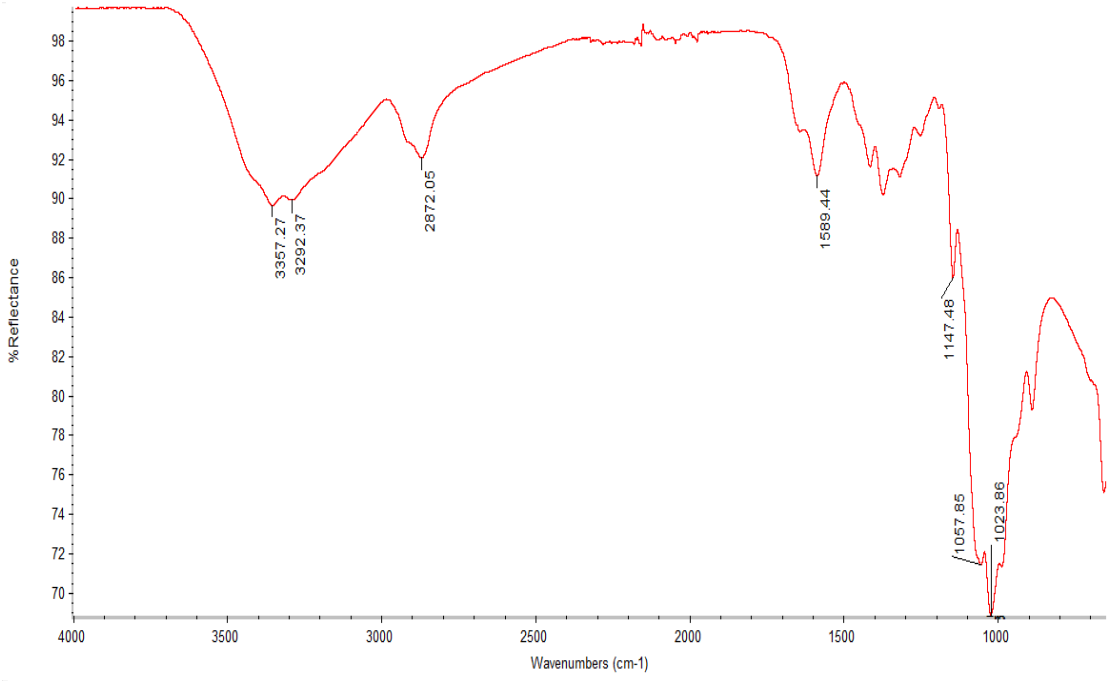

Figure A2. ATR-FTIR spectrum of chitosan

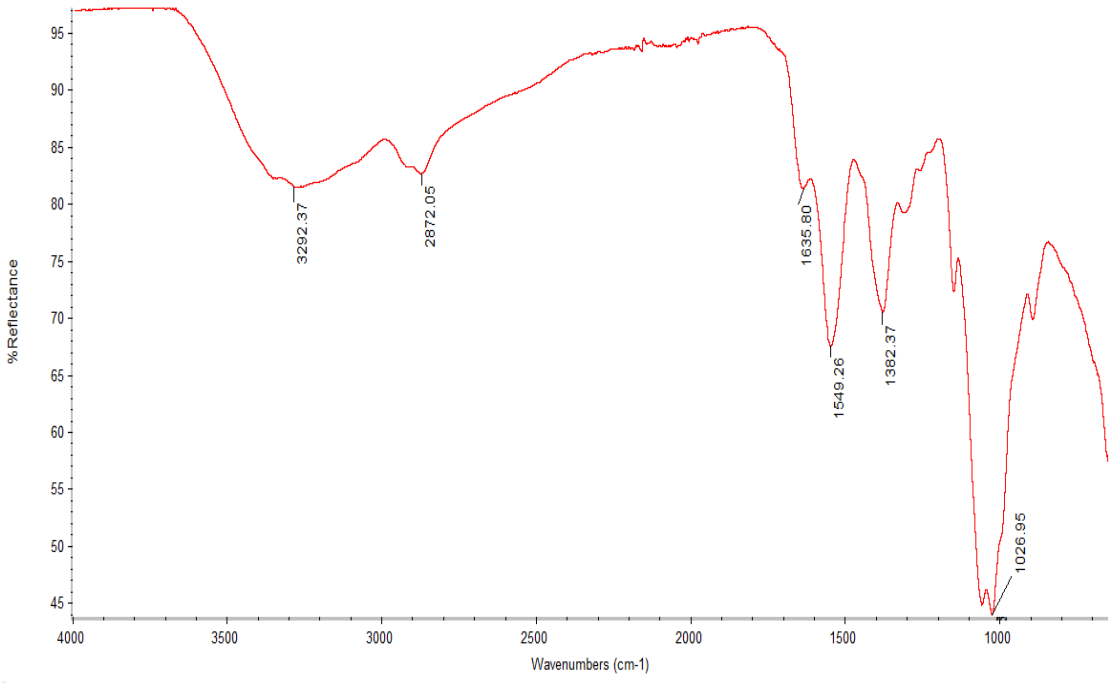

Figure A3. ATR-FTIR spectrum of *N*-succinylchitosan (N-SC)

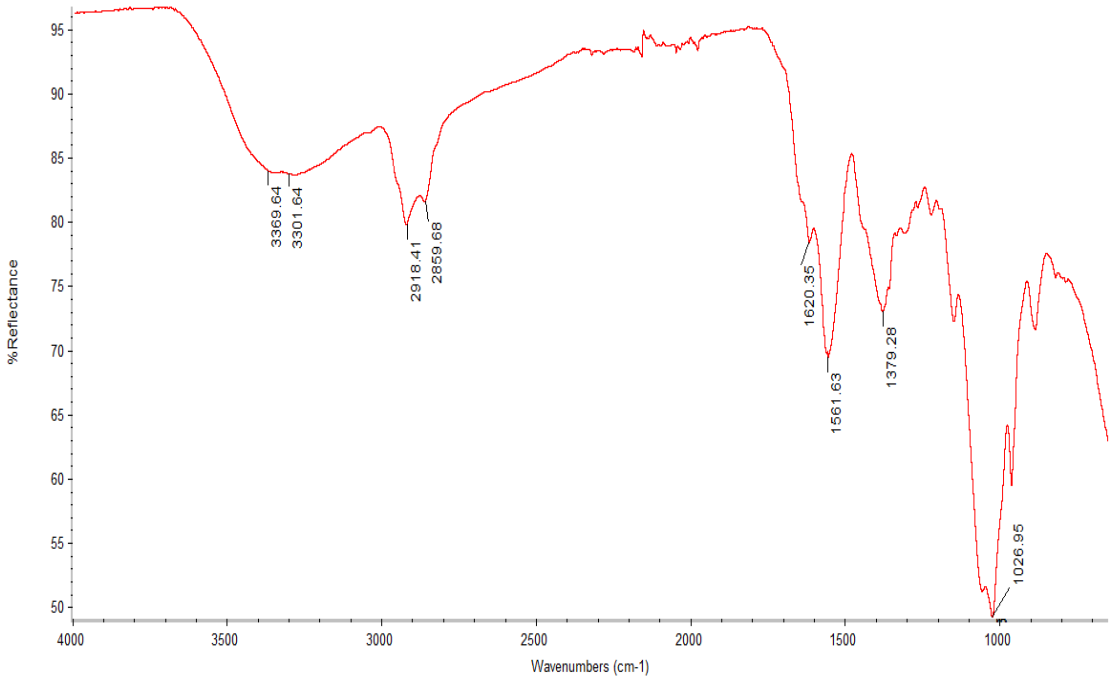

Figure A4. ATR-FTIR spectrum of retinilidenesuccinylchitosan

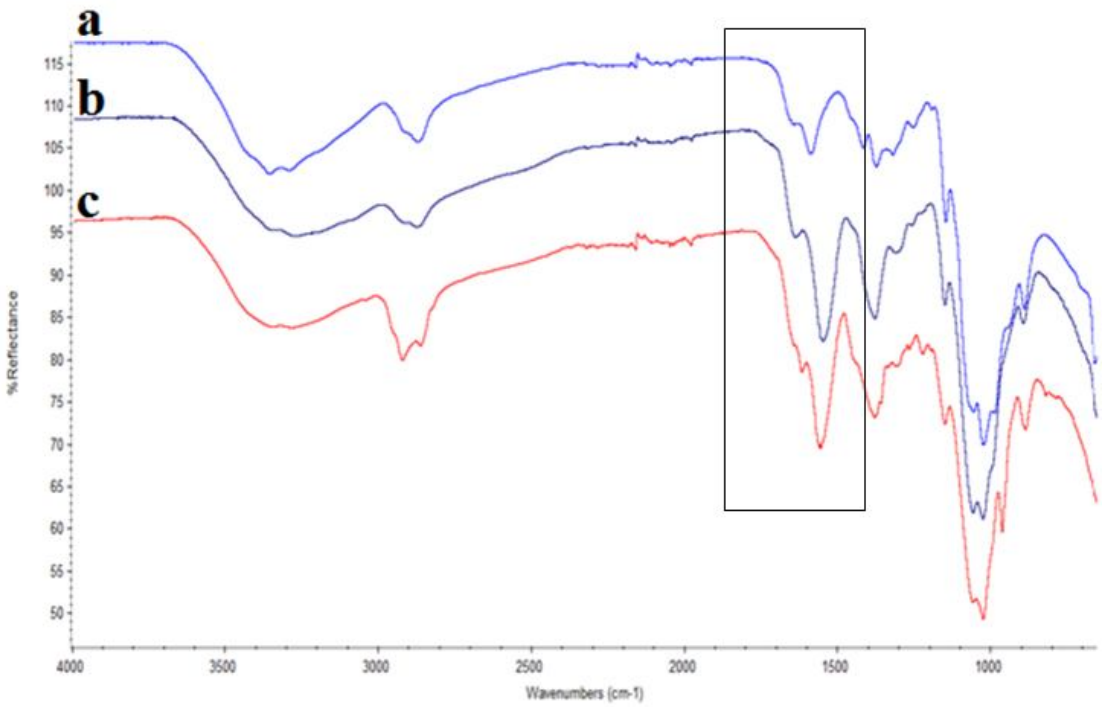

Figure A5. ATR-FTIR spectra of (a) chitosan (b) N-SC and (c) retinilidenesuccinylchitosan.

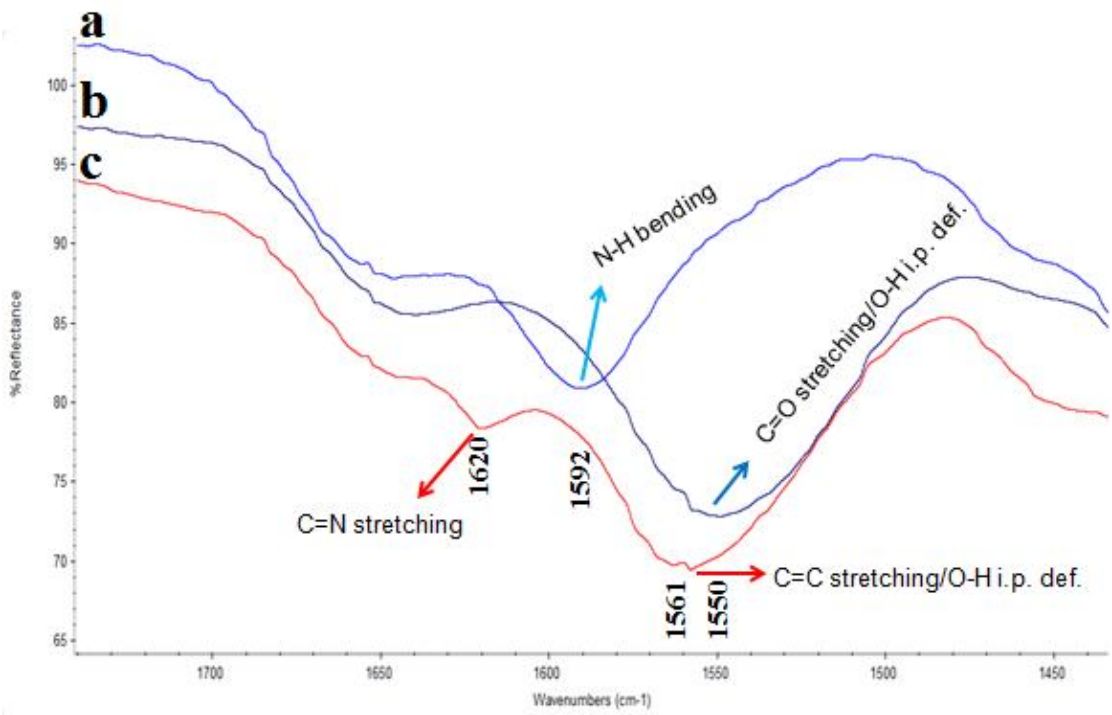

Figure A6. Expansion of ATR-FTIR spectra of (a) chitosan (b) N-SC and (c) retinilidenesuccinylchitosan.

APPENDIX C

2. Determination of degree of retinilidene moiety grafting (imine functionality)

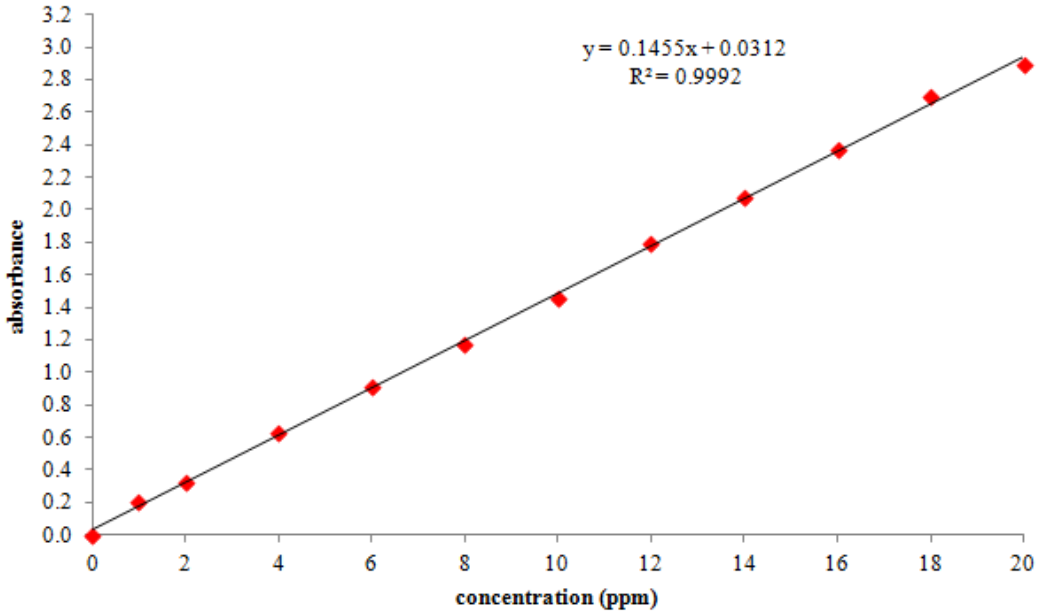

Figure A7. Calibration curve of retinaldehyde at 375 nm

The amount of extracted retinaldehyde from retinilidenesuccinylchitosan was estimated with the aid of the calibration curve:

$$Y = 0.1455X - 0.0312 \quad (1)$$

From equation (1) $0.905 = 0.1455X - 0.0312$

$$X = 6.4344 \text{ ppm}$$

Dilution factor = 160

$$X = 6.4344 \times 160$$

$$X = 1029.50 \text{ ppm}$$

Weight of grafted retinaldehyde in 15 mL = 1029.50 x 0.015

= 15.44 mg

Molecular weight of retinaldehyde = 284.44 mg/mol

∴ Mole of retinaldehyde = 15.44/284.44 = 0.0543 mol

The amount of N-SC = 46.28 mg, molecular weight = 185.12

∴ Mole of N-SCS = 46.28/185.12 = 0.25 mol

Degree of grafting (DG) = mol of grafted moiety/mol of N-SC

DG = 0.0543/0.25 = 0.22

The degree of vanillin grafting could be estimated as 0.22.

APPENDIX D

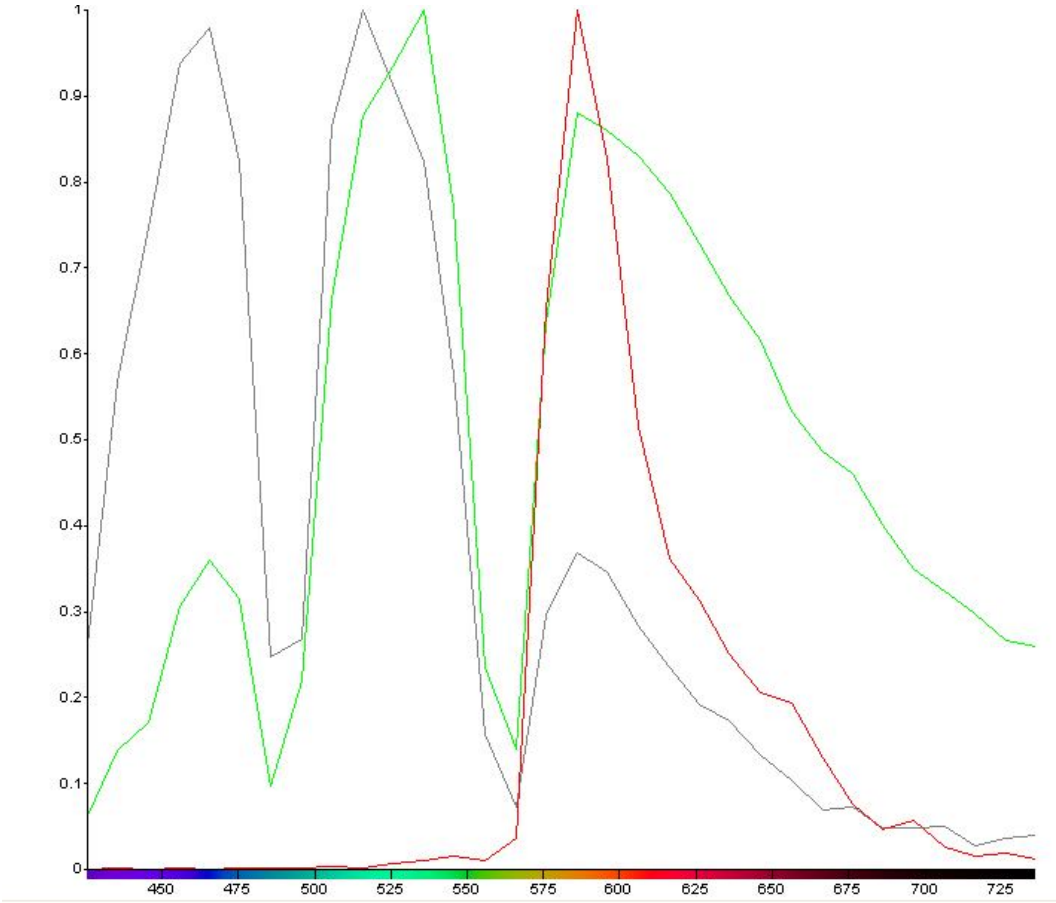

Figure A8. The fluorescent spectra of: retinaldehyde (green), Rho B-N-SC (red) and porcine ear skin (gray).

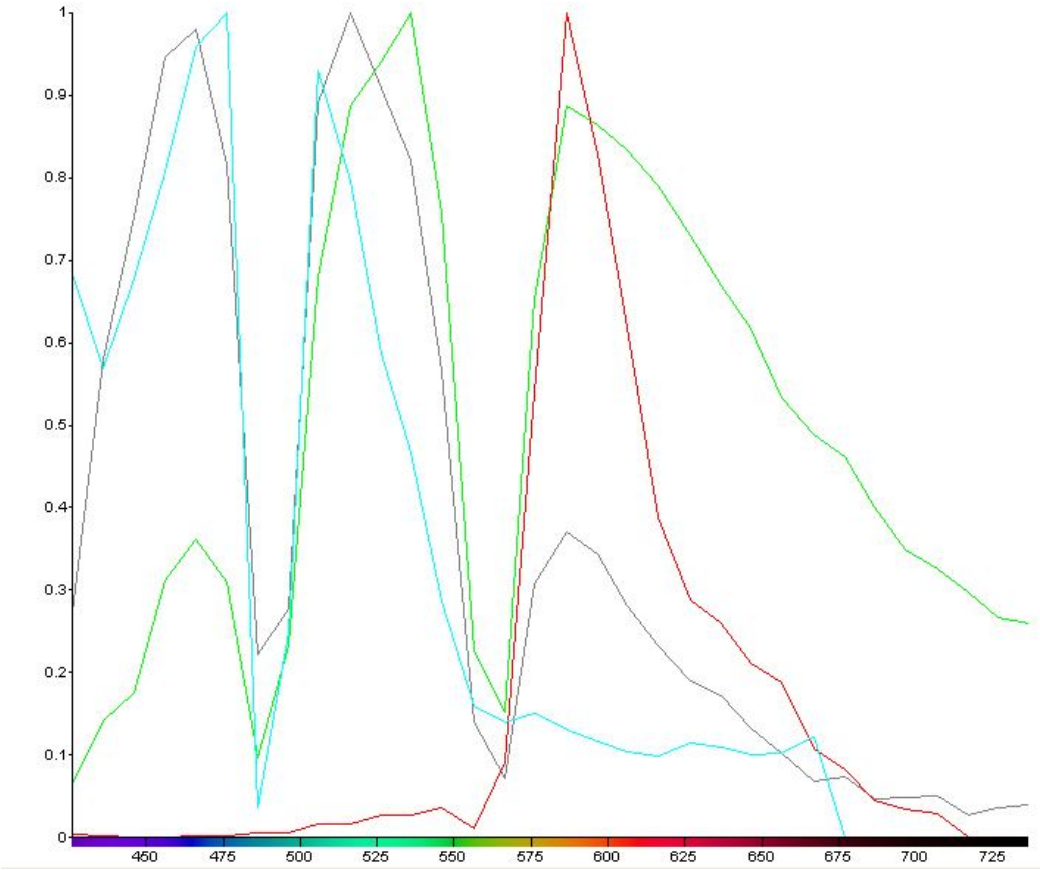

Figure A9. The fluorescent spectra of: retinaldehyde (green), Rho B-N-SC (red), vitamin E (light blue) and porcine ear skin (gray).

VITAE

Miss Piyapan Supmuang was born on September 11, 1986 in Bankok, Thailand. She received a Bachelor's Degree of Science in Biotechnology from King Mongkut's Institute of Technology Ladkrabang in 2008. Then she started her graduate study on Master's degree in the Program of Biotechnology, Faculty of Science, Chulalongkorn University. During master study, she had the great opportunity to present her work in poster session in the topic of "Nanoparticles of retinaldehyde using chitosan" at the Pure and Applied Chemistry International Conference 2012 (PACCON 2012), Chiangmai, Thailand.

Her present address is 148/5 M. 6 Klongdan, Bangbo, Samutprakarn Thailand 10550.